Space Programs Summary No. 37-9, Volume I

for the period March 1, 1961 to May 1, 1961

jpl

JET PROPULSION LABORATORY
CALIFORNIA INSTITUTE OF TECHNOLOGY
PASADENA, CALIFORNIA

June 1, 1961

NATIONAL AERONAUTICS AND SPACE ADMINISTRATION
CONTRACT NO. NASw-6

Space Programs Summary No. 37-9, Volume I

for the period March 1, 1961 to May 1, 1961

JET PROPULSION LABORATORY
CALIFORNIA INSTITUTE OF TECHNOLOGY
PASADENA, CALIFORNIA

June 1, 1961

o auth

Preface

The *Space Programs Summary* is a two-volume bimonthly publication of the Jet Propulsion Laboratory. Research and development activities conducted by JPL having specific application to space programs under the sponsorship of the National Aeronautics and Space Administration are reported in this publication. Unclassified and classified activities will be documented in Volumes I and II, respectively.

The projects reported herein were undertaken in partial fulfillment of National Aeronautics and Space Administration Contract NASw-6.

W. H. Pickering, *Director*
Jet Propulsion Laboratory

Space Programs Summary No. 37-9
Volume I

Contents

Contents (Cont'd)

Editor's Note:

Additional documentation of the Lunar and Planetary–Interplanetary Programs and their associated Advanced Development can be found in Volume II of this summary. Also to be found in Volume II is a discussion of the *Juno II* Program.

PART ONE
RÉSUMÉ

I. Lunar Program

A spacecraft-vehicle compatibility test, using the *Ranger* RA-1 proof test model (PTM) and *Agena* No. 6001, was successfully completed at Lockheed Missile and Space Division (LMSD), Sunnyvale. The *Ranger* RA-1 spacecraft completed all tests and has been shipped to AMR. *Ranger* RA-2 is ahead of schedule, having completed magnetometer calibrations and preliminary system tests. The RA-3 PTM is in assembly.

II. Planetary–Interplanetary Program

Mariner activities are proceeding on schedule. Spacecraft-vehicle compatibility test criteria and schedules were coordinated and agreed upon between JPL and MSFC. Both the *Centaur* and the *Mariner* project development plans are nearing completion with June 1 as the publication goal. Allocation of *Centaur* vehicles C-4 and C-5 to *Mariner* missions P-37 and P-38 has been confirmed.

III. Deep Space Instrumentation Facility

Contact with the planet Venus by coherent CW radar was successfully made from Goldstone. Ranging, reflectivity, polarization, and true doppler measurements have been made. More accurate measurements of the astronomical unit have been obtained. Study contracts on a large aperture antenna will be completed in May. Installation of the South Africa station is proceeding on schedule. Installation of equipment for the first *Ranger* launch will begin in May.

IV. *Juno II*

The *Juno II* program is essentially the continuation of the original *Juno I* (or *Jupiter C)* series with the substitution of a *Jupiter* for the original *Redstone* booster. Only slight structural modifications were made to the JPL cluster to adapt it to the heavier payloads used on this series.

The first two *Juno II* vehicles were assigned the mission of launching JPL's lunar probes *(Pioneers III* and *IV).* Since then, the vehicle has successfully orbited *Explorer VII* (IGY payload), *Explorer VIII* (ion probe satellite) and *Explorer XI* (gamma-ray astronomy satellite). All these payloads fall into the 75- to 100-pound class.

PART TWO
LUNAR PROGRAM

I. Ranger

On March 13 to 31, the *Ranger* RA-1 proof test model (PTM), associated ground support equipment (GSE), and *Agena* Vehicle No. 6001 were mated at Lockheed Missile and Space Division (LMSD), Sunnyvale and a highly successful compatibility test was conducted (Fig 1). *Atlas* and *Agena* RF sources were simulated, and as many as possible of the on-board systems were operated to determine compatibility and interference effects. Apart from undesired 400- and 800-cycle modulation on the *Agena* telemetry readout of spacecraft data, no major problems were encountered.

During the month of April the RA-1 flight spacecraft and associated GSE were operated in a series of dummy run, or mock flight, tests for the purpose of refining and correcting the operating procedures and training the operator team. Throughout these tests the equipment performed excellently, and a compatible set of detailed operating instructions was created. At the completion of the dummy runs the RA-1 spacecraft had accumulated a total of 600 hours of running time. Because results of the initial RA-1 vacuum–temperature test had not agreed with predictions, another test in the space simulator was scheduled following the dummy runs. After this second test it was concluded that some portions of the spacecraft paint pattern should be altered, but the final pattern has not yet been selected and the alterations will have to be made at AMR. Time for this activity was already included in the AMR operation schedule.

During this temperature control test, subsystem spares were substituted for five of the six cases in order to take

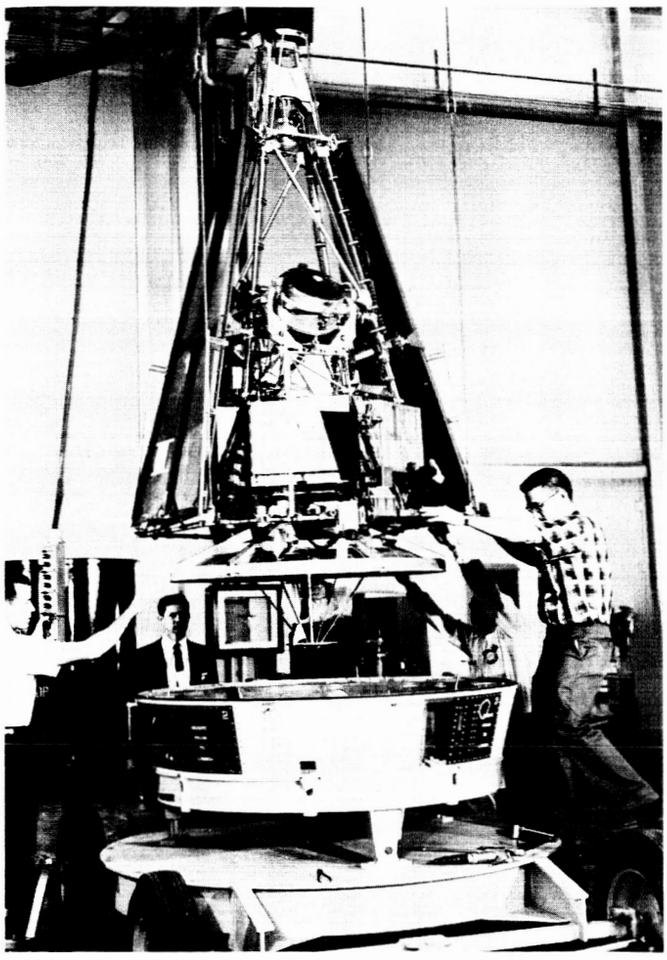

Figure 1. Spacecraft to adapter mating

advantage of the vacuum–temperature environment. One equipment failure was encountered during the test, resulting in the loss of one commutator sync signal. This failure was the result of a cold solder joint in the sync sensor relay circuit.

After the vacuum–temperature test, a final system test was made to confirm flight readiness of the spacecraft. Minor problems were found in the GSE; flight equipment performance was completely satisfactory.

Assembly and testing of the RA-2 spacecraft have proceeded smoothly and this activity is now several weeks ahead of schedule. At the end of April, RA-2 was placed in the Space Technology Laboratories magnetic test facility at Malibu and the magnetic field calibration was accomplished. Following this test, vehicle match-mate and vacuum–temperature tests are planned. A portion of the time gained will be used in an extended life test in the space simulator; however, this test will probably have to be shorter than it could ideally be because of the limited number of available personnel. RA-1 experience indicates that round-the-clock operation of the space simulator and monitoring of the spacecraft is a demanding, exhausting task.

Assembly of the RA-3 PTM has begun. The mid-course propulsion unit and the lunar capsule electrical mock-up are on hand, and other components are in qualification test. However, some late deliveries are now expected and it is likely that a part of the value of the RA-3 PTM will be lost because there will not be enough time to incorporate changes between tests of the PTM and of the actual RA-3 flight spacecraft.

A. Systems

1. Ranger RA-1 Testing

Compatibility testing of the *Ranger* RA-1 proof test model (PTM) with the Lockheed adapter and *Agena* vehicle demonstrated sufficient technique of both systems working with negligible interaction. Systems problems uncovered during compatibility tests at Lockheed Missile and Space Division (LMSD) were primarily the type that were independent of the match-mating.

According to procedure the following steps were planned and accomplished:

(1) Entire GSE complex was set up.

(2) Spacecraft was assembled and mated to the *Agena* adapter.

(3) The shroud was installed over the spacecraft.

(4) Spacecraft was joined with the adapter to the *Agena*.

(5) Complete RF interference tests were made with the shroud installed and also with the shroud removed.

A telecommunications error developed at communications Case II on Connector 2J3. Improper installation of the connecting cable between 2J3 and the omni-antenna was the cause, and the cable was replaced with a slight delay in test schedule.

Irregular counting was experienced in the spacecraft controller. This existed as a difficulty before compatibility testing, however.

As an expedient means of keeping the 0.25-watt transmitter turned off during certain portions of the compatibility test, a device was constructed to accomplish the task. Premature exhaustion of the mercury battery pack of this device failed and, as a consequence, the transmitter was allowed to transmit over the week-end. This device will not be used in flight and so this problem will not recur.

The spacecraft RF signal telemetered by the *Agena* experienced spurious signals superimposed on the normal signal. An 800-cps interference tone below spacecraft Channel 3 was present as well as a 400-cps tone causing the Channel 1 discriminator to momentarily lose lock.

Match-mating was hampered insofar as connecting cables were concerned. The foreward support ring of the *Agena* dolly interfered with the spacecraft umbilical plug and the catenary cables. A fix was obtained after a short delay in schedule by removing a section of the support ring.

Wiring problems were narrowed to a single error in the adapter and it was rectified by LMSD.

a. Interface tests. A number of tests on items of interface have been conducted during this period.

Shroud and spacecraft separation tests. Shroud and spacecraft separation tests are being conducted by LMSD at their Burbank, California facility. Results of tests to date indicate that no major difficulties will be encountered. Final results will be reported at a later date.

Match-mate tests. Match-mate tests were made on February 16 through 18, 1961 with the adapter and shroud for *Agena* B 6001 vehicle and *Ranger* RA-1 spacecraft.

Duplicate tests were made using first the serrated plate type shear connection, then the type with close tolerance tight fitting bolts and holes. Both systems appear to be satisfactory (*SPS 37-7*). A decision as to which type shear connection shall be used is still forthcoming because of incomplete tests on the serrated plates.

Vibration tests. JPL furnished a dynamic model of the spacecraft to LMSD on April 10 for running a composite vibration test of *Agena*–spacecraft adapter and the spacecraft and shroud. In these tests, the package was shaken in all three axes over a range of 6 cps to 2 kc. Loads varied from 1 g at the low ranges to 7.5 g at the high range with intermittent 0.5-*g* levels at particular table resonance conditions. Data from this test consisted of accelerometer data from the shake table, the adapter, the spacecraft and the shroud, and of data taken from distance probes on both spacecraft antennas to determine any possible bumping or interference. Final results of the test are still pending; however, the package appears to be sound and no interference was detected. Upon completion of the vibration tests the dynamic model of the spacecraft was sent to Lockheed's Santa Cruz test base for use in the *Agena* B hot firing tests.

Shroud material qualification tests. During the months of March and April, LMSD ran qualitative tests to prove the acceptability of the materials used inside the shroud. It was determined that a number of the materials initially considered for use on the shroud were unacceptable from the standpoint of contaminating spacecraft surfaces by smoke and/or gasses generated from aerodynamic heating. These materials were eliminated and replaced by nonsmoking materials.

Tests were again made at LMSD Van Nuys for final acceptance of the shroud materials. These tests consisted of exposing optic samples, provided by both LMSD and JPL, to the products emitted when shroud materials were under simulated flight altitude and temperature conditions. Three tests were run: one on materials which may reach 750°F, one on materials which may reach 350°F, and a third test on red cerro cement, the use of which was questionable at the time of test and which has since been eliminated. The results of the tests indicate reflectance of the Lyman-alpha mirror sample used in the first test to be down about 50% in the 1215 Angstrom unit wavelength. All other tests of JPL samples indicate satisfactory transmissibility in the visible light range.

Shroud ground-cooling tests. A demonstration of ground cooling of the shroud with spacecraft power dissipation simulated therein was made at Lockheed Van Nuys plant on April 26, 1961. The method of cooling was by means of a cooling blanket which fitted closely the exterior contour of the shroud. Air of controlled temperature and in varying quantities was pumped through ducts to the blanket and distributed to annular ducts running around the shroud. Air flowing through the annular ducts picks up both solar heat from the outside and spacecraft dissipated heat from inside the shroud and exhausts it into the atmosphere. The blanket is to be left on the shroud until the missile actually lifts off the pad. A cable attached to the umbilical tower releases the blanket along its entire fore and aft length. As the umbilical tower moves away from the missile it pulls the cooling blanket with it. The blanket is expected to be damaged and burned sufficiently by the missile exhaust to require a new one for each flight.

b. Systems tests. The combined systems compatibility test was conducted at LMSD, Sunnyvale, California, during the period of March 13 through March 31, 1961. For the performance of this test, MSFC provided over-all management direction. LMSD and JPL supplied personnel to perform the necessary tasks in their respective areas. These personnel were under the control of LMSD and JPL test directors who reported to a LMSD test conductor. The test conductor reported to MSFC personnel.

The purpose of this test was to demonstrate the mutual compatibility of the *Ranger* RA-1 PTM and the *Agena* B 6001 vehicle. The test was conducted in accordance with LMSD specifications and was divided into three major areas.

Mechanical compatibility. The intent of this test was to go through, as completely as possible, the operations necessary to mate the spacecraft with the *Agena* shroud and adapter (Fig 2), and to determine if the ground handling equipment were compatible with the flight hardware.

Electrical compatibility. The intent of this test was to determine if the spacecraft–*Agena* adapter wiring was mutually compatible.

Radio frequency compatibility. The intent of this test was to determine: (1) RF compatibility between on-board electrical and electronic systems, and (2) RF compatibility between on-board electronic systems and certain simulated AMR sources.

During this portion of the test, the *Agena* and spacecraft were simultaneously put through complete system checkout runs while being exposed to a simulated AMR RF environment. Three different system runs were made: the first run was accomplished without the shroud installed (Fig 3). In the second run, the shroud was installed

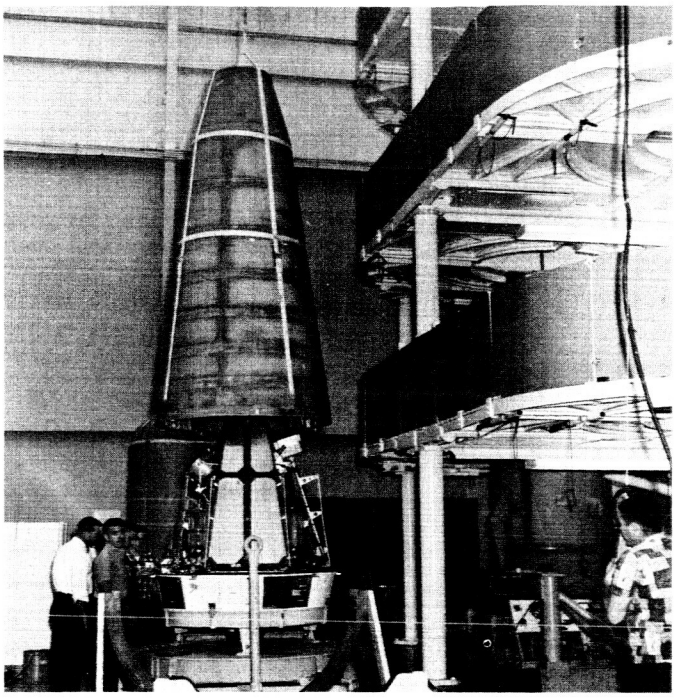

Figure 2. Installation of spacecraft shroud

and was removed manually (Fig 4) at the time it is normally ejected during flight. During the third run, efforts were made to simulate flight conditions as nearly as possible. External monitoring cables were removed and the preflight countdown was simulated. At $T - 0$ the spacecraft and *Agena* umbilicals were removed and a simulated flight sequence was conducted.

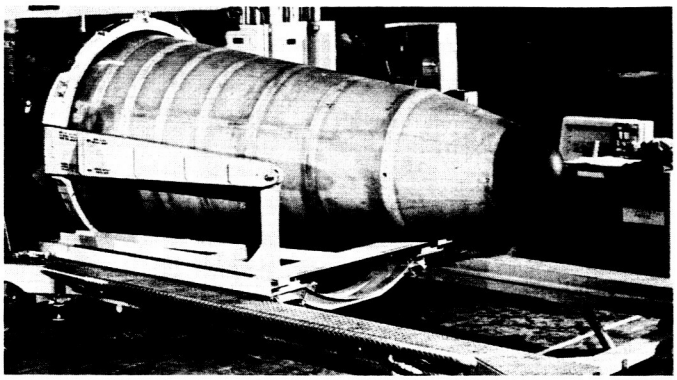

Figure 4. Spacecraft–adapter–shroud assembly

The RF environment equipment was designed to simulate AMR conditions as nearly as practical. The equipment consisted of signal generators feeding directional antennas aimed at the spacecraft (Fig 5). JPL acted as over-all coordinator for the environmental simulation.

The objectives of the mechanical, electrical, and RF interference tests were met. A number of problems were encountered; however, these were minor in nature and were resolved during the course of the test. Evaluation of the spacecraft telemetry and central recorder records has revealed no abnormalities in spacecraft operation due to the RF environment. However, two major incompatibilities were uncovered during the course of this test.

c. Electrical incompatibility. Task Assignment Directive No. 008 from MSFC to LMSD established the feasibility of providing certain telemetry measurements over

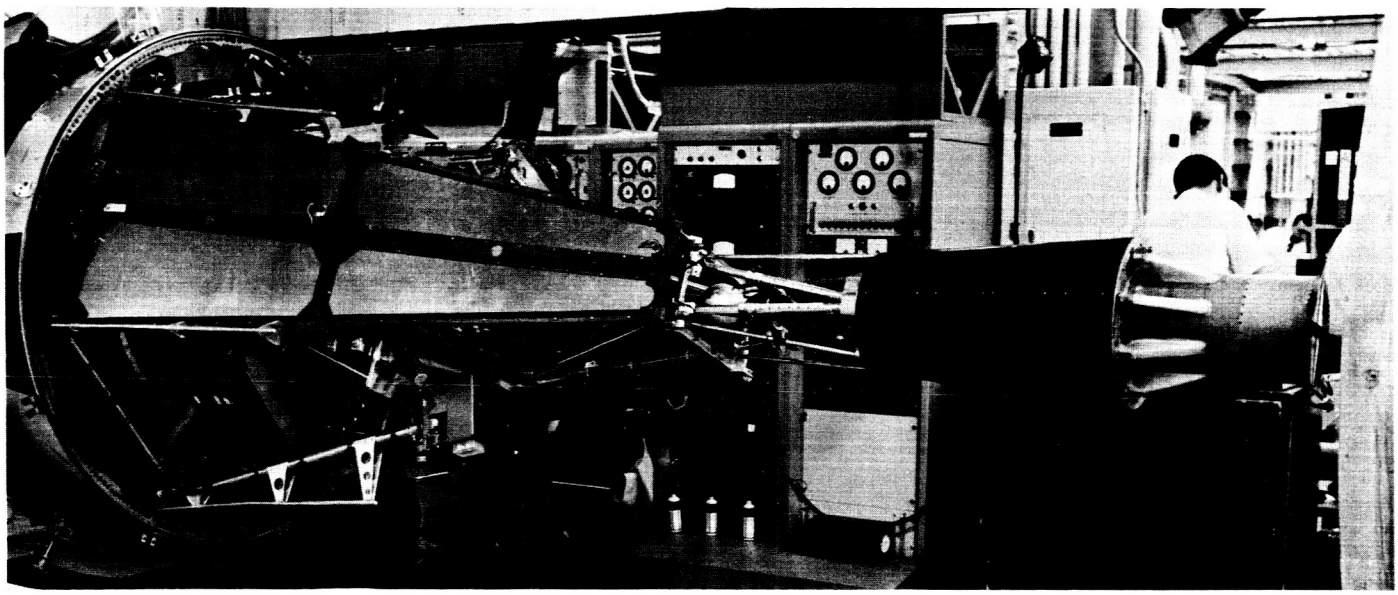

Figure 3. Spacecraft mated to *Agena*

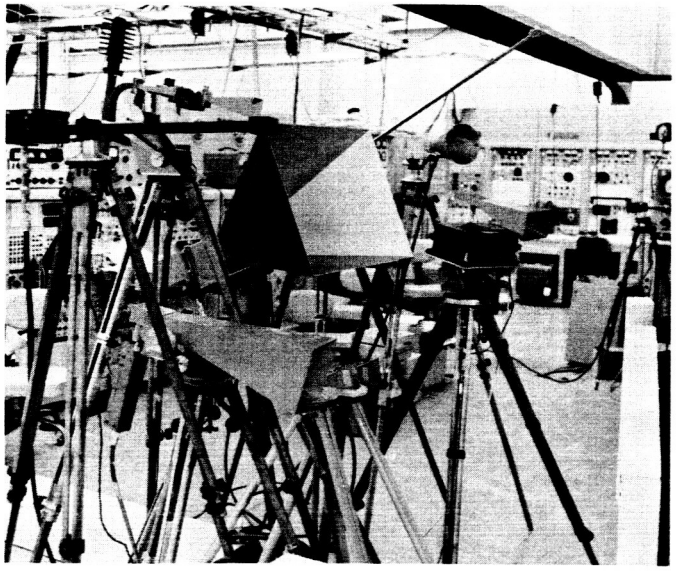

Figure 5. Spacecraft RF test setup

the *Agena* system, and the required measurements are noted in JPL Specification No. 30331.

One of the requirements was that the spacecraft (audio) telemetry signal be utilized to modulate the *Agena* telemetry. This modulation, then, provides spacecraft information during those periods of flight when the *Ranger* 960-mc signal is not received (from loss of signal at the Cape to signal acquisition at the South Africa DSIF site) and when the *Agena* 244.3-mc signal is received (through the standard AMR telemetry receiving stations, including assigned ships). The method agreed upon is shown in Figure 6 (*SPS 37-7*, Fig 5).

Figure 6 shows that the spacecraft (audio) mixed tones (370 to 3220 cps) are used to modulate both the spacecraft telemetry and the *Agena* telemetry, and that this mixed-tone signal is monitored in the blockhouse. A 600-ohm, transformer-coupled balanced line is used between the spacecraft, the *Agena*, and the blockhouse. A low-pass filter is installed in the LMSD base-band coupler.

Test results. The spacecraft data encoder observed no effects on the RF interference environment tests at LMSD. The only problems were in the spacecraft signal telemetered by the *Agena*. These were an 800-cps interference tone about 6.5 db below the spacecraft Channel 3 signal and an odd 400-cps tone occurring every 40 to 45 seconds causing the Channel 1 discriminator to momentarily lose lock.

Observations of the spacecraft signals after coming through the *Agena* telemetry system showed a noticeable 800-cps component which interferes with the spacecraft Channel 3. This interference is shown in Figures 7, 8, and 9. Figure 7 was taken from the tape made during the tests. This shows Channel 3 on the spacecraft modulation line and after passing through the *Agena*. The two pictures were taken when Channel 3 was at the same frequency. Figure 8 was made from a dub of the recording Lockheed made of the *Agena* telemetry signal during the test and shows the same effect. Figure 9 was taken at Lockheed during the test.

This 800-cps tone occurred throughout the test and seemed to be constant in amplitude. It was determined that the tone was not caused by the instrumentation gyro in the spacecraft. Analysis of the spacecraft and *Agena* signals with a HP Model 302A wave analyzer are shown in Table 1. Thus, the *Agena* telemetry signal contains an 800-cps component which is 20 db greater than that in the spacecraft and only 6.5 db below Channel 3.

Another interesting phenomenon is shown in Figure 10. This increase in amplitude occurred regularly every 40 to 45 seconds and only on Channel 1 of the *Agena* telemetry signal and nowhere else. This transient, under no noise conditions, causes the Channel 1 discriminator to momentarily lose lock. The situation becomes worse under noisy conditions. This can cause an error in the 400-cps timing reference used in the decommutator and in decommutating the scientific data.

This latter condition, the 400-cps transient, should be considered as the most serious problem. The 800-cps interference tone should only affect the data in extremely noisy conditions as it is far enough away from the data frequencies on Channel 3 so as not to be seen by the phase locked discriminator. All the information available on this problem has been supplied to LMSD for review and possible action. In addition, dub tapes have been provided to LMSD to aid in their analysis. Neither the cause of the problem nor its solution is known at this time.

d. RF incompatibility. From approximately 24 hours prior to launch until the shroud is ejected during the *Atlas* boost phase of flight, the spacecraft is completely enclosed within a metal box, that is, the shroud, the adapter, and the *Agena* forward equipment rack. Thus, a fundamental incompatibility arises in that the antennas are not radiating into free space with the result that a large voltage standing wave ratio (VSWR) exists within the RF system.

As shown in Figure 6 the spacecraft has three RF cavities which provide the RF power output: two at 3.0 watts and one at 0.25 watt, through coaxial cables,

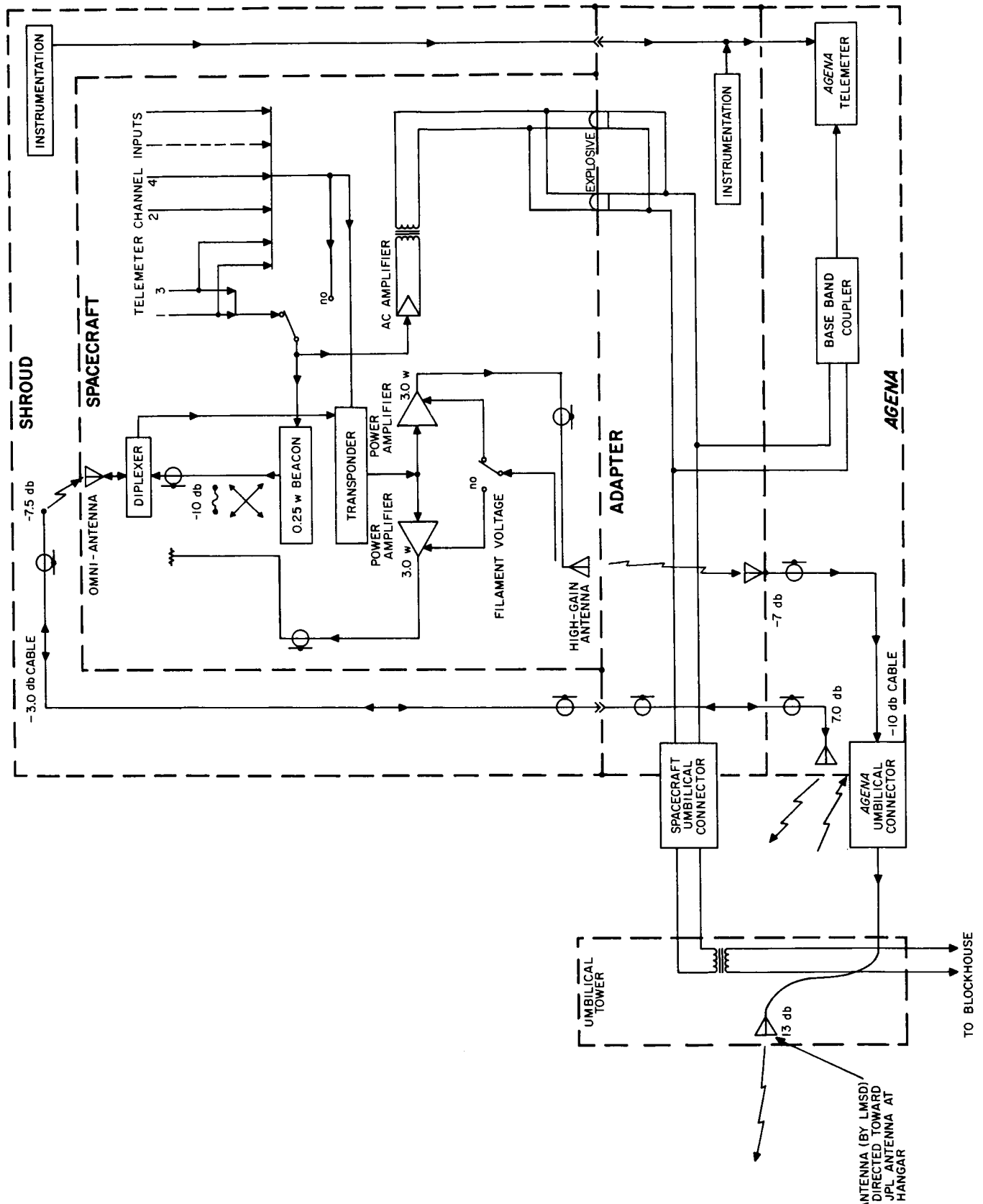

Figure 6. RF and telemetry interface

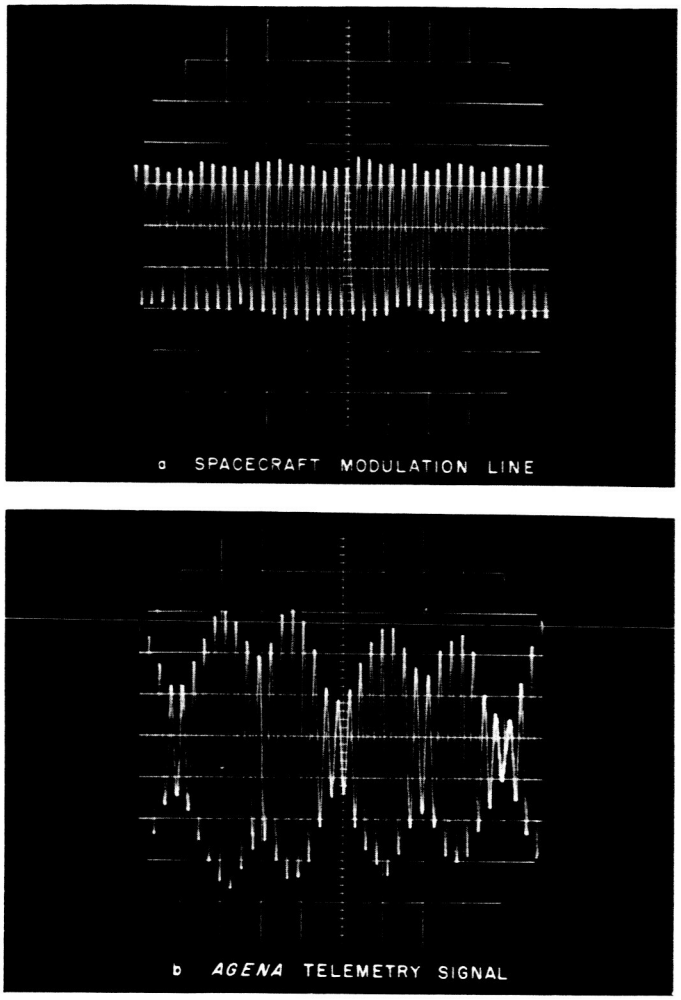

Figure 7. Channel 3 output

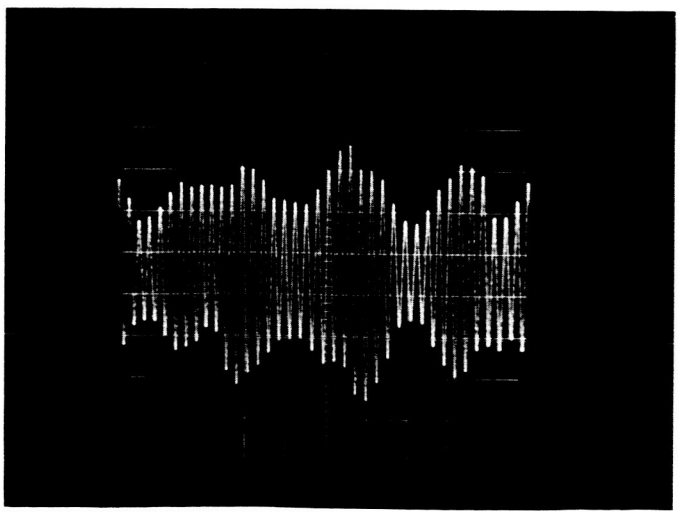

Figure 8. Channel 3 output taken from LMSD telemetry tape

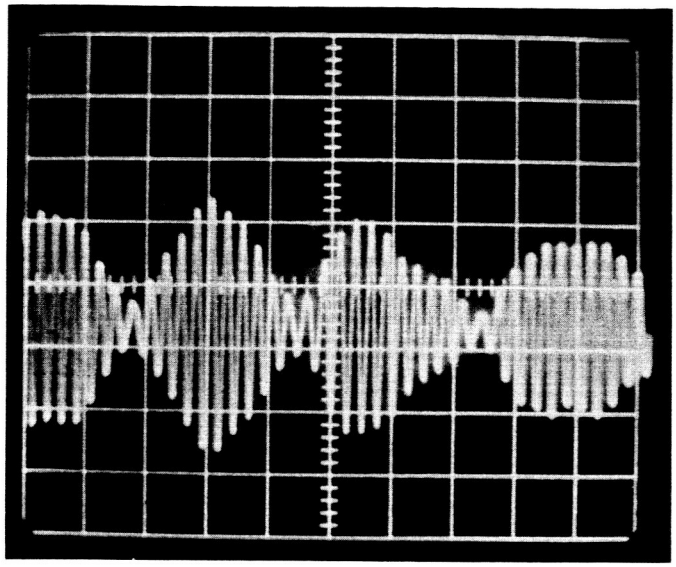

Figure 9. Channel 3 output on *Agena* telemetry signal

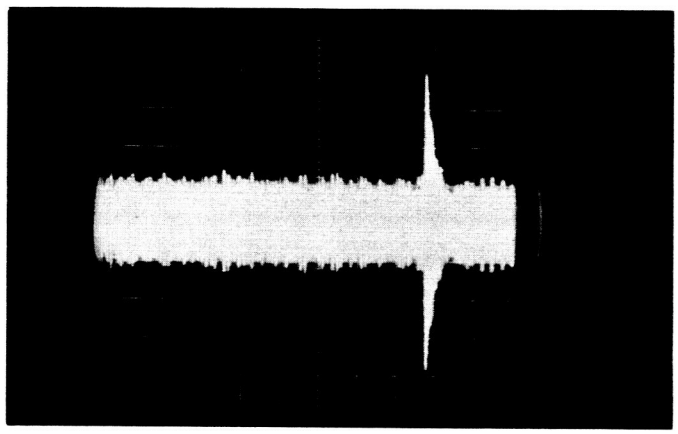

Figure 10. Channel 1 amplitude change

etc., to the spacecraft antennas. Task Assignment Directive No. 007 from the MSFC to LSMD established the feasibility of coupling a portion of this RF energy from the antennas to the exterior of the vehicle, and the system design parameters are noted in JPL Specification

Table 1. Analysis of spacecraft and *Agena* signals

Signal	Spacecraft signal, db	*Agena* signal, db
Channel 1	−12	−12
Channel 2	0	0
Channel 3	−7	−6.5
Channel 4	0	0
800 cps	−33	−13

No. 30331. Thus, two-way communication links are provided through an integrated RF system.

Test results. The large VSWR was found to degrade the performance of the spacecraft RF cavities. The performance of the Lockheed designed and installed RF couplers was not degraded.

The combined systems compatibility test showed degraded performance through the integrated RF system, with especially poor performance (compared to the original LMSD laboratory tests) through the high-gain antenna coupler system. The power output through the omni-antenna to parasitic-antenna system was 5 db less than anticipated; and through the high-gain antenna *Agena* umbilical connector system was 13 db less than anticipated. (Values shown on Figure 6 are the anticipated values.)

Further tests were made at JPL with the *Ranger* RA-1 PTM and previously-supplied mock-ups of the adapter, shroud, and *Agena* forward equipment rack. (These mock-ups are considered to be reasonable approximations of the flight hardware.) The results of these additional tests are as follows: (1) With a signal generator serving as the RF power source, the results essentially duplicated those of the original LMSD laboratory tests. (2) With the *Ranger* RA-1 PTM as the RF source, the results duplicated those obtained during the combined systems compatibility test.

It was established that the large VSWR in the spacecraft coaxial cables, which is the load seen by the RF cavities, was degrading the performance of the RF cavities. The mismatch detuned the cavity with resultant reduction in power output; and detuning the cavity caused a large, detrimental increase in the plate current. The mismatch was alleviated by changing the length of the spacecraft coaxial cables in order that each RF cavity see as little mismatch as possible. It is planned to take whatever coordinated action is necessary both at JPL during the match-mate tests for Vehicles Nos. 6002 through 6005 and at the Cape prior to launch to establish the proper cable lengths for each set of flight hardware.

2. Ranger RA-3 Testing

Basic test plans for the *Ranger* RA-3, -4, and -5 program, and particularly RA-3 PTM, call for a test program quite similar to the one followed by the *Ranger* RA-1 PTM. The main changes are: replacement of the scientific superstructure by the lunar landing capsule and specific testing to accommodate this mission. Notably, the special requirements, time, and facilities necessary for magnetometer checkout and calibrations have been deleted. The remaining subsystem testing of the assembled spacecraft, calibrations, system testing, weight and inertia measurements, sensor alignment, environmental tests, dummy run, and match-mate checking will follow the same basic concepts as used in RA-1 PTM testing.

The capsule assembly will be checked out by Aeronutronics. Electrical and dynamic equivalent mock-ups will be furnished JPL for use in spacecraft testing. Operating and monitoring the capsule electrical equivalent mock-up will be limited to specific test operations on the spacecraft. RF or electrical interference between the spacecraft and capsule will be the main things checked. The limited hard-wire interfaces, mainly for squibs, between the two units will also have their functioning and compatibility verified during system test operations.

The system test complex will be set up in the new spacecraft assembly facility. Originally a 50- by 50-foot test complex was planned to allow utilization of the cable trenches built into the floor, but previous commitments necessitated the reduction to a 40- by 40-foot test area. Test positions have been turned around in the test area to best utilize the existing trenches rather than have the floor covered by protective troughs as was done for *Ranger* RA-1 and -2 testing.

It is planned that the test complex be set up during the week of May 8, thus allowing 2 weeks to check out the test complex and incorporate any last minute changes or additions. May 29 is the presently scheduled date for the initial power turn-on of the spacecraft. A listing of all test procedures and their due dates has been compiled.

The test equipment utilized for nearly all the test positions has been fabricated exclusively for and will be initially used with the RA-3 PTM program. On April 27 the GSE used with RA-2, through its system test phase, was made available for direct use or modification for use with RA-3. Approximately 50% of the *Ranger* RA-2 GSE will be usable directly with RA-3 or can be economically modified. The GSE used with RA-1 and -2 will be made available on August 10 for conversion into a system test complex for RA-4 and -5.

Test operations for RA-3, -4, and -5 will follow much the same plan as PTM, but with a different sequence and without a vibration test of the assembled spacecraft.

3. Spacecraft Integration

a. Weight. As *Ranger* RA-3 components are received for installation on the proof test model (PTM) they are

weighed. These weights are compared with their estimated weights (which are listed in the Design Parameter Functional Specification and used as weight allotments) to get a practical look at the final weight of the spacecraft. Some weight saving techniques were introduced too late to be incorporated into the PTM. In such cases, the item is weighed and an estimate is then made of the flight item's weight. In the main, the *weighed* weights have been comparable with, or lower than, the weight estimates.

b. Power. Total power requirements for *Rangers* RA-3, -4, and -5 have been firmed and allocations for battery and solar panel are complete. The 5 watts originally reserved for thermal control (heaters) have been eliminated, in that no heaters will be employed. Sufficient contingency is contained in the battery for meteoric perturbation (which would require re-acquisition of the sun for solar panel use) and for delayed sun acquisition after a normal maneuver.

c. Design status. The basic *Ranger* design is firm and last minute changes have been few. This is (for the most part) attributed to the fact that the *Ranger* RA-3, -4, and -5 bus design is in most respects identical to the *Ranger* RA-1 and -2. However, some changes have been required. A lens cover for the vidicon camera will be employed and actuated (opened) by pyrotechnics approximately 5 minutes before the vidicon is used. This cover is designed to protect the vidicon from micrometeorite and direct solar radiation during spacecraft maneuvers, and also reduces heat leakage from the vidicon.

An intensive investigation has been underway to determine a method of telemetering lunar reflectivity data from the lunar capsule radio altimeter (13.3 kmc) without jeopardizing test and flight scheduling and weight. This data is of value in determining radio altimeter design parameters for future lunar soft landers. A method has been uncovered whereby commutation between the gamma-ray radiation experiment and the radio altimeter may be accomplished within the science circuitry and still meet the required restraints. Commutation would only be required for the last minute before lunar impact in that this is the sole period of operation for the radio altimeter.

d. Proof test model. The spaceframe selected for the PTM has been modified to the *Ranger* RA-3 configuration and completely thermally controlled (i.e., gold plating and paint); the component assembly is now underway on this spaceframe.

e. Interface requirements. The final interface requirements for the *Ranger* RA-3–*Agena* B have been firmed. The major difference in interface between *Rangers* RA-1 and -3 is the change in design and location of the omni-antenna. The omni-antenna to be used on *Rangers* RA-3, -4, and -5 is conical in shape and will be mounted on the forward end of the lunar capsule. In effect, this moves the antenna aft from the RA-1 location by approximately 41 inches. The same design of omni-antenna coupler will be used by merely relocating it within the shroud by the appropriate amount.

B. Telecommunications

Antennas and RF Components

Past work on development of the antennas and radio frequency components for *Ranger* spacecraft has been reported in previous issues of this summary. Activity in the present reporting period has been limited to investigation of temperature problems in the coaxial rotary joint used in the feed line to the high-gain antennas. In order to determine the effect of high temperatures on the driving torque requirements of the rotary joint, tests were made at 200°F. During the course of these tests, the drive torque exceeded 15 in.-oz, well above the room temperature requirement of about 2 in.-oz. Internal examination showed one of the ceramic spacers to be broken, with one piece of the ceramic completely out of place.

Examination of the breakage planes in the ceramic led to the conclusion that failure was caused by a localized stress concentration as the beryllium copper conductor expanded within the ceramic. This stress concentration was probably brought about by improper distribution of the adhesive between the ceramic and the conductor.

Further evaluation of expansion breakage of these spacers has been conducted. Five dummy conductors with a total of nine ceramic spacers cemented in place were baked at temperatures ranging from 125 to 400°F in 25°F increments. Pieces were baked for 30 minutes at each temperature. No total separation failures occurred in this test. Each ceramic failure consisted of only single hairline cracks even at 400°F. Results of the tests are shown in Figure 11.

It is believed that, because of the type of bearing loads carried by these spacers, a hairline crack failure would not impair the reliability of the rotary joint. To insure the soundness of this hypothesis, shake tests are being scheduled for the cracked ceramic spacers. If no further failure occurs, it can be assumed that, with proper care in cementing the ceramics, elevated temperatures offer no threat to rotary joint reliability.

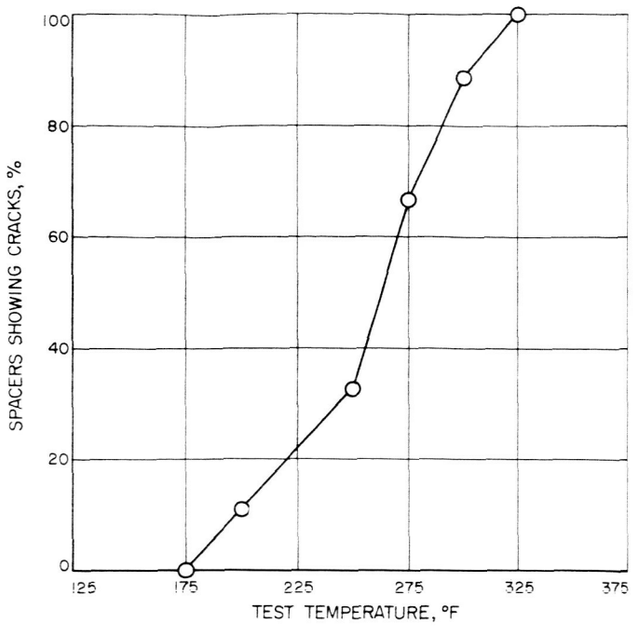

Figure 11. Ceramic spacers temperature test

C. Electrical Power

1. Rangers *RA-1 and 2*

The *Ranger* RA-1 power system (*SPS 37-6*) derives its power from two solar panels with a total area of 20 ft^2 and a primary battery which provides power during those intervals when the solar panels are not illuminated. The raw dc power from the solar panels and battery is fed to a booster regulator which produces a 1% regulated dc voltage to feed several converters and inverters which, in turn, supply individual users.

a. Batteries. The main battery, which will supply the launch and backup power for the spacecraft, has undergone several changes from the original Eagle-Picher (MAP 4059) battery. The present battery (Fig 12) now consists of 16 Eagle-Picher silver-zinc reinforced primary cells in a JPL-designed magnesium casing. The purpose of this new egg-crate design case is two-fold: to increase the structural support of the 16 cells in order to meet the environmental requirements, and to facilitate the dissipation and distribution of heat generated within the battery in order to prevent the occurrence of a thermal run-away condition. The reduction in the number of cells from 17 to 16 was the result of power systems tests which indicated that a 16-cell battery would have longer flight life and greater backup capacity because there would be less power sharing with the solar panels. The battery is now operating in a voltage range between 25.6 and 29.5 volts. The new batteries have undergone flight acceptance and type approval tests and have experienced no failures either from shock, vibration, or thermal run-aways. Individual cells have been subjected to test to destruction experiments and found to exceed vibrational environmental specifications by a factor of 50%.

Two studies into the nature of the thermal run-away of the Eagle-Picher (MAP 4059) batteries have been performed. The initial study was directed toward the determination of the relative magnitudes of heat generation and of heat rejection under steady state conditions. According to this analysis, the capacity for heat rejection appears to be ten times greater than the capacity for heat generation and, therefore, the battery should not experience a thermal run-away.

The second study consisted of determining for this particular battery and critical temperature the maximum allowable rate of electrical energy extraction without precipitating a thermal run-away. The concern of this study was with the non-steady state heat transfer from a body which contains heat sources. The results of this study are presented in Table 2 which lists the maximum localized battery temperature as a function of current at various ambient temperatures. The conclusion of this study was that the theoretical increase in temperature is not severe unless the current drain is very large. It has also been found that the poor thermal conductivity of the plastic case is the one significant factor that makes it difficult to dissipate the heat generated within the battery.

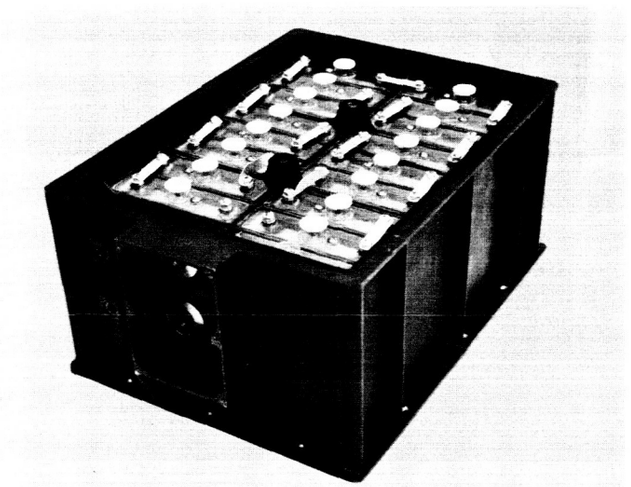

Figure 12. *Ranger* RA-1 and -2 battery

Table 2. Battery hot spot temperature

Current, amp	$T_s = 32°F$ -	$T_s = 70°F$	$T_s = 110°F$
	T_o, °F	T_o, °F	T_o, °F
2	32.0	70.0	110.0
5	32.2	70.2	110.2
10	32.8	70.8	110.8
50	49.9	87.9	127.9
100	78.1	116.1	156.1
150	99.5	137.5	177.5
200	110.5	148.5	188.4
∞	122.0	160.0	200.0

Note: Battery hot spot temperature, T_o; surrounding temperature, T_s.

b. Electrical converters. All electrical converters have been delivered to the spacecraft assembly building and several sets have been utilized in the various testing areas. Two sets of converters have been sent back for an added vacuum–temperature flight acceptance test which is now in progress and due to be completed before June 1, 1961.

Testing. The PTM spacecraft has completed low-frequency vibration testing, mating, and interface testing with the *Agena* at Sunnyvale, and various special tests without failure or malfunction of the power conversion system. Prior to the spacecraft's shipment to Sunnyvale, the power system had been modified to eliminate oscillations which had been observed at various times during the spacecraft system testing. No oscillations have been observed since the PTM hardware was modified. At the conclusion of the special tests the spacecraft had been operated approximately 660 hours.

The RA-1 spacecraft has completed flight acceptance level vibration, vacuum–temperature, and magnetometer tests. It also has completed several system tests and a second complete vacuum–temperature test. The power system has had two malfunctions during the 525 hours of operation. The first of the malfunctions was a power sync subassembly diode failure which occurred during spacecraft vacuum–temperature testing. This diode was cracked; the failure was traced to the use of an improper Conformal coating technique. The second of the malfunctions encountered was an out-of-band telemetry signal from the attitude control converter. The signal was in tolerance but the tolerance was not compatible with the telemetry bands. The signal was adjusted to meet the telemetry limits requirements.

The RA-2 spacecraft has completed systems testing and is currently undergoing magnetometer tests. It has been operated approximately 100 hours. There have been two malfunctions in the power system. The first of the malfunctions was a transistor failure in the telemetry circuitry of the power switch-logic subassembly. The second was caused by a cover mounting screw which was longer than clearances allowed. The screw intermittently touched a terminal and caused the communications converter to go into its overload mode of operation. Both of the problems were found during preliminary testing so that the subassemblies were repaired prior to the systems and magnetometer tests.

System modifications and failures. Because of the improper coating techniques involving a large number of diodes, and the functional position of the power sync subassembly in the power system, all power sync diodes were replaced. During the replacement of the diodes it was found that some of the Cerafil capacitors soldered to the same terminals as the diodes were affected by the soldering heat and later failed. The Conformal coating prevented proper heat sinking of the capacitors during rework. This resulted in the replacement of many Cerafil capacitors.

The power sync subassembly was modified to provide a separate synchronizing signal to the rate gyro inverter. This modification was implemented to stop the power system from oscillating. These oscillations were intermittent and had been observed only a few times during the PTM and RA-1 spacecraft operation.

Life testing. The life test effort to date consists of one booster regulator which was designed and manufactured by ITT. This type of booster regulator is not scheduled for flight, but it is representative of ITT manufacturing techniques. It has now operated for over 2480 hours without a malfunction.

2. Rangers *RA-3, -4, and -5*

The *Ranger* RA-3, -4, and -5 power system with all revisions as of April 24, 1961 is shown in Figure 13. The squib firing chassis and the GSE battery test connector are included in this latest block diagram. Other revisions and additions were made for nomenclature clarification.

a. Batteries. The delivery of the *Ranger* RA-3, -4, and -5 batteries has started on schedule with the arrival of the prototype. Figure 14 shows a spacecraft case with this Electric Storage Battery Company battery potted in place. All type approval, flight, and spare batteries will be similar in appearance to the prototype. Reduction in the battery weight from 31 to 25 pounds has been accomplished without loss of electrical capacity or change in voltage range by using the spacecraft case as the battery container. This is a secondary battery (synonymous with

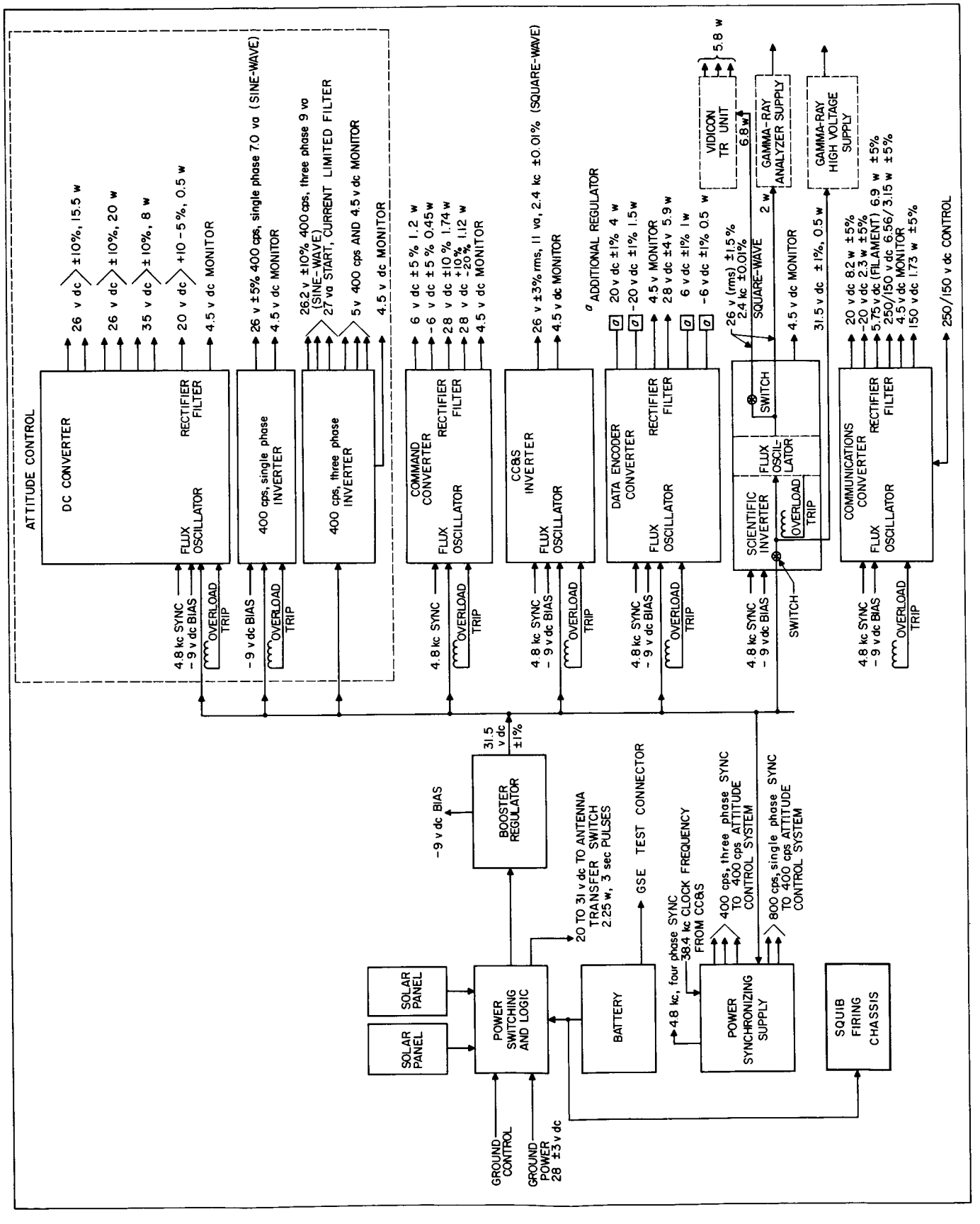

Figure 13. *Ranger* RA-3, -4, and -5 power system

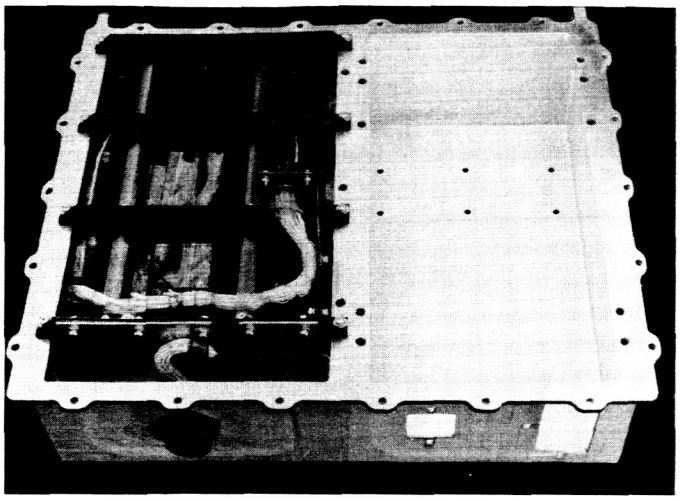

Figure 14. Ranger RA-3, -4, and -5 battery

rechargeable battery), and it is delivered to JPL in a completely discharged state. A battery charger has been purchased from the Electro Development Corporation of Seattle, Washington. The charger, Model No. 2-271, is a constant current unit with an output current regulation from 0.1 to 10 amperes. This charger is unique in the fact that it has electronic sensing ($\pm 0.5\%$) for the charge voltage as compared to a conventional charger's meter relay type control ($\pm 2\%$). This $\pm 0.5\%$ voltage control is required to prevent excessive gassing at the end of the battery charge cycle which could rupture the sealed battery.

b. Electrical converters. Changes in the RA-3 communication equipment have required an increase in the filament voltage. Therefore, the 5-volt dc filament voltage output from the communication converter has been increased to 5.75 volts dc. This change will become effective with the first set of flight equipment, Serial 003. The lower voltage will be used for the Serial 001 and 002 converters, PTM and TA sets, to be compatible with the communications units that are scheduled for use with these sets.

Hardware delivery. Delivery of the first set of RA-3 power equipment, Serial 001, was completed on April 12, 1961. The second complete set, Serial 002, was delivered as of April 24, 1961. Of the remaining sets, deliveries have been made on two power switch and logic modules, Serials 003 and 004, and on three more booster regulators. As explained in *SPS 37-8*, these booster regulators will not be used as flight equipment because the revised power specifications exceeded the capabilities of the booster design. These booster regulator modules will be used during the early PTM and system checkout effort until the redesigned booster flight equipment is received. Delivery of the complete Serial 003 set of power equipment is scheduled for May 12.

Booster regulator. The revised booster regulator, capable of operating at high efficiency over an input range of 18 to 31 volts dc, is being designed by a local vendor. Their design effort has advanced to the breadboard temperature testing phase. Efficiency figures have been lower than anticipated, but the vendor is confident that this will be improved. Package assembly design of the new booster may require an increase in the package width and weight over that of the earlier design. Present estimates are for a package width of $2\frac{7}{16}$ inches and a weight of 5.5 pounds. The first prototypes of the new booster design are scheduled for delivery on June 15. After a short electrical evaluation, these units will be substituted into the power systems in place of units of earlier design.

Subsystem tests. The first set of RA-3 power converter modules, Serial 001, have been undergoing electrical testing. All units have been given their flight acceptance tests and engineering evaluation by the manufacturing vendors before delivery. These vendor tests are conducted on the individual power modules. The first JPL tests are designed to confirm the vendor's results by repeating some of the tests at room temperature. Once it is confirmed that each element of a power set is operating, all modules are connected and operated as a complete power system using resistive loads. These tests should reveal any interactions between units that might present problems.

After the power system evaluation is completed, additional tests can be made using actual power user loads. Many of these mating tests have had to be eliminated for the Serial 001 equipment because of the extremely short time between the receipt of units from the vendors and the scheduled delivery of the PTM system on May 1. Most of these tests will be included during the checkout of the second set before it is subjected to the type approval tests.

In general, the test results on the Serial 001 power equipment have shown fairly good conformance to the JPL design specifications. Several minor items have been uncovered that resulted from a difference of interpretation by the vendor of the design details, but no serious problems are anticipated.

One failure was found during the preliminary test phase. Power synchronizing supply, Serial 001, which furnishes sync signals to all converters and inverters, lost the sync signal for the 400-cps, three phase inverter. A component failure was suspected as no output could be detected on the subject sync lines. This unit, Serial 001,

has been returned to the vendor for troubleshooting and repair. The sync supply, Serial 002, was installed in the power system so that testing could continue. Operation has been satisfactory with this combination.

The first set of power modules will be delivered to the spacecraft assembly building on May 1, as per the PTM schedule. The set will include sync supply, Serial 002, the 23- to 31-volt dc booster regulator, and Serial 001 modules of all other power units.

Flight acceptance testing. One of the power equipment manufacturers is conducting much of the flight acceptance testing in their own testing laboratory. The remaining tests for this vendor and all tests for the other vendors are contracted out to a commercial testing laboratory. Members of the vendor's engineering staff are always present during testing and are responsible for conducting all electrical testing on the power modules. The test laboratory staff operate their own test equipment as required to obtain the proper environmental conditions.

During a recent visit to one of these testing laboratories, testing of Serial 003 power modules was in progress. Two modules were mounted on a special heat sink inside a vacuum chamber. The heat sink temperature was controlled by external equipment which circulated a liquid coolant. The vacuum and temperature equipment was monitored and operated by a testing laboratory technician. A technician from the manufacturing vendor handled all power operation and electrical testing of the module under test. All equipment used for this electrical testing, including power supplies, meters, scope, and necessary switching, was furnished by the vendor. Test data was recorded on approved data sheets as specified by JPL.

These tests are witnessed periodically to confirm confidence in the equipment and procedures used by the test laboratory and by the vendors. Each test presents its own unique problems for proper instrumentation and control. A proper environmental evaluation depends on both an adequate test procedure and on the careful work of competent test personnel. The details observed on this trip have continued our confidence in the test program.

D. Scientific Instruments

1. Seismograph

Under a NASA contract, the California Institute of Technology (Caltech), Seismological Laboratory, has been assigned the task of designing and fabricating a single-axis lunar seismometer capable of withstanding a lunar impact for *Ranger* flights RA-3, -4, and -5. Caltech, in conjunction with the Lamont Geophysical Observatory of Columbia University, will reduce, analyze, and interpret the subsequent seismograph data. JPL has been assigned the responsibility of technically monitoring this contract and ensuring the proper integration of the seismometer into the lunar capsule, which will be supplied (under a JPL subcontract) by Aeronutronic, a Division of Ford Motor Company.

Development of the seismometer began with preliminary design of several different types of instruments and high-g impact testing of electrical and prototype mechanical components. Results of these studies led to the design of a suspended-magnet type seismometer, which was selected because of its inherent stability, wide operating range, and ruggedness. Prototypes of this instrument have been constructed and delivered (on schedule) to JPL. Environmental testing of a proof test model (PTM) is presently being carried out.

The basic instrument consists of a coil, a spring suspended magnet, a centering system, and an internal calibration device. The relationship of these components is shown in Figures 15, 16, and 17. Figure 18 is an electrical schematic of the instrument. The seismic mass consists of a permanent magnet suspended from the body of the instrument by a helical spring and two cantilever spring rings. The spring ring acts to maintain concentricity of the seismic mass within the instrument body and allow the seismometer to operate at any inclination of its longitudinal axis from 0 to 90 degrees. Movement of the coil, which is rigidly attached to the instrument body relative to the seismic mass, generates the output of the transducer. Several additional permanent magnets are embedded in the body so as to repel the seismic mass, thus extending the natural period of the instrument from approximately 0.4 second to a range of 0.9 to 1.2 seconds.

a. Description. The seismometer is 5.250 inches long and 4.375 inches in diameter. It weighs 7.25 pounds without caging fluid and 8.13 pounds when filled with caging fluid. While in the lunar capsule, the seismometer will be packaged in a rigid breech so that it is supported everywhere except at the terminals and drain vents. To damp the rapid movement of the seismic mass upon lunar impact, the instrument will be vacuum filled with a protective fluid. This fluid (N-Heptane) was chosen due to its relatively high vapor pressure, viscosity, density, and its compatibility with the materials of the instrument. The seismometer will be set into operation shortly after impact following venting of the caging fluid.

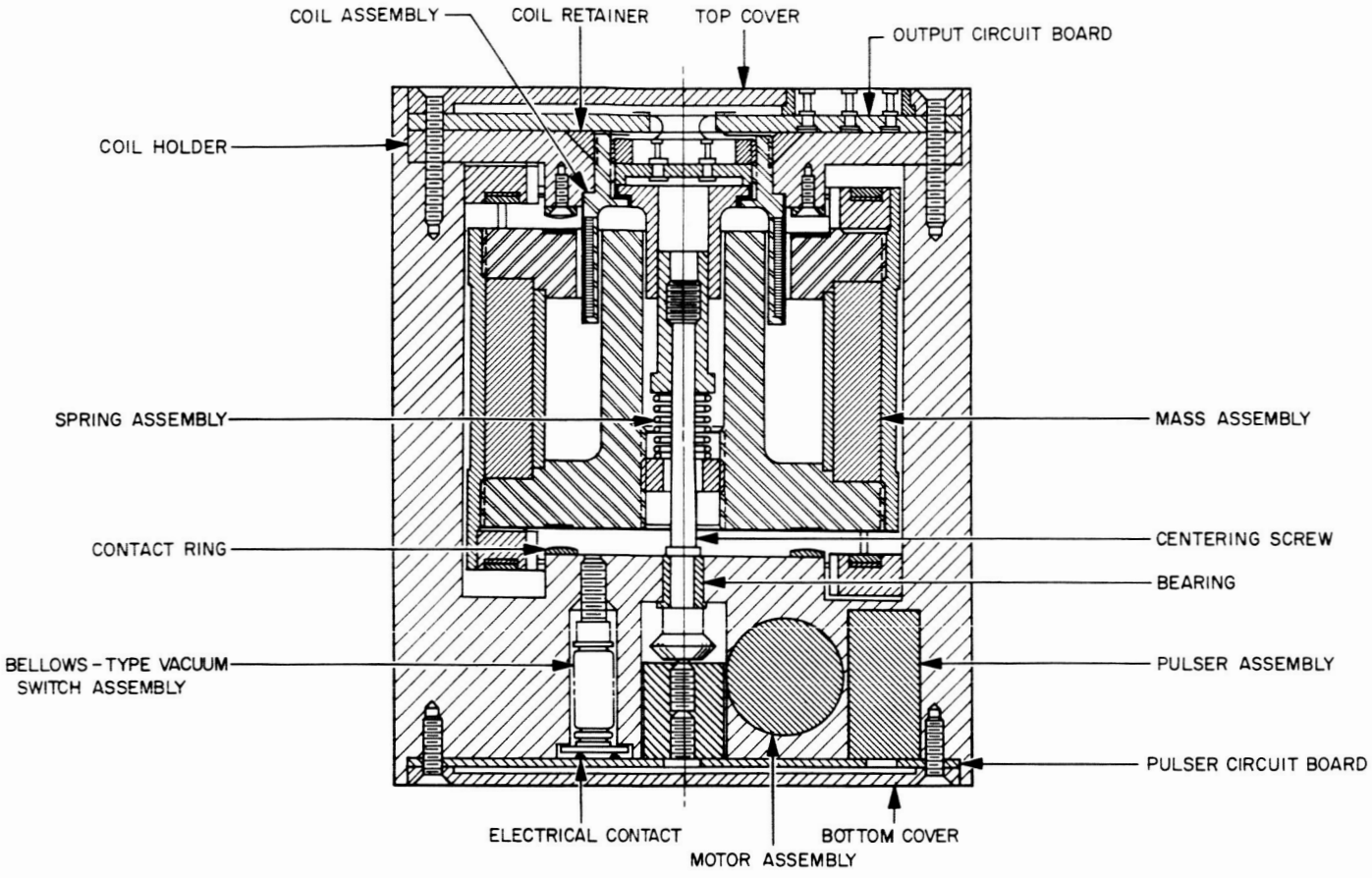

Figure 15. Suspended magnet seismometer, internal view

The internal power required by the calibrating device or pulser circuit will be provided by six batteries, arranged to give an output of +1.2 volts and −1.2 volts—at 0.75 milliwatts of power, continuously for the lifetime of the lunar capsule (estimated at 77 days). The centering motor for the seismic mass requires 6 volts which is exter-

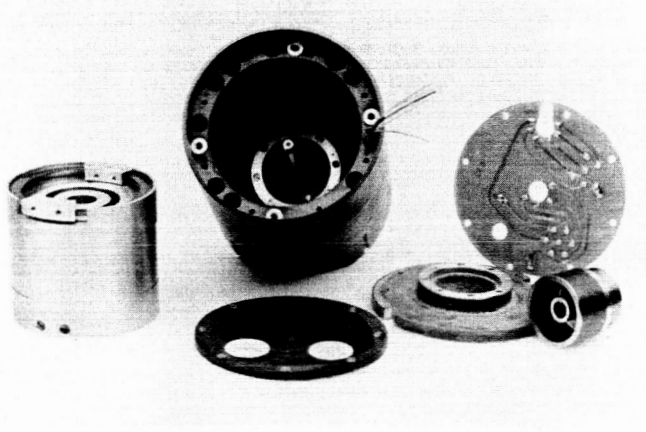

Figure 16. Suspended magnet seismometer assembly

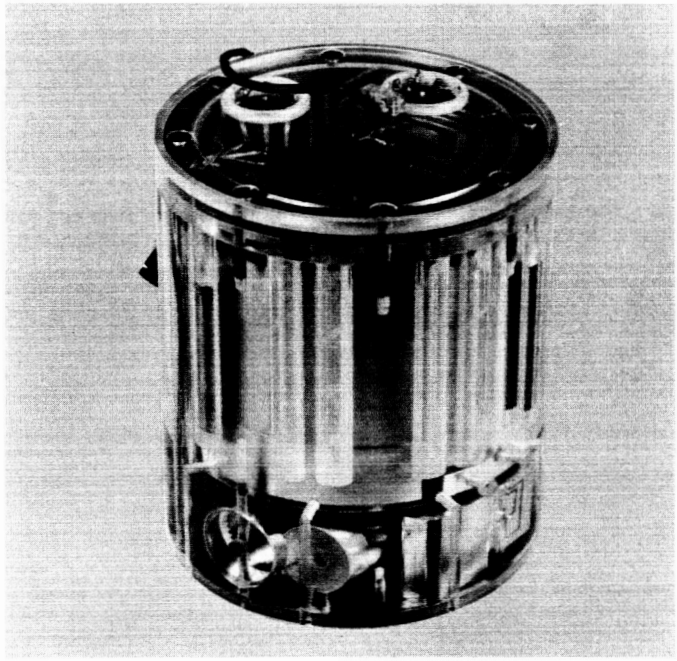

Figure 17. Plastic model of seismometer

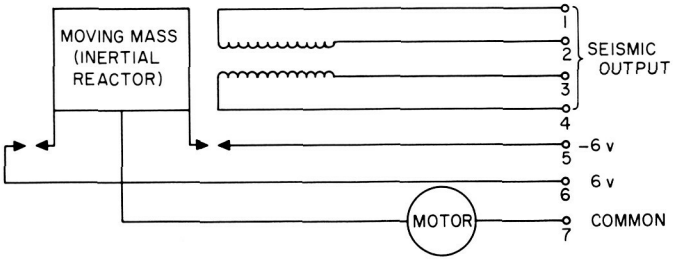

Figure 18. Suspended magnet seismometer schematic

nally supplied by batteries in the lunar capsule. The seismic transducer itself is self generating.

Movement of the seismic mass is limited to 0.25 inch by stops within the instrument. The centering system is designed to keep the seismic mass from resting on these stops. The motor is activated whenever the seismic mass contacts the rings on the stops. Motor activation causes rotation of the center shaft through the gear system, thus shifting the frame and helical spring attachment point. This shift causes an increase or decrease of the force exerted by the helical spring on the seismic mass, thereby lifting it off the contact ring and breaking the circuit. Over-run of the motor is sufficient to bring the mass to a position which is well off the stop.

Calibration of the voltage output of the transducer and monitoring of its operation will be provided by the pulser throughout the lifetime of the experiment. The pulser consists of a solid-state multivibrator and divider which periodically energizes a coil magnet. The magnet displaces the seismic mass and thus generates a standard output signal. A schematic of this circuit is shown in Figure 19. Figure 20 shows the technique used in packaging the circuit. The package shown and its batteries will be potted in the body of the instrument. The pulser will be activated shortly after impact and venting of the caging fluid by an internal bellows-type pressure switch.

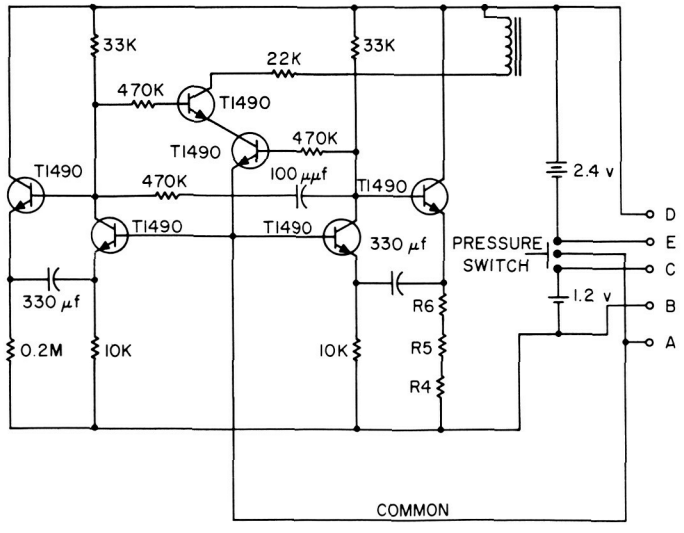

Figure 19. Seismometer pulser circuit

The output of the instrument at 1 cps is 0.75 microvolt per millimicron of ground amplitude (peak-to-peak deflection). The output characteristics provide a 6 db/octave rise for periods short compared to the natural period (0.9 to 1.2 sec) of the instrument and 18 db/octave falloff for periods long compared to the natural period.

b. Environmental tests. The seismometer has been designed to withstand all environmental limits prescribed for equipment inside the survival capsule. Although design–proof tests have not been completed, preliminary drop tests of a prototype unit indicate that it is capable of surviving an impact of approximately 5000 *g* along its longitudinal axis. During the testing of the seismometer it will be housed in a fixture which will simulate its packaging in the survival sphere. The seismic mass will be caged with N-Heptane. Provisions have been made to bring out signal leads to permit an accurate determination of the instrument performance. Following each test the performance record will be compared to a standard record obtained from the seismometer before any of the tests were conducted. A block diagram of the test setup for obtaining the performance records is shown in Figure 21.

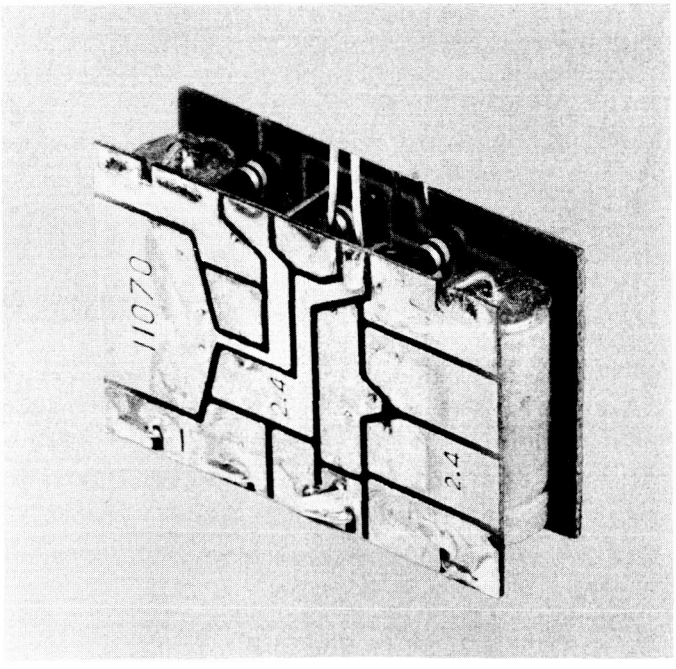

Figure 20. Seismometer pulser

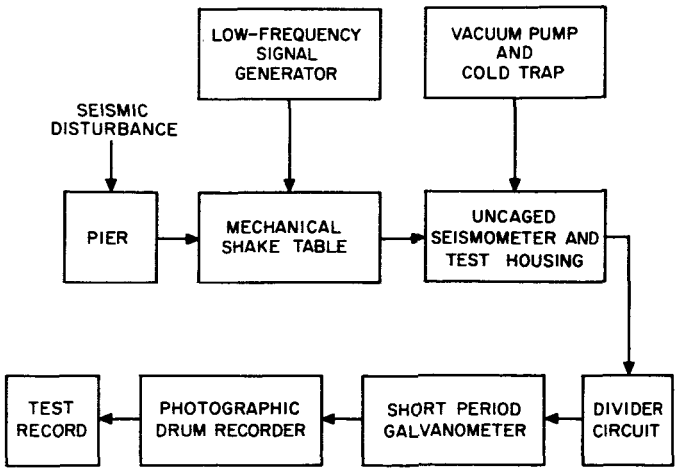

Figure 21. Seismometer performance test setup

c. Sterilization. Construction of the instrument and the techniques by which it will be packaged in the lunar capsule will necessitate the use of both sterilization techniques (thermal and ethylene oxide gas) in order to comply with the NASA lunar impact sterilization policy. The instrument less the batteries and pulser circuit will be heat soaked. Following the heat soak, these components will be added by sterile assembly in a dry box and the complete instrument will be tested for flight approval. Details of the assembly procedure and precautionary measures, which will be followed so as not to recontaminate the inside of the sterile instrument during the flight acceptance tests, are being developed.

d. Data handling. Upon impact on the lunar surface the survival package will be permitted to float into an upright position. After a predetermined time the survival sphere will be punctured permitting the seismometer caging fluid to vent. The reduction of pressure within the seismometer will actuate its pressure switch which will initiate the seismic experiment.

The lunar seismic disturbances will then be detected and converted into electrical analog signals by the seismometer. These electrical signals will then be passed through the seismometer amplifier which will modify its characteristic in a precisely calibrated manner. A simplified block diagram of the capsule's data system is shown in Figure 22. The output of the seismometer amplifier is used to frequency modulate the standard Channel 2 subcarrier ($F_0 = 560$ cps). The subcarrier is then used to phase modulate the main capsule transmitter.

The three DSIF sites (Fig 23) will alternately receive the telemetered data. The subcarrier will be recovered from the main carrier by a phase discriminator and an appropriate subcarrier filter and will then be recorded on

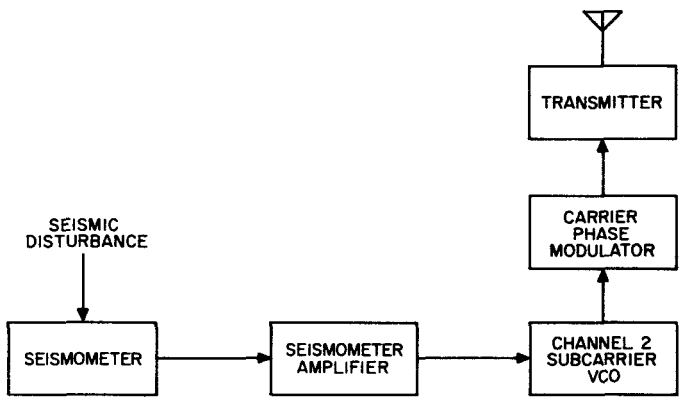

Figure 22. Capsule data system

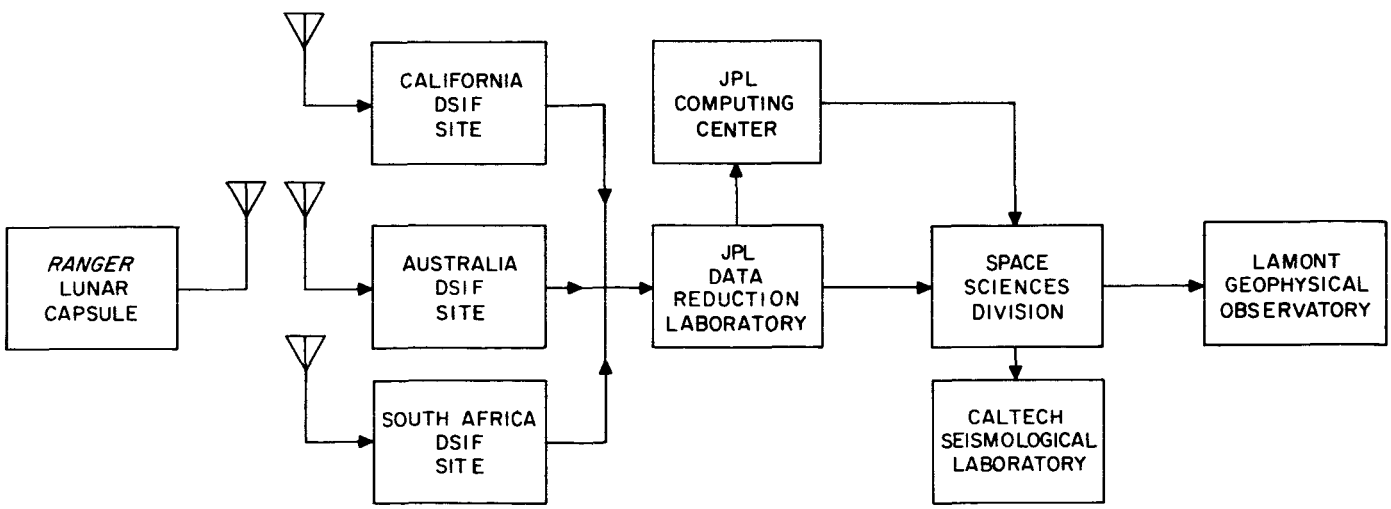

Figure 23. Seismic data flow

magnetic tape along with standard timing signals. The tapes will then be forwarded to the JPL data reduction laboratory as expeditiously as possible.

It is currently planned that the DRL will perform two operations on the data tapes received from DSIF: (1) The analog seismic data will be digitized to facilitate processing on the digital computing. (2) Two sets of magnetic tapes bearing analog seismic signals in subcarrier form and timing signals will be dubbed.

Each experimenter, the Caltech Seismological Laboratory and the Lamont Geophysical Observatory, will receive one set of analog data tapes and the necessary terminal equipment to extract the data. The digitized data will also be made available to the co-experimenters.

To facilitate analysis of the seismic information obtained from the ground adapter the Caltech Seismological Laboratory will filter the signal before it is recorded so that it corresponds to that obtained from familiar seismograph systems. Those which will be simulated are a short period seismometer with a short period galvanometer, a short period seismometer with a long period galvanometer, and a long period seismometer with a long period galvanometer. Specifically, the seismometer period (T_0) and the galvanometer period (T_g) will be as follows: ($T_0 = 1.0$, $T_g = 0.2$; $T_0 = 1.0$, $T_g = 90$; and $T_0 = 30$, $T_g = 90$ seconds). The final data output and timing signal will appear on three separate recorders as indicated in Figure 24. Figure 25 shows a typical earthquake trace from the lunar seismometer. The output was filtered through the Caltech system to simulate the familiar Bennioff short period seismometer (i.e., $t_0 = 1.0$, $t_g = 0.2$).

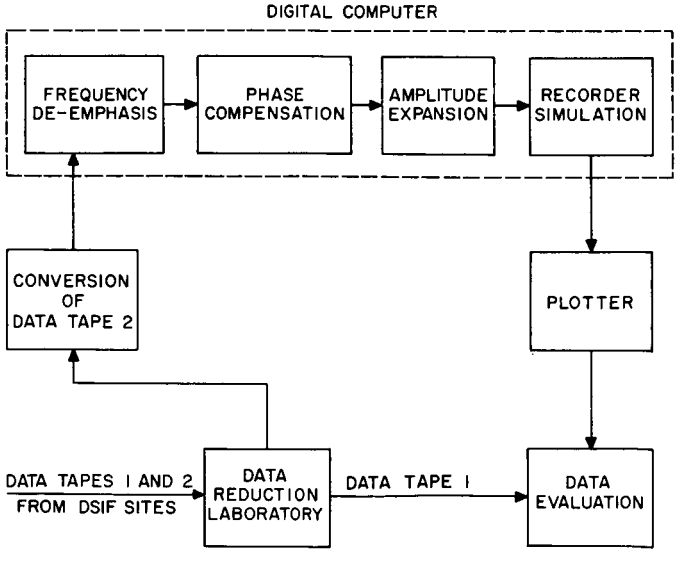

Figure 24. Data handling system

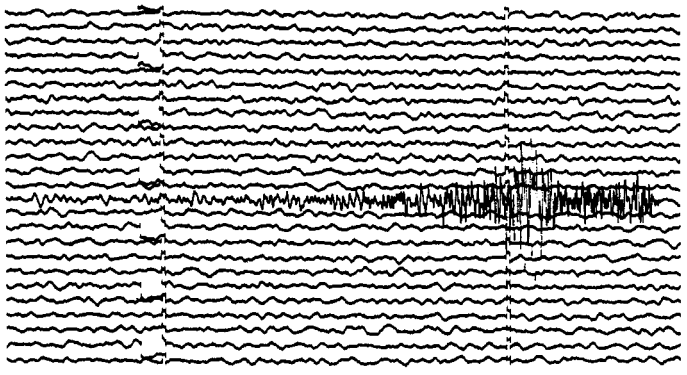

Figure 25. Typical earthquake trace

The system through which Lamont will process the data from the ground adapter has not been specified as yet.

e. System tests. Aeronutronic and the Caltech Seismological Laboratory have been conducting joint tests in order to establish adequate performance criteria for the lunar capsule data handling system and to verify the compatibility of the system transfer function with the objectives of the lunar experiment. The tests are being conducted using actual earth seismic disturbances and prototype circuits of the Aeronutronic seismometer amplifier and ground adapter.

Due to a number of difficulties, one being the random occurrence of characteristics of the seismic waves, only qualitative results have been obtained, thus far. In order to obtain closer control of the experimental conditions and to obtain more useful quantitative results, JPL has proposed and will direct the recording of several earth seismic disturbances on magnetic tape using the system shown in Figure 26. These recordings will then be cataloged and calibrated by reproducing them on the Caltech Seismological Laboratory data handling system. The recorded waves can then be used to establish the minimum acceptable mean square signal-to-noise ratio for the Caltech system. The setup which will be used to accomplish this is shown in Figure 27. Tape recorded waves will also be used to establish the program transfer functions for the capsule seismometer amplifier, the telemetry channel, the ground adapter, and, in general, to verify the adequacy of the communication channel design.

2. Telescope Vidicon Camera

Space Programs Summary 37-7 (p 38) notes: "The mission of the *Atlas–Agena–Ranger* RA-3, -4, and -5 is to direct a scientific payload to the surface of the moon and to take high resolution pictures of the landing area of the capsule." Similarly, Dr. Robert Jastrow, Chairman of the NASA Lunar Explorations Working Group has

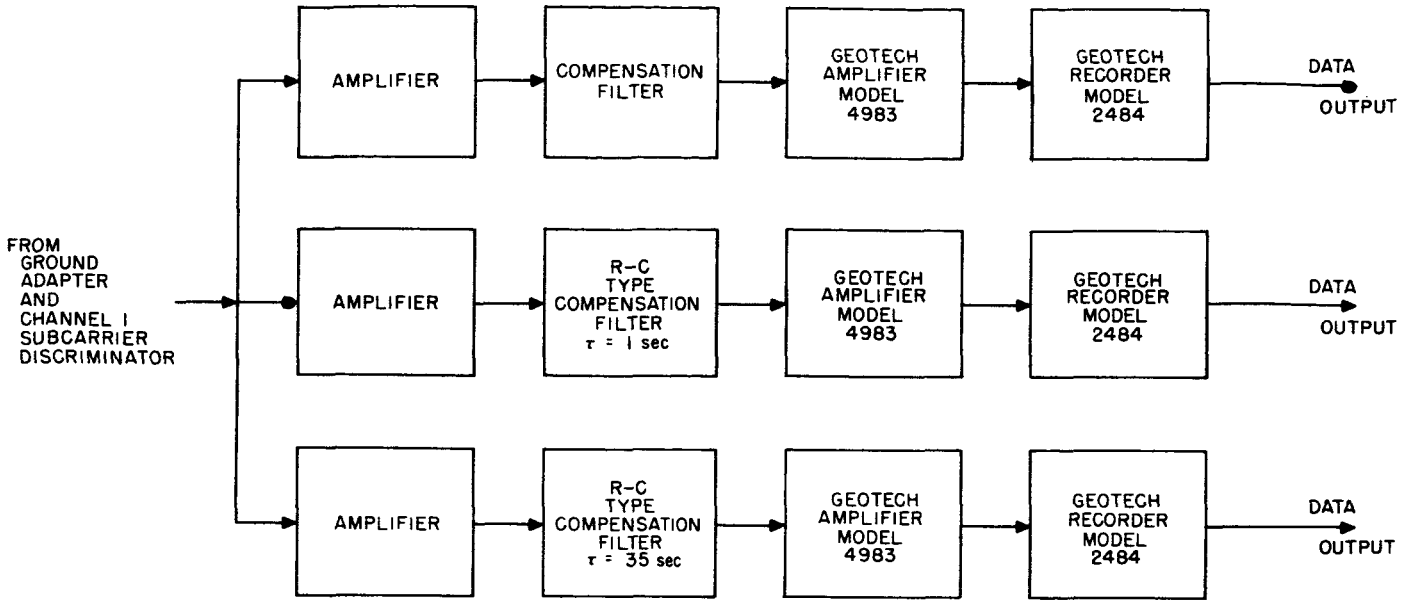

Figure 26. Caltech data recording system

noted: "One of the first objectives of the lunar exploration program will be to obtain views of the surface that are more detailed than those available from telescopes on the earth... The images may be obtained by television or by photography;... both methods will be developed and tried" (Ref 1).

A telescopic television system (Fig 28) has been developed by JPL to go aboard *Rangers* RA-3, -4, and -5 to accomplish this mission in the 30 minutes before impact of the spacecraft. It can be demonstrated that, with a 40-inch equivalent focal length telescope which is perhaps the maximum for the *Ranger* payload, photographs secured with a 200 TV line scan vidicon at 4000 km distance will just about equal the best resolution secured from earth based telescopes. Therefore, there is little purpose in attempting recordings at a greater distance from the moon. The present vidicon telescope system will

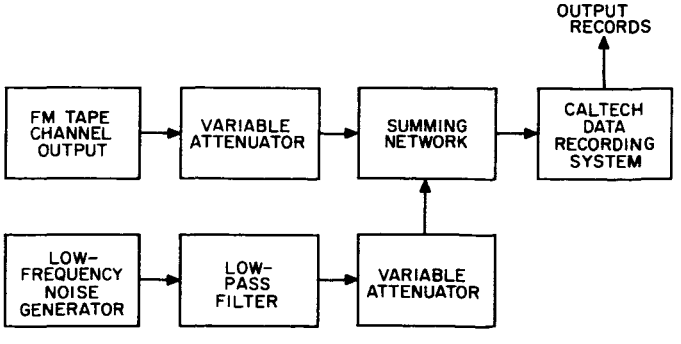

Figure 27. Signal-to-noise test setup

transmit from 4000-km down to 24-km altitude, where the capsule is ejected and earth contact with the high-gain antenna will probably be lost due to subsequent tumbling of the spacecraft. At 24 km, an area 350 meters square on the moon would be recorded with a surface resolution of approximately 2 meters. The spacecraft and vidicon telescope longitudinal axes will be aligned nearly normal to the lunar surface during the recording period. The lunar phase-angle, as viewed from the spacecraft, may vary from approximately 20 to 70 degrees depending upon the date and azimuth of launch within the proposed launch windows. This will result in a sufficiently oblique sun angle to yield shadows on the lunar surface, thus providing greater surface detail rendition because of the increase of contrast. It is anticipated that the improvement in lunar surface resolution will be from 100× to 1000× that secured from earth based telescopes under the best conditions, depending upon a number of instrumental and environmental factors which will be encountered by the vidicon telescope system.

The television recordings of the lunar surface from *Rangers* RA-3, -4, and -5 may be put to a number of uses. Primarily, the images will indicate the type of lunar terrain in which the seismometer capsule will land, and should assist in the proper evaluation of the data. The vidicon images will also permit determination of the coarse surface structure, small scale geological land forms and features, altitudes and slopes of lunar surface features, and the general environmental condition close to the moon. At the same time, the vidicon photographs will

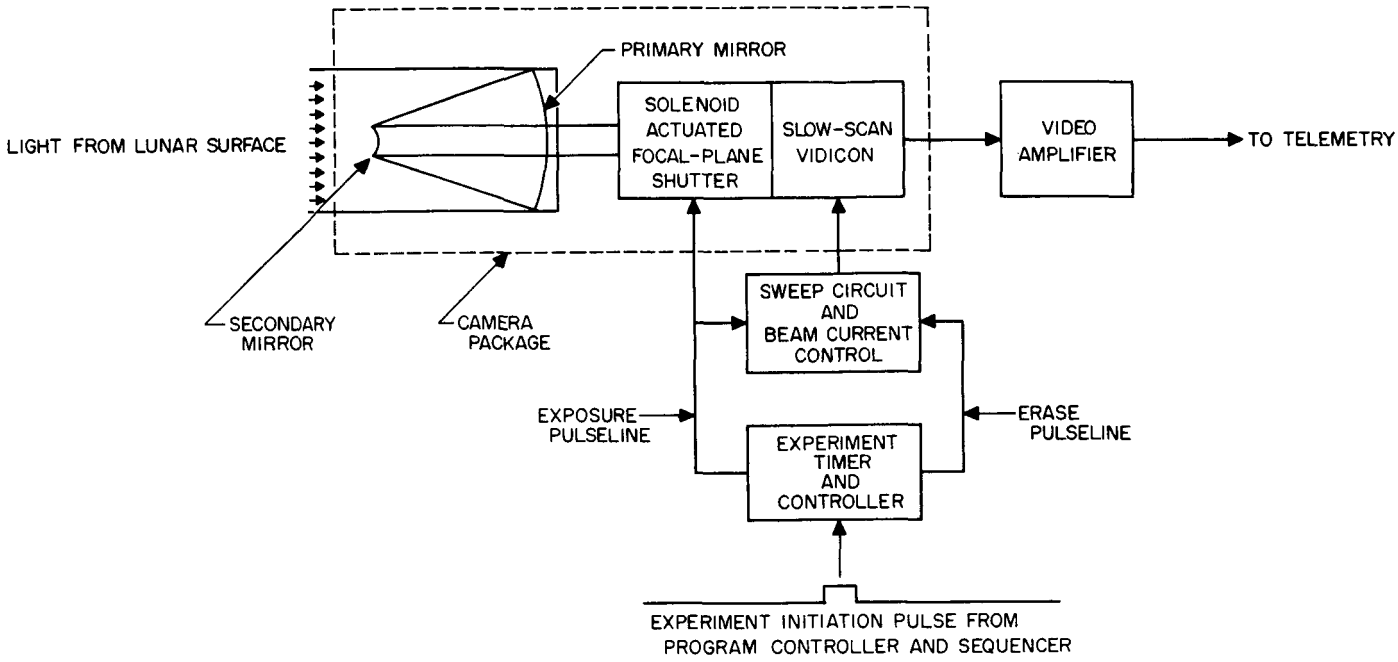

Figure 28. Vidicon system

be a first approach to the selection of possible landing sites for future instrumented and manned lunar probes.

a. Vidicon system. The television system for *Rangers* RA-3, -4, and -5 has been tailored specifically for the experiment and thus departs in several areas from typical designs. A vidicon sensor was chosen for imaging because of its simplicity and ease of operation. Quite unlike other vidicon camera systems, an all-electrostatic deflection and focus vidicon is employed which combines a special *sticky* target with rapid erase capability. In operation an image is shuttered onto the faceplate for 20 milliseconds and the slowly decaying image is subsequently scanned at a rate which yields one complete frame in 10 seconds. Two hundred scanning lines are employed per frame in order to achieve the desired resolution. The video bandwidth out of such a system for equal vertical and horizontal resolution is of the order of 2000 cycles.

Since each frame is different from the rest, no averaging technique for a large number of frames may be employed for background shading or dc restoration; thus, the lowest frequency in the video signal must be considered to approach dc. In order to accommodate this, the vidicon beam current is modulated by a high frequency which chops the target current and creates an amplitude modulated signal. After sufficient amplification, the demodulated video is mixed with blanking pulses to form a composite video signal for presentation to telemetry. The line-deflection circuit is triggered from a 20-cps generator clocked, in turn, from the spacecraft 400 cps. Since this 400-cps clock is available in the ground receiver, line synchronization is guaranteed even in the presence of rather severe noise; or, in turn, the 400-cps clock may be retrieved from the line sync pulses should the 400-cps signal be lost. The commands for shutter and erase are obtained from the CC&S in the form of 1-millisecond switch closures. The shutter command terminates erase, triggers the shutter solenoid drives and, following a fractional second delay, causes initiation of the frame sweep. The erase command terminates the frame sweep and initiates the erase mode which consists of illumination of six filamentary lamps mounted on the periphery of the vidicon target, acceleration of line and frame scan rates over the surface of the target, and increased beam current. Although this process normally requires less than 1 second, circuit simplicity is maintained by continuing erasure for the full 3 seconds allotted for readout of the gamma-ray data.

b. Vidicon sensor. The proper vidicon sensor was chosen as the result of an extensive evaluation program. All available sensors were investigated by RCA as a preliminary phase of the impact television contract. The specific requirements on the vidicon are:

(1) Adequate sensitivity for low light levels anticipated.

(2) Sufficient dynamic range to allow perception of detail for lower than normal illumination as well as possible strong highlight detail.

(3) Capability of survival of the thermal requirements of bulk sterilization.

(4) Minimum weight and power requirements.

(5) Adequate storage time of a shuttered image combined with ease of erasure prior to shuttering of a new optical image.

These requirements of the sensor were not mutually compatible in light of present commercial practice. Thus, it was evident that a completely new sensor would have to be developed which combines the best features of existing sensors and yet meets the rigors of spacecraft environment. Since this is an evolutionary development which normally requires extensive time, it is a credit to the participating organizations that a task of this nature was actually accomplished within the demands of the *Ranger* schedule. The resultant sensor combines all the required features.

The target material chosen for this vidicon is an antimony sulfide oxysulfide surface which is a proprietary development of RCA and combines the necessary retention of the image for slow scan readout together with rapid erase capability. The latent image may be scanned slowly off the target with less than 10% reduction in highlight detail for periods in excess of 10 seconds. Sensitivity of the surface is maintained at light levels as low as 0.01 ft-candle-sec following the 24-hour soak at 125°C for sterilization; the useful dynamic range of some units extends from 0.001 to 0.1 ft-candle-sec with an opening of f/6 and 20-millisecond exposure. The image may be erased in 700 milliseconds.

The electron gun structure and deflection system is a ruggedized version of the 1-inch diameter electrostatic unit manufactured by General Electrodynamics Corporation (GEC). Electrostatic focus is accomplished by a saddle field lens arrangement and electrostatic deflection is accomplished through the use of special deflection plate configuration designed by Schlesinger called a Deflectron. The conventional crossed pair deflection plates cause the electron beam to be deflected sequentially; that is, in passing between the first set of plates, it is deflected in one plane and, then, when reaching the second set of plates, it is deflected in the other plane. The Deflectron causes the beam to be deflected both horizontally and vertically simultaneously as in magnetic deflection. This common center of deflection reduces the undesirable effects of fringe fields, defocusing, and other distortion found in conventional plate scanning.

Physically, the Deflectron is a tube of insulating material, the inside of which contains the printed deflection plate pattern. This yields an exceptionally rugged structure capable of surviving present spacecraft environment. In addition, the use of an all-electrostatic structure removes the considerable weight and power penalty of electromagnetic deflection yokes, while resolution comparable to electromagnetic systems is maintained through the use of post-deflection focusing.

The faceplate complete with target material is supplied by RCA and is bonded by GEC to their gun structure by an indium-glass seal process tailored specifically for this particular vidicon. The electron gun structure has been modified to permit a larger beam diameter. This was done in order to facilitate rapid erasure of the sticky target, since erasure is accomplished by simultaneous application of external light stimulus and rapid-scan of the target in *fire hose* fashion by the electron beam. Dark-current slipping over wide temperature ranges is facilitated by including a deposited mask on the faceplate to obscure a portion of the image. This mask covers a narrow strip along the faceplate which obscures less than 5% of each scan line. Present vidicons have this mask vapor deposited externally; however, experimentation with internal deposition is in process and, if successful, will eliminate the slight amount of optical defocusing presently observed with this mask.

c. Optical telescope. Basically, the telescopic optical system (Fig 29) developed by JPL is a conventional Cassegrain-configuration astronomical telescope employing a primary concave parabolic mirror and a centrally located secondary convex hyperbolic mirror to reflect the lunar image picked up by the primary back to the vidicon photoconductive image surface 0.5 inch in front of the

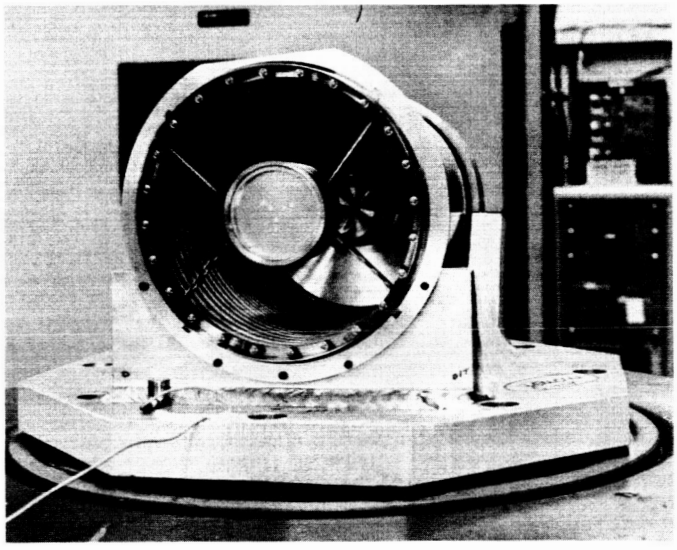

Figure 29. Vidicon telescope

primary mirror. An aperture of 7 inches and equivalent focal length of 40 inches is provided, yielding an equivalent light grasp of f/6.3. An initial optical resolving power of 5 seconds of arc, or 40 optical line pairs/mm over the 1-degree telescope field of view will be secured. This will, of course, be deteriorated by the vidicon scan to approximately 34 seconds of arc or 6 optical line pairs/mm resolution.

The significant deviations from usual astronomical telescope design consists of the use of fuzed quartz for the telescope mirrors, Invar for all temperature sensitive metallic parts and, primarily, the use of an 8-inch diameter fuzed quartz tube as the basic rigid tubular structure separating the primary and secondary mirrors. These features have been emphasized in the design because of the large range of vehicle temperatures anticipated in the cislunar environment. Engineering models of the vidicon telescope employing this JPL design have successfully survived the simulated *Atlas–Agena* takeoff vibration tests without mechanical or optical deterioration.

A mechanical rotating sector shutter operating on inertial principles with solenoid actuation has been included in front of the vidicon face. This provides an exposure time of 20 milliseconds on the photoconductor surface with a uniformly illuminated field. The shutter will prevent blurring of the optical image of the lunar surface, due to motion of the spacecraft during the exposure time, and will also provide a closing of the optical system during the 13-second scan and erase operation of the vidicon electronic system.

The unit for holding the telescope optical elements and the vidicon tube and associated electronics within the telescope structure have been carefully designed to survive the shake, shock, and temperature environments anticipated. An auxiliary capping mechanism is provided to shield the telescope optics and the vidicon surface from the light of the sun during mid-course maneuver, and to provide protection from micrometeorites and a proper temperature balance within the telescope in cislunar space. The telescope structure will be mounted to the spacecraft in such a way as to minimize misalignment of the longitudinal optical-mechanical axes during takeoff and under the temperature environment anticipated.

In the generation of the present optical telescope design, three different optical firms were contacted for detailed design studies. In addition, a fourth, backup design was undertaken by JPL. Three engineering models resulted from these design studies. These were all subjected to optical tests for image quality, resolving power, and position of the image plane with reference to the vidicon face before and after *Ranger* system vibration testing. The only design which satisfied the strict optical-mechanical requirements both before and after shake was the JPL backup telescope. This design is being constructed by a vendor for RA-3, -4, and -5 to meet the mission schedule requirements.

3. Gamma-Ray Spectrometer Experiment

The gamma-ray spectrometer was discussed in *Space Programs Summary 37-3*. The following information is intended to bring that discussion up to date.

The scintillation crystal to be used will be cesium iodide in the shape of a cylinder, 2¾ inches × 2¾ inches and having a weight of 2.7 pounds. A double scintillator or phoswitch system has been chosen for coincidence rejection of charged particles with pilot scintillator B, the material which generates the reject pulses. The phototube will be a 3-inch CBS type, Model CL 1029. The phototube and scintillators, together with an appropriate emitter follower and anti-coincidence circuitry, are to be mounted in a hermetically sealed aluminum container whose total weight is just under 7 pounds. Within the container will be small quantities of Ce^{144} and Hg^{203}. The characteristic low-energy radiations produced by the decay of these isotopes will calibrate the instrument.

The high-voltage supply developed for the experiment can produce a fixed value between 1400 and 1800 volts according to the requirements of the detector. Input-output voltage regulation will be 0.1%. The output voltage is well compensated against temperature drift. The high-voltage supply will sit next to the detector at the end of a 6-foot telescopic boom. Supply and detector will be enclosed in a thin sphere of aluminum designed for optimum temperature control. The weight of the boom and sphere should be under 5 pounds.

The 32-channel pulse height analyzer weighs about 5.2 pounds and requires 1.2 watts of power. In addition to amplifier, converter, and storage, it contains provision for a factor of five change in gain.

The instrument will be turned on 4 hours after liftoff and will operate in 8-minute periods until the terminal maneuver. Readout of information will occupy about 0.5 minute of each period. The two gain levels, which are expected to be 0 to 0.6 mev and 0 to 3 mev, will alternate from period to period.

Two and a half hours after mid-course maneuver is initiated, the boom will be extended.

After terminal maneuver, and starting approximately 4000 km above the moon's surface, the telemetry channel

will be time shared with the vidicon. Readout will take 2.5 seconds of each 52-second period. There will be only one gain change during this mode, with the 0 to 3 interval remaining fixed during the final 30 minutes of flight.

E. Supporting Activities

1. Celestial Simulator

The construction phase of the celestial simulator facility has been concluded and final cleanup operations are now in progress. On completion of building cleanup, black carpeting will be placed on the floor in the dome area.

The artificial sun source has been installed and preliminary optical alignment has been accomplished. On completion of control wiring, cooling system additions, and final optical alignment, the source will be operational. Final alignment of the sun source and installation of the heliostat will await receipt of the two remaining mirrors which complete the optical system. Both mirrors were ground, polished, aluminized, and overcoated, but were rejected prior to delivery because of the discovery of severe scratches on the optical surfaces. The mirrors are currently being refinished and delivery is expected within 2 weeks. The two-axis heliostat mount and drive system is complete and has been tested with its associated electronics in the laboratory. Closed loop acquisition and stability tests were accomplished by mounting a two-axis sun sensor on the controlled member and acquiring a fixed, high intensity light source. Although the test was contrary to the normal mode of operation in which the mirror is controlled to reflect a moving source (the sun) onto a fixed sensor, the acquisition and stability considerations are equivalent and the test results confirmed predicted performance. After acquisition, observations with a Wild T-2 theodolite revealed no detectable motion of the mirror mount in either axis.

The communication capacity of the three-axis, air-bearing supported spacecraft simulator is being expanded with the addition of a 30-channel command and a 30-channel telemetry system to facilitate operation and evaluation of onboard experiments. The command receiver system consists of 30 tone operated latching relays driven by two RF receivers. All *command on* signals are transmitted over one carrier while *command off* signals appear on the second carrier. The 30 different tones on each carrier range in frequency from 400 to 6500 cps and are spaced at 10% frequency increments. The command transmission system consists of two AM transmitters modulated by two unijunction transistor relaxation oscillators. Tuning networks for the oscillators are selected by push buttons on the operating console. The telemetry system consists of a pulse-amplitude-modulated transmitter driven by a 30-channel solid state commutator. Of the 30 sampled channels, 28 carry information and the remaining two are used in automatic zero and calibration loops. The sequentially sampled inputs are mixed with a synchronizing pulse and are then fed to a 17-channel VCO phase which phase modulates a crystal controlled transistorized RF transmitter. The receiver for the system is a wide-band FM type whose output is further discriminated to restore the PM information. The sync signal is separated and the remaining information restored by a solid state decommutator operating into 30 zero order hold circuits. A switch panel enables simultaneous read-outs to a monitor CRO, meters, and recorders.

2. Vacuum and Space Simulation

Four new 18- by 30-inch vacuum bell jars have been added to the environmental laboratory and will be ready for use in May. These chambers will help fill the increasing need for life testing of components and assemblies in a vacuum environment. The systems were specially built by CVC and use a PMC 1440 diffusion pump with LN_2 cooled Chevron baffles over the diffusion pump. With the cooled baffles to reduce any backstreaming of diffusion pump oil, the system should be capable of holding a pressure of 5×10^{-7} mm Hg over long periods of time and with a minimum of contamination of test articles by diffusion pump oil.

3. Vibration Testing

An order has been placed for a 175-kva amplifier which should permit the operation of a 28,000 force-pound (vector force rating) vibration system by August 1961.

A hydraulic vibration system is also on order with a scheduled delivery in October. This system is rated at 25,000 pounds (vector), and is intended to be used in conjunction with the above electrodynamic system. The hydraulic system, with its 6-inch stroke, will be used primarily in the 1- to 50-cps frequency range. The electrodynamic shaker, with its 1-inch displacement, will handle the range from 20 to 2000 cps. Because of the high force output of these shakers, it is possible to excite a 1200-pound package or system along with roughly 1200 pounds of fixtures to a level in excess of 5 g rms.

II. *Surveyor*

A letter contract for initiating the *Surveyor* spacecraft development was executed with the Hughes Aircraft Company on March 1, 1961. This contract is to extend through June 13, 1961. The fundamental objectives for this 105-day period are as follows:

(1) To continue *Surveyor* systems analysis and trajectory studies leading to a definitive design specification which will be the key document governing the spacecraft system development.

(2) To formulate specific development and test programs which take into account the revised development schedule; i.e., an earlier start date and a later initial launch date.

(3) To provide engineering support to JPL's Space Sciences Division by assisting in the present instrument breadboard development and, thus, to acquire sufficient background so as to take on the responsibility for the procurement of scientific instruments by July 1961.

During March, the first draft of the design specification was submitted to JPL for review and comment. A program plan for the 105-day effort showing major milestones was prepared. Investigation into the use of a modified PERT system for the entire program was carried on jointly with JPL. Sample networks were drawn up and processed by the established programming techniques.

On May 1, the design specification for the spacecraft system, which will be the key governing document for *Surveyor* development, was submitted to JPL for final review and approval. During April, a team of five resident cognizant engineers from Hughes was assigned to JPL to support the current programs of developing breadboards for the various scientific instruments. Limited-objective subcontracts were established with the Elkton and Reaction Motors Divisions of Thiokol for the main retro and vernier propulsion systems, respectively. The initial testing of the vernier system using prototype hardware at low L^* is highly encouraging.

The spacecraft vehicle configuration was modified to accommodate the latest complement of scientific instruments. Other configuration changes included (1) a single spherical tank instead of multiple integral cylindrical gas tanks for the propellant feed pressurization; (2) a 6-inch increase in length of each of the landing legs for greater stability; and (3) a more rigid interconnect structure between *Surveyor* and *Centaur* so that the spacecraft can better withstand the vibrational boost environment of the launch vehicle.

An analysis of the telecommunication system transmission parameters was completed and led to the conclusion that the transmitted power should be substantially increased (1 to 10 watts). This higher power, principally due to the larger threshold value of the FM/FB network in the presence of noise, makes a solid-state transmitter impracticable.

A study in conjunction with Martin Nuclear was conducted on adapting an RTG power source to *Surveyor*; a decision on the use of RTG for the initial spacecraft will be made in mid-May. RFP's on the precision altimeter and doppler navigator were issued and replies solicited by early in June 1961.

The master development plan was revised to take into account the earlier start date and later launch date for *Surveyor*. The 4-month relaxation in initial launch dates permits an additional 2 months of systems tests for each spacecraft and a 2-month integration and dummy run of each spacecraft with the *Centaur* flight vehicle at Convair, San Diego, prior to shipment to AMR.

The NASA research centers of Lewis Laboratory and Langley Field were made aware of the special technical problems associated with *Surveyor*. It appears that these research centers can be of specific assistance in investigating the behavior of dust in a hard vacuum, the disturbances induced in dust layers by rocket engine impingement, and the effect of engine exhaust on RF performance.

PART THREE
PLANETARY—INTERPLANETARY PROGRAM

I. Program Status

A. Objectives

The primary long range objective of the NASA Planetary–Interplanetary Program is the development of automatic, unmanned, interplanetary spacecraft technology and the use of this technology in the form of space probes to gather fundamental scientific knowledge concerning the planetary and interplanetary environments, the planets themselves, and solar phenomena, both out of and within the plane of the ecliptic.

The secondary long-range objective of the program is the development of technology and the collection of scientific data which will contribute to the successful manned exploration of the planets and interplanetary space.

The primary objective of the program by 1970 is to have rather completely demonstrated and, to some reasonable extent, exploited (in terms of acquired scientific data) spacecraft capable of (1) being put into orbit around and (2) landing on the surface of Mars and Venus.

A secondary objective during this period will be the initial efforts toward extending the above capability toward the planets Mercury and Jupiter and space shots out of the plane of the ecliptic and in toward the sun.

The immediate objective of the program is the initial probing of Mars and Venus.

B. Missions

To ensure reasonable confidence of successful Mars and Venus missions in 1964, it is important that three spacecraft developmental flights occur in 1962–1963.

The *Centaur* vehicle will be the launch vehicle used in the *Mariner* program. In 1962, this program will be limited to two launchings which will be at Venus. The Venus probes in 1964 and on will use the same basic design as that used in 1962.

The launching scheduled in 1963 will be a prototype of the 1964 Mars mission. The trajectory to be flown will be chosen to provide the best overall test of this spacecraft involving some variety of an earth return orbit. As a prelude to the *Voyager*, employing *Saturn* launch vehicles, the 1963–1964 mission will incorporate experiments as are deemed practical, leading to orbiting landing capability; e.g., terminal guidance experiments. Beyond this time, the missions are envisioned to evolve first to complete sophisticated orbiters in 1965–1966, and landing experiments beginning in 1966 or 1967 using *Saturn* vehicles.

Planetary orbiters are a necessary part of the evolution and are a logical step in the development of spacecraft technology. Orbiters are required to permit sufficient observation of the planet to know how to proceed with the landing missions. Furthermore, orbiters may well constitute an important step in the actual landing experiments. The emphasis on planetary orbiters, therefore, will be to contribute to the successful accomplishment of the landing objective.

The missions of the planetary–interplanetary program as defined above are subject to change because of such influences as new scientific discoveries or unexpected developments in vehicle availabilities.

C. Program Activities

1. Compatibility Tests

The criteria and schedule for compatibility tests between the *Mariner* spacecraft and the *Centaur* vehicle have been generated and agreed upon between JPL, MSFC, and Convair.

2. Vehicle Allocation

Allocation of Vehicles C-4 and C-5 to *Mariner* missions P-37 and P-38 has been confirmed.

3. Mariner Missions

The P-38 mission has been changed from a deep space probe to a Venus fly-by. Both P-37 and P-38 now are identical and are scheduled for launch during the summer of 1962.

4. Project Development Plans

JPL project personnel visited MSFC in early April for the purpose of generating a management structure for the *Centaur* and *Mariner* projects. A mutually acceptable organization was developed and is being incorporated into the *Centaur* and *Mariner* project development plans.

5. Vehicle Interface Meetings

Regularly scheduled biweekly meetings involving JPL, MSFC, and Convair personnel have been started with the intent of resolving vehicle interface problems. These meetings are turning out to be extremely valuable in integrating the *Mariner* spacecraft with the *Centaur* vehicle.

6. Mariner Design Status Reviews

On April 25, the *Mariner* Project Office initiated a series of intensive status reviews of the *Mariner* spacecraft. These reviews consist of a 1- to 2-day detailed presentation by each JPL technical division, indicating the status of design, fabrication, documentation, and actual or potential problem areas. Demonstration of existing hardware was included.

II. Mariner A

A. Systems

1. Flight Sequence

The *Mariner* A flight sequence and some of the subsystem interactions required for executing various functions are shown in Figure 30.

In the flight sequence, liftoff from AMR is considered as zero time. The spacecraft and the *Centaur* stage are separated after injection into the interplanetary trajectory. At $T + 44$ minutes the solar panels are unfolded and the planetary horizontal platform (PHP) is unlatched and extended to the cruise position. The PHP is in the cruise position for most of the flight so it will not shade

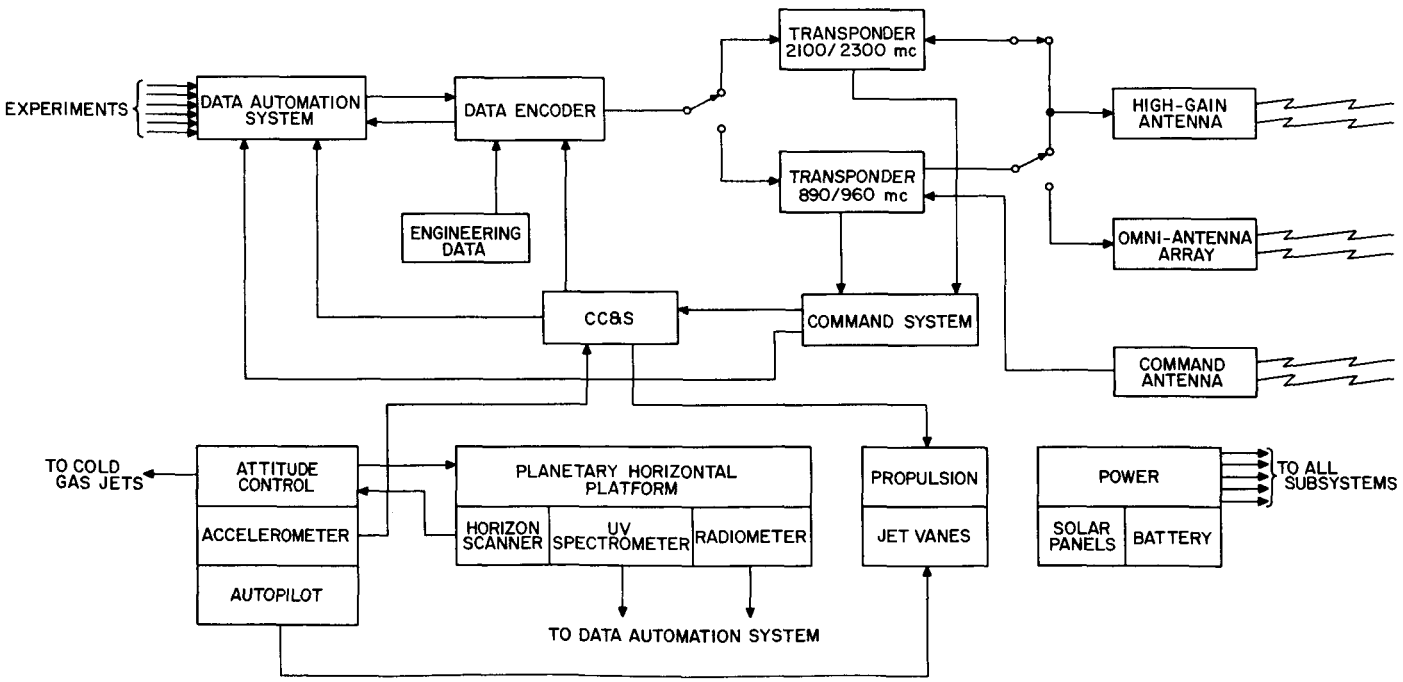

Figure 30. Subsystem interrelationships

the electronic packages on the hexagonal structure. One hour after launch the attitude control system is activated.

Through most of the flight the attitude control system keeps the spacecraft oriented so that solar panels face the sun and the high-gain antenna tracks the earth. This is accomplished by a cold gas mass expulsion system and a servoactuator drive of the high-gain antenna. Short- and long-range earth sensors are attached to the antenna boom to generate error signals for the servoloop. Two earth sensors are required because the wide field of view of the short range sensor results in insufficient sensitivity after the first 6 days of flight.

The data automation system (DAS) is to be turned on at $T + 90$ minutes. In turn, the DAS regulates the various experiments at certain times during flight. The DAS operates throughout the mission except during the propulsion maneuvers. Transmission of scientific data occurs only over Goldstone during a 4-hour period at the end of the Goldstone pass.

At various times during flight it may become necessary to send ground commands to the spacecraft. Ground commands can only be transmitted when the spacecraft is over Goldstone. The aft command antenna is receptive to 890-mc transmission frequency, while the high-gain antenna is used to receive ground commands on the 2100-mc frequency. These commands are fed into the command system which distinguishes between real time commands and stored commands, sending each to its proper destination. Use of ground commands permits many useful functions to be performed. It will be possible to select the data rate, the telemetry mode, the antenna or the transponder being used, the times of various maneuvers and their magnitudes, and the choice of several DAS data sampling programs. The insertion of a new science program of a maximum size of 10,240 bits is also possible by ground command.

Telemetry data is transmitted throughout flight from either the high-gain antenna which tracks the earth or the omni-antenna array. The former can be used for transmission of either the 960- or 2300-mc signal, while the latter can be used only for 960-mc transmission. Scientific data is transmitted from the DAS upon receipt of sync pulses from the data encoder. Daily transmission of stored science data occurs during a 4-hour period over Goldstone. Engineering data is transmitted in real time during the remainder of the day.

A mid-course maneuver is anticipated for the second pass over Goldstone. Following completion of the mid-course maneuver computations at JPL, the required turn durations and velocity increment are sent to Goldstone for transmission to the spacecraft. During the mid-course maneuver the PHP is stowed in its nested position to ensure proper cg location with respect to the motor thrust axis. The roll turn and pitch turn are executed prior to motor ignition. The autopilot controls the jet vanes during motor burning so the thrust axis passes through the cg of the spacecraft. Motor burning termination is effected by the closure of a valve when the integrated signal of the accelerometer matches the preset value in the central computer and sequencer (CC&S) memory. After motor cutoff the attitude control system again reorients the spacecraft so that the sun and earth acquisition can be attained.

Following reacquisition the magnetometer boom and solar plasma boom are extended and the PHP is moved to its cruise position. This configuration of the spacecraft is maintained until planet encounter when the PHP is servoactuated so it tracks the planet.

Dependent upon the launch date the closest approach to the planet occurs 86.5 to 153.5 days after liftoff. At 8.5 hours prior to closest approach the PHP will begin tracking the planet, employing servoactuators which receive signals resulting from error signals generated in the horizon scanner. While the PHP remains normal to the Venus radius vector the scan actuator causes the radiometer and ultraviolet spectrophotometer to scan the surface of the planet to obtain data about the temperature profile and the spectral energy distribution of the planet, respectively. The time to start the planet encounter sequence is programmed into the memory of the CC&S before liftoff and can be adjusted by radio command after the actual trajectory has been computed.

An advanced development propulsion experiment will be performed 4 days after planet encounter. However, this restart capability may have to be utilized for a second trajectory correction some 30 days prior to encounter. In this case no propulsion maneuver after encounter will be performed.

2. System Integration

Effort by the agencies [MSFC, Convair (C-VA), and JPL] involved in the system integration of the *Mariner* spacecraft with the *Atlas–Centaur* launch vehicle has resulted in significant progress.

a. Task Assignment Directives. To aid in resolution of interface problems TAD (*SPS 37-7*) have been initiated by JPL, approved by MSFC, and assigned to C-VA. It is anticipated that there will be few further requirements for additional TAD during the *Mariner* A program since the program has been contractually implemented to

insure adequate support in all remaining technical areas. A complete list of TAD is as follows:

TAD 1. Determination of spacecraft pressure environment during nose fairing ejection (October 5, 1960).

TAD 2. Determination of the basic loads and deflections for *Mariner* A spacecraft (October 5, 1960).

TAD 3. Telemetry measurements for *Mariner* A spacecraft (January 9, 1961).

TAD 4. Payload capability of *Atlas–Centaur* for *Mariner* A missions (January 30, 1961).

A review of the spacecraft injection energy requirements indicated that a study task was needed to clarify the performance compatibility of the *Centaur* vehicle. At the request of MSFC, TAD 4 was initiated by JPL. Specifically, the task was to prepare a weight analysis of the required spacecraft support equipment to be carried on the *Centaur* launch vehicle; to determine the payload capability as a function of several parameters (i.e., parking orbit altitude, launch azimuth, injection energy levels); to determine possible payload weight increases by taking advantage of various launch-to-injection trajectory characteristics peculiar to the *Mariner* missions; and to determine payload improvements obtainable through the introduction of launch vehicle improvements.

TAD 5. RF propagation for *Mariner* A spacecraft (February 2, 1961).

In considering the task of performing an on-pad checkout of the spacecraft communications systems, it became apparent that problems would exist in obtaining reliable and accurate RF propagation from the spacecraft, located on the launch pad, to the checkout receiving station. This was due to the fact that, in the mated configuration, the spacecraft directional antenna will be buried within an enclosure of the *Centaur* consisting of a metal adapter, numerous electronic packages and instrumentation, coupled with the fact that the service tower nearly surrounds the vehicle. The purpose of TAD 5 was to establish a method by which reliable and accurate communication links between the spacecraft antennas and the launch checkout station could be accomplished.

TAD 6. Mariner A spacecraft *Centaur* interface design (February 3, 1961).

It was the purpose of TAD 6 to initiate an early design of hardware for the attachment of the spacecraft to the *Centaur* vehicle. With contractual negotiations still incomplete for the *Centaur*, and because of the limited time available, it was considered essential that a TAD be initiated on major long lead time items. Subsequently, TAD 6 was incorporated into the over-all mission tasks now under contract. TAD 6, as a formal document, has been cancelled.

TAD 7. Pre-injection trajectories for *Mariner* A missions (March 22, 1961).

To support range instrumentation planning and verification of *Centaur* performance, pre-injection trajectory computations were requested by TAD 7.

b. Completed TAD. A number of reports of study accomplished under the TAD have been completed:

TAD 1. Results of this study (February 9, 1961) concluded that the environment within the *Centaur* nose fairing at the time of jettisoning will be tolerable to the spacecraft and no associated modifications to the fairing are required.

TAD 2. This task was primarily for assembling design load information for use in evaluating the *Mariner* spacecraft structural compatibility with the *Centaur* launch vehicle. Two problems appeared as a result of the study (February 16, 1961): (1) was physical interference; (2) was an incompatibility between the required and the permissible cg envelope. Both problems have subsequently been resolved.

TAD 3. Results of this study (April 3, 1961) culminated with proposals to carry two telemetry subsystems on the *Centaur* vehicles for the *Mariner* missions in place of the three systems which will be used on earlier *Centaur* flights. One of the two subsystems requires no changes, while the other will require minor additions of subcarrier oscillators to support the JPL-requested measurements.

TAD 4. The report of study (February 20, 1961) includes an analysis of vehicle inert weight, telemetry requirements, performance, and performance improvement potential. It was concluded that, based upon the proposed instrumentation configuration for the *Centaur* and upon a modified approach to propellant tanking criteria, the *Centaur* vehicle has the performance capability for injecting the *Mariner* spacecraft at the desired weight and hyperbolic velocity. The results of the study must be modified to take into account that the *Mariner* missions have since been scheduled for *Centaur* vehicles earlier in the series. JPL will make written comment on the report to MSFC which, in turn, must ultimately define and approve the basic configurations and related modifications.

TAD 5. The preliminary report (April 28, 1961) is currently being evaluated by JPL.

*c. Spacecraft–*Centaur *integration schedule.* It was necessary to develop a planning schedule in order to link the integration design and development effort to the C-VA vehicle and to the JPL spacecraft. Through the combined efforts of MSFC, C-VA, and JPL, an integration schedule was defined and approved. This document contains schedule milestones for such activities as:

(1) Complex 36, AMR, and Sycamore test stand (S-4) facility requirements and criteria.

(2) Interface engineering design of vehicle peculiars.

(3) Spacecraft–*Centaur* mock-up match-mate tests.

(4) Fabrication of component and system test articles.

(5) Separation equipment and related component system tests.

(6) Combined systems compatibility tests at Sycamore.

d. Interface design. Preliminary design of the major spacecraft–vehicle interface hardware has been accomplished. The basic design approach has been reviewed and approved in most of the interface areas. Emphasis is now directed toward resolution of design detail and hard-design. The characteristics of the spacecraft–vehicle interface are as follows:

(1) The spacecraft will be attached to the *Centaur* adapter at six equally spaced points (Fig 31); three to carry tension loads; all six to carry shear loads.

(2) The three tension ties (Fig 32) will be released at the time of in-flight separation by pyrotechnic actuated latches initiated by a *Centaur* vehicle timed discrete.

(3) Separation of the spacecraft from the *Centaur* will be the action of three compression springs (Fig 33) located symmetrically at the three alternate attaching points. Velocity imparted to the spacecraft at separation by these springs will be approximately 1 ft/sec.

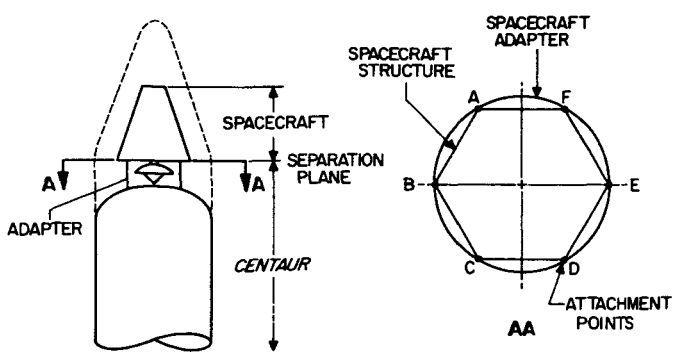

Figure 31. Spacecraft–*Centaur* attachment

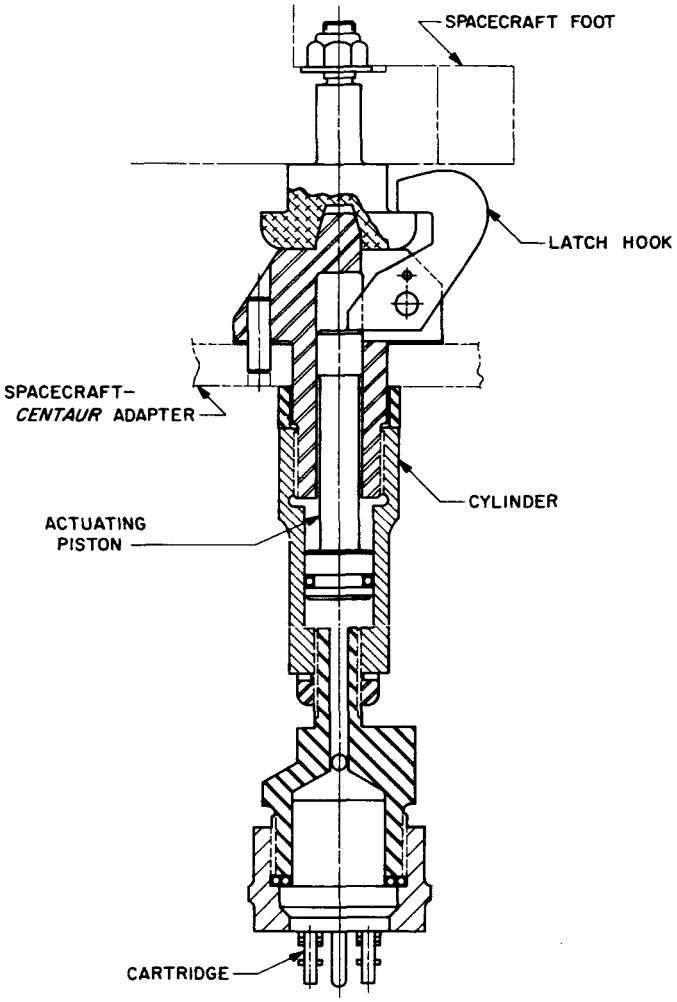

Figure 32. Tension ties

(4) Electrical connections between the spacecraft and the blockhouse monitor and control console will be disconnected by ground control approximately 10 seconds prior to liftoff. The connector, a specially designed unit by C-VA, will be mounted near the spacecraft attachment plane and will carry all spacecraft connections with exception of two circuits which must be maintained until actual flight separation. Upon execution of the pre-flight electrical separation, a signal will be received in the blockhouse to indicate complete and satisfactory separation.

(5) Two spacecraft electrical circuits will be routed through one small, in-flight disconnect. These circuits are the spacecraft emergency shutdown func-

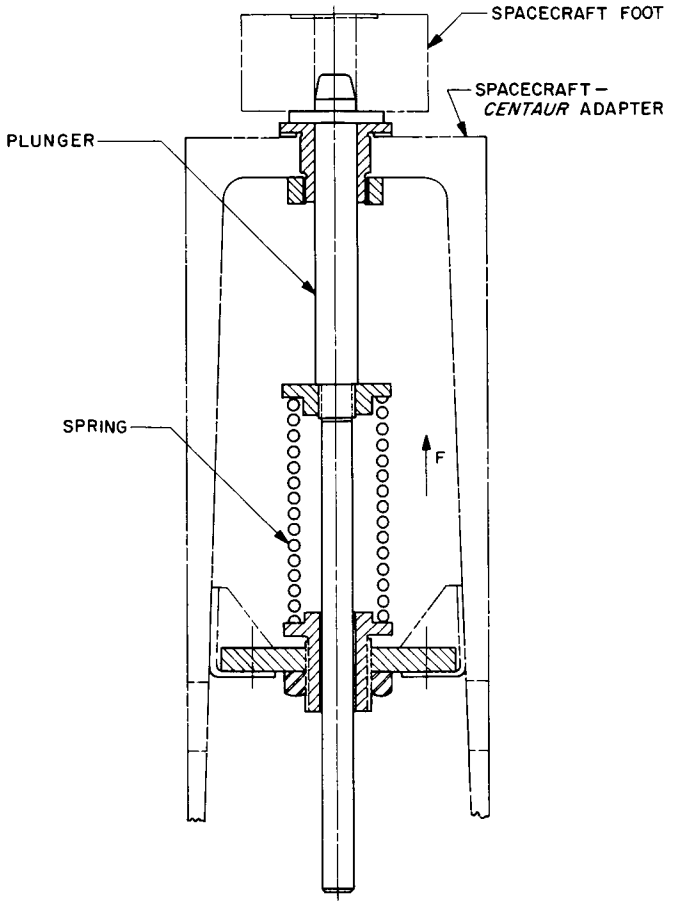

Figure 33. Shear ties

tion and the connection between the spacecraft telemetry and the *Centaur* telemetry used during the launch-to-injection telemetry phase. Separation of this connector will be by force of the spacecraft having been accelerated from the *Centaur* by the separation springs. This connector is, in other words, a fly away type, not requiring a distinct event to be generated by the vehicle. The approach selected for the design of electrical disconnects was as a result of an attempt to make the spacecraft as independent of the launch vehicle as possible and, thus, to improve the reliability of separation.

3. Testing

A proof test model (PTM) of the *Mariner* A-1 spacecraft is being built to demonstrate that the design will perform in a manner consistent with the mission intent. This demonstration will be in the form of a series of tests on the PTM.

a. Systems tests. The objective of this test will be the verification of transfer functions through more than one subsystem and to verify that the spacecraft performs properly by executing a complete flight operations sequence. Also, sufficient subsystems monitoring will be performed to permit isolation of system deficiencies.

b. Environmental tests. These tests simulate the deleterious vibration conditions which accompany *Atlas* and *Centaur* operation as well as transportation vibration. Also included are tests to demonstrate that the spacecraft will operate satisfactorily in a combined temperature–vacuum environment.

c. Vehicle compatibility tests. This test involves mating of the spacecraft with the *Centaur* vehicle and serves to demonstrate both mechanical and electrical compatibility between spacecraft and launch vehicle. The test will be performed at Convair and spacecraft functions will be monitored in the preflight and launch through separation sequence.

B. Space Sciences

Magnetic Spectrometer

The magnetometer experiment aboard *Mariner* A has as its goals the measurement of the interplanetary field in the region between the orbits of the earth and Venus as well as the Cytherean magnetic field itself. Complete vector measurements will be made, the direction and magnitude of the field being of great importance in both regions of interest.

The magnetometer instrument is a three-component fluxgate type which will have a maximum value of zero offset of 0.5 gamma and will be capable of resolving fields to within 0.25 gamma on the most sensitive scale. It will have a dynamic range of from essentially 0.5 to ± 3000 gammas, which is covered in three ranges. The basic magnetometer will measure fields with periods down to a fraction of a second, although data sampling will increase this to several seconds.

In addition to obtaining information regarding dc and slowly varying interplanetary and planetary magnetic fields, the *Mariner* magnetometer will obtain information regarding the magnetic fluctuations in the region from 1 to 30 cps in three bands. This will be obtained by opening up the bandpass and tapping a signal out prior to synchronous detection. This signal is passed through three bandpass filters (the amplitudes of which are peak detected) and then passed through low pass filters, thereby allowing one to measure the level of field variations in these three regions. Variations in amplitude of these fre-

c. Rotary joint. A coaxial rotary joint, similar to that used on the *Ranger* spacecraft, is being developed for *Mariner* A. System considerations require that the rotary joint be capable of handling a maximum power of 25 watts with a VSWR of less than 1.4 and an insertion loss of less than 0.2 db, for frequencies of 960, 2113, and 2295 mc.

Because of mechanical strength and environmental requirements, all insulators in the rotary joint will be of ceramic material. These materials present some problems because of the high dielectric constant and the several frequencies involved. Several systems of matching out the effects of these ceramics are under consideration.

A prototype rotary joint has been ordered, designed so that all of the approaches may be tested with it. Testing and evaluation are expected to begin by the middle of June.

d. RF coaxial switch. An RF coaxial switch is employed so that the high-gain antenna may, by command, be switched to either a low-power L-band transmitter or a high-power L-band transmitter. The required switch for this application is a coaxial single pole, double throw unit with high reliability and relatively light weight. The switch must carry 25 watts at 960 mc with a VSWR of less than 1.2 and an insertion loss of less than 0.2 db. It must switch reliably at voltages and currents within the spacecraft power supply capability throughout the expected environmental range.

Two commercial switches are presently under consideration. One is operated by a stepping motor. The other utilizes a solenoid operated plunger. Both switches are well within the RF electrical requirements. Neither switch requires holding power upon completion of switching. The plunger switch, however, weighs only 8 ounces as compared to 24 ounces for the stepping switch, and requires only 1.75 peak amperes for switching as compared to 3 peak amperes for the stepping switch.

Orders have been placed for three of each model switch in order to test and evaluate them further. It is expected that tests will start on the stepping switch about May 7, and on the plunger switch about June 14.

D. Electrical Power

The *Mariner* A power system was discussed in *SPS 37-7* and the block diagram was illustrated. Since that publication several changes have been made as shown in Figure 34. The 2400-cps power amplifier loads were redistributed. Individual load power requirements were changed. Several changes were made on the block diagram to more descriptively indicate the functional operation of the power system. Other modifications and additions were made for nomenclature clarification such as telemetry and GSE monitoring points.

The *Mariner* A derives its primary power from solar panels. A rechargeable battery is used to supply peak power and sustain the load during those periods when the solar panels are not illuminated. The *Mariner* A booster regulator requires a wider dynamic range of input voltage than the *Ranger* booster regulator. (This voltage range is caused by the change in solar intensity along the flight path from the earth to Venus.) The status of development and procurement of the *Mariner* A hardware is as follows:

Solar panels and batteries. Solar panels and batteries will be purchased items. Contracts are now being negotiated for the development and procurement of these items.

Electrical converters. The design and development of the electrical converters and associated subassemblies are being done by the Laboratory and are now in the completion phase. Latest system requirement changes are being implemented. The flight units will be industry built, and proceedings for request for bids have been initiated on three out of ten subassemblies.

Hardware. Prototypes of both 2400-cps power amplifiers have been built and have undergone temperature tests. Prototypes of booster oscillator-regulator and three booster amplifiers have been built and are undergoing temperature and system tests. A prototype of the synchronizer has been built and has undergone temperature tests. Mating tests of synchronizer and both 2400-cps power amplifiers have been completed over extreme temperature conditions and showed satisfactory results.

Breadboards of the charger, pyrotechnics control, power switch, and logic are undergoing tests. Prototypes of these units will not be built because the breadboard tests under temperature will be sufficient proof of the design.

Because of thermal problems, the spacecraft configuration was modified and some of the hardware relocated. This led to a mechanical redesign and repackaging of several subassemblies which will now be installed on the intercoastals. The building of prototypes for two of these subassemblies is under consideration for evaluation under

quency components will be measured to within 1.5 gammas and peak amplitudes up to 150 gammas can be measured. This part of the magnetometer instrument is primarily for a survey type experiment as frequency components in this realm may not be measurable by any previous instrument system, although some indication may be obtained from RA-1 and -2.

The instrument also includes circuitry which will cause the data system to go into a high data rate plasma sampling mode if the field fluctuation level goes above a prescribed value which has been set prior to launch, or if the dc field level causes a scale change from the most sensitive to the intermediate range. Either of these can be squelched by ground command in case it is found that the level has been chosen incorrectly. This will decrease the probability of missing any magnetic field variations of short time duration associated with blobs of plasma ejected from the sun.

C. Telecommunications

Spacecraft Antennas and RF Components

The *Mariner* A vehicle will carry three sparate antenna systems, a high-gain parabolic antenna, a command antenna, and an omnidirectional telemetry antenna. The high-gain antenna will be used with the 960-mc telemetry transmitter during the later portions of the vehicle flight when greater gain in the communication channel will be necessary. The high-gain antenna will also be used with the advanced development S-band transpoder. The command antenna will be used on the ground-to-spacecraft link at 890 mc and will handle the signal that contains all the command information for the spacecraft. The omnidirectional antenna will be used to provide 960-mc telemetry communication during the early portions of the spacecraft flight, during mid-course maneuvers and during any other interval of time when it is not possible to direct the high-gain antenna toward the earth. Associated with these antennas are various ancillary items. A broad-band coaxial rotary joint is used to pass the RF signals between the spacecraft proper and the movable high-gain antenna. A band separator is used to separate the S-band signals and the L-band signals from the high-gain antenna. An S-band diplexer is used to separate the receiver signal and the transmitter signal of the S-band transponder from the antenna input. An L-band filter is used in the input to the transponder receiver. Other items to be supplied will include an RF switch, a directional coupler, and power monitoring devices.

a. High-gain antennas. The type of parabolic reflector to be used and several illuminating feed approaches were discussed in *SPS 37-8*. The feed type finally selected is an equiangular conical spiral. This particular feed is a balanced feed and, therefore, requires a balun transformer to carry the signal from the coaxial feed line to the higher impedance balance feed. The balun transformer that was described in *SPS 37-8* is being used. The match of this balun transformer to 100 ohms was better than a VSWR of 1.1 to 1. The efficiency of the balun was 0.1-db loss at 960 mc and approximately 0.3-db loss at S-band. Measurements have been made with the prototype equiangular conical spiral feed mounted in the 4-foot parabolic dish. Gain efficiencies of approximately 50% were measured at both 960 mc and at S-band. (The S-band frequencies are 2113 mc and 2295 mc.) The major problem area at the present time is maintaining low ellipticity at these frequencies. Items that tend to degrade the ellipticity of the antenna are the support structure for the feed and focus. The proper focus has been determined; however, the effect of the feed support structure has not been completely determined. Ellipticities of less than 3 db have been obtained on a rough full-scale model, and a more accurate model is now being built which will closely resemble the final design in order to determine better the true ellipticities or ratios.

b. Omnidirectional antenna. The omnidirectional antenna is required to have a minimum antenna gain of 5 db below isotropic to linear polarization in all directions. To produce this type of antenna coverage a polarization diversification technique was developed. This system includes multiple antennas so located that their patterns overlap, thus providing radiation in all directions over a spherical surface. When nulls are detected at a linearly polarized monitoring antenna, as a result of the interference pattern produced by the radiation of the number of antennas making up the omnidirectional antenna, it is found that enough crossed polarized energy remains in the null so that by rotating the monitoring antenna's polarization 90 degrees, an acceptable signal can be received. Thus, by merely rotating the polarization of linear ground station antenna, a polarization can always be found such that the effective antenna gain of the flight omni-antenna will never drop below 5 db below isotropic.

Full-scale measurements have been made on a part of the omni-antenna system. One-quarter scale antenna measurements with a one-quarter scale *Mariner* A vehicle are now in progress. Typical patterns for a *Mariner* A vehicle based on the one-quarter scale measurements will be available soon.

shock and vibration environments. It is believed that a higher vibration may be encountered on the intercoastals.

Power amplifier. The 400-cps inverter was designed to supply three-phase and single-phase ac power to the gyros and motors, respectively. In addition, a constant single-phase voltage is required to operate the receiver. A three-phase sine-wave supply was designed with the intent of utilizing one phase for the motors when in use. The unbalance produced by these unbalanced loads was compensated for by tuning the output filters to specific load combinations.

Table 3 shows the power requirements for the various loads and Figure 35 the load profile for the interior delineating the various load combinations. The figure is

Table 3. System power requirements

Parameter	A Control gyros	B Rate gyros	C Horizontal scanner motor	D Data automation system motors	E Receiver
Sine-wave, phase	3	3	1	1	1
Power factor	0.5	0.9	0.9	0.9	Resistive load
Harmonic distortion, %	3 max	10	10	10	
Voltage variation, %	±5 line to line	+15 −8	±10	±7	
Starting power, watts	22.5	—	7.5	—	

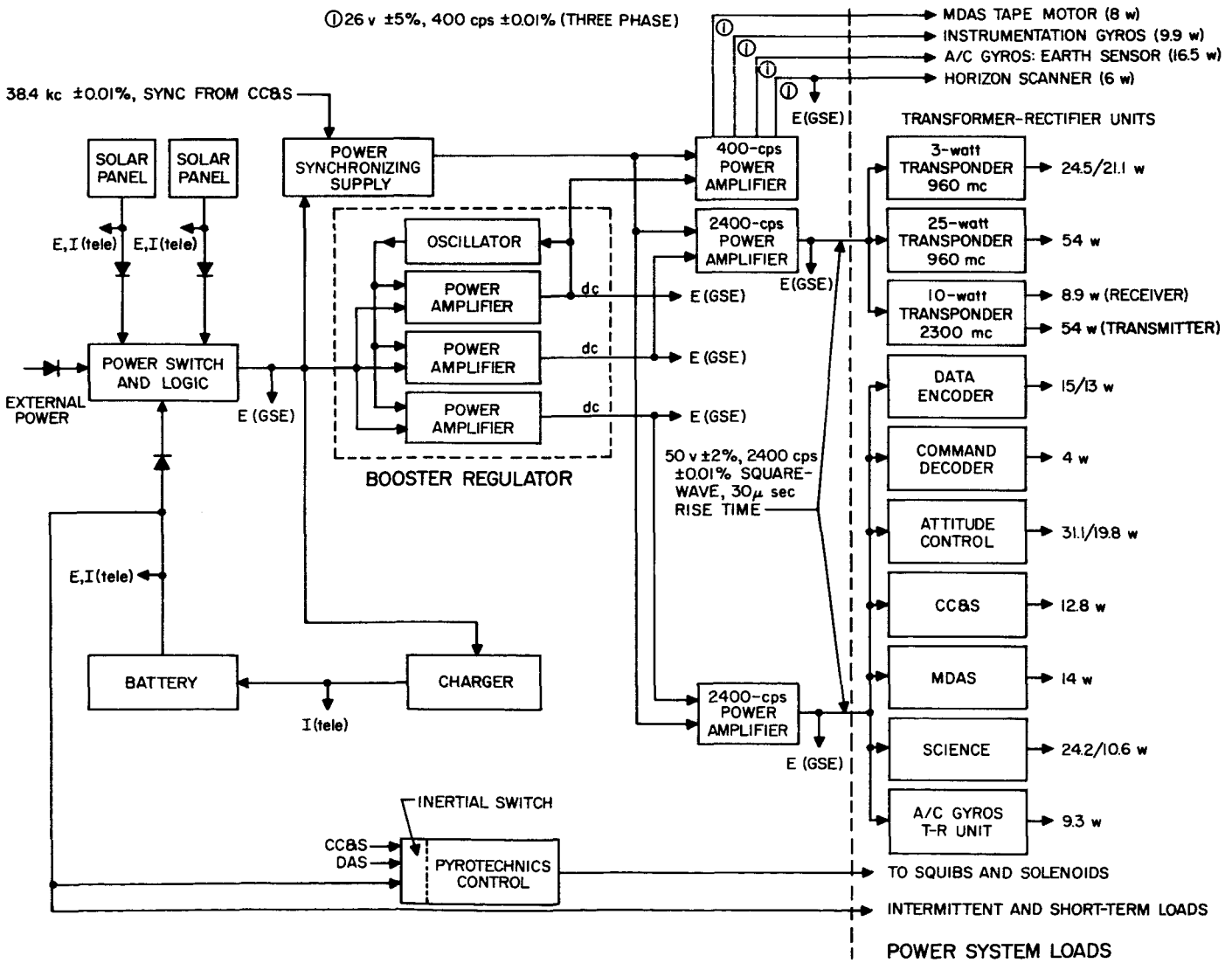

Figure 34. Power system

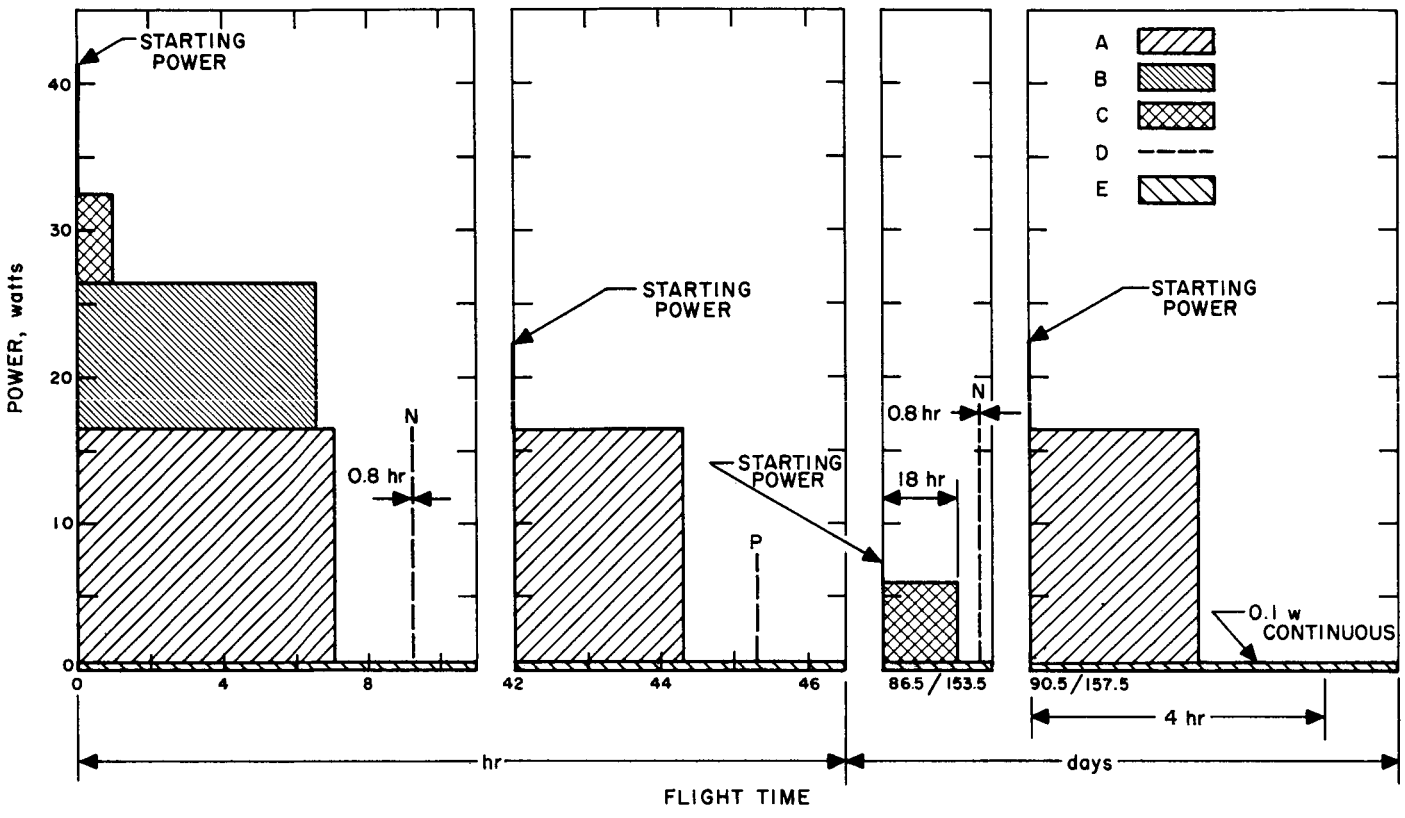

Figure 35. Power amplifier lead requirements

a functional description of the 400-cps inverter amplifier (Fig 36).

The 400-cps amplifier consists of three identical channels each comprising a preamplifier, a power amplifier,

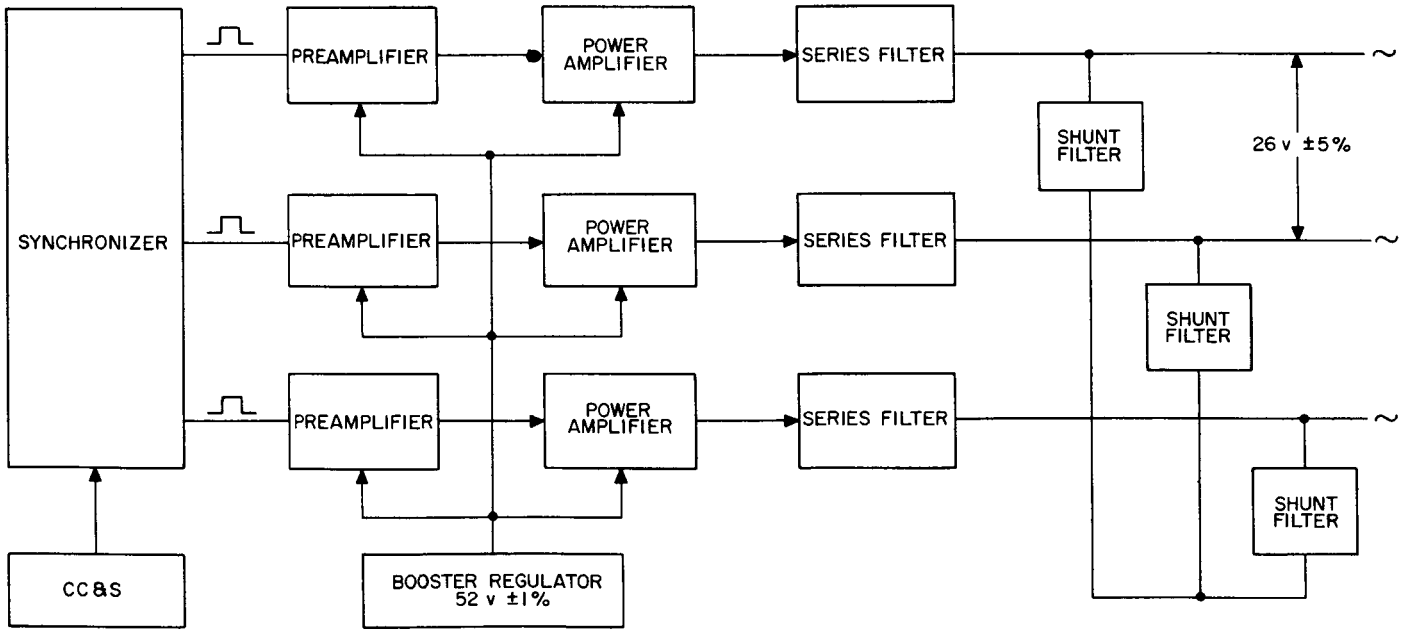

Figure 36. Inverter amplifier

a series filter, and a shunt filter. Each of the preamplifiers and power amplifiers consists of two transistors operating in push-pull and a coupling transformer. Two stages of amplification are necessary to provide the required power gain of approximately 1000. Each channel amplifies and filters a square-wave received from the synchronizer to produce a sine-wave output. The sync circuits provide the proper phasing of the square-waves to produce in the output of the amplifier three-phase sine-wave voltages with the proper phase rotation. The frequency is crystal controlled to 0.01% in the CC&S.

The filter network is composed of a series filter and a shunt filter. Both filters are tuned around 400 cps. The series filter provides a low-impedance source to components of the waveform with frequencies below 400 cps while the shunt filter provides a high-impedance source for frequencies below 400 cps. The filter is tuned for the *E*-load condition shown in Figure 35, and power factor corrections are to be introduced at the load by the users. Tests with the actual loads are being performed to establish the power factor correction components. These components are to be installed in the users equipment and provide for the necessary compensation for the unbalance in any one particular load combination.

E. Engineering Facilities

1. Space Simulator

The design for the 25-foot space simulator has progressed satisfactorily during the past 2 months. The liquid nitrogen cooled panels, which cover all the inside surfaces of the chamber, except for the overhead parabolic mirror, are being fabricated from thin aluminum extrusions to minimize weight and liquid nitrogen consumption. Out-gassing of these panels, while higher than stainless steel at ambient temperatures, will be less than stainless steel at the liquid nitrogen temperatures. A black anodize and dye penetrant process is being applied to the inside faces of the shroud and it is hoped that the resultant emissivity will approach 0.93 to 0.95.

The 2.5-kw Mercury–Xenon lights being utilized by the facility have demonstrated 500- to 600-hour life under severe test conditions with intensity falloff in this time of the order of 15 to 20%. A solid state selenium rectifier has been developed to supply the dc power for the lights which operate at 50 amperes and 50 volts dc. The contractor has an intensive program underway to develop a 25-foot cool parabolic mirror which fills the top of the chamber; this mirror will operate at approximately $-200°$F.

All high-vacuum valves and diffusion pumps have either been shipped from the prime contractor or are in final stages of fabrication. The initial carloads of steel consisting of the chamber bottom, legs, and first ring sections were shipped April 21. All foundation work in the basement and equipment room is complete and ready to erect steel thereon. Connecting utility lines between the simulator site and the wind tunnel area have been installed by outside contractors and are waiting connection by JPL. Figure 37 shows the site as of April 28, 1961.

The 6-foot space simulator in the environmental laboratory has been operating with carbon arc lights as a source of radiation, but because of a lack of collimation and uniformity in the resulting light patterns, a contract has been awarded Bausch and Lomb Company to equip the chamber with a solar simulator similar in concept and function to that being utilized in the 25-foot chamber. Completion of this modification for the 6-foot chamber is scheduled for November 1, 1961.

2. New Optical System

A unique concept of producing solar radiation within a vacuum chamber has been experimentally demonstrated. Light from Xenon lamps was collected and collimated as indicated in Figure 38. Experiments were conducted using a 4-foot diameter section of a surplus searchlight

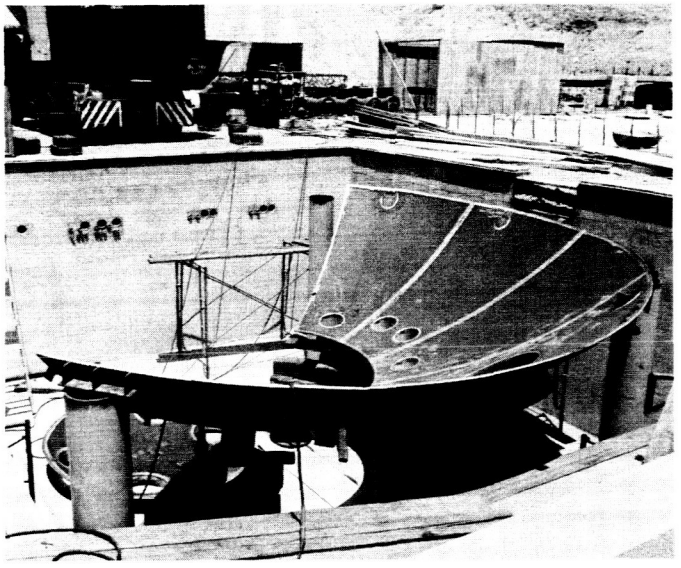

Figure 37. Simulator building

parabola which resulted in a collimated (6 to 7 degree) light beam with a ±2 to 3% variation in intensity over a broad annular test area. Further work is planned to achieve a better definition of the spectral distribution (Fig 39) and to obtain a more uniform radiation intensity across the entire circle.

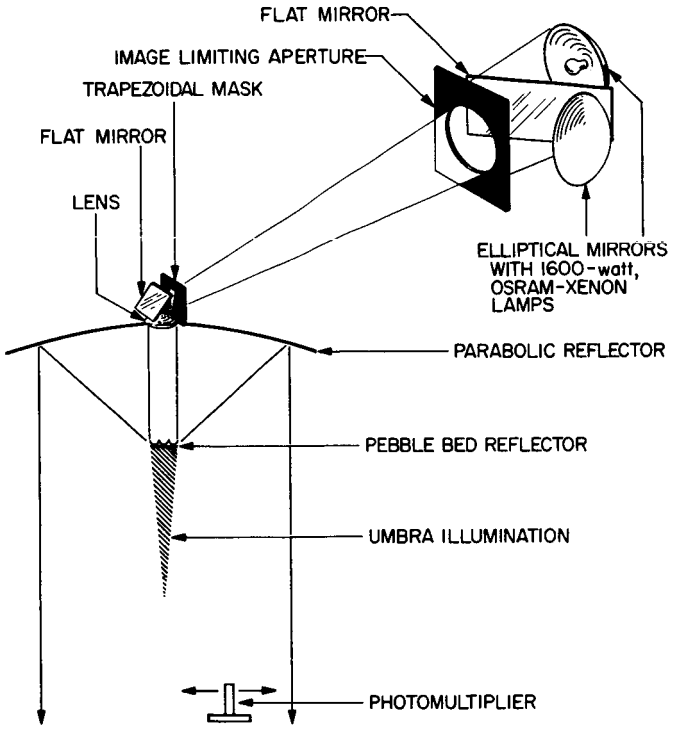

Figure 38. Solar simulator

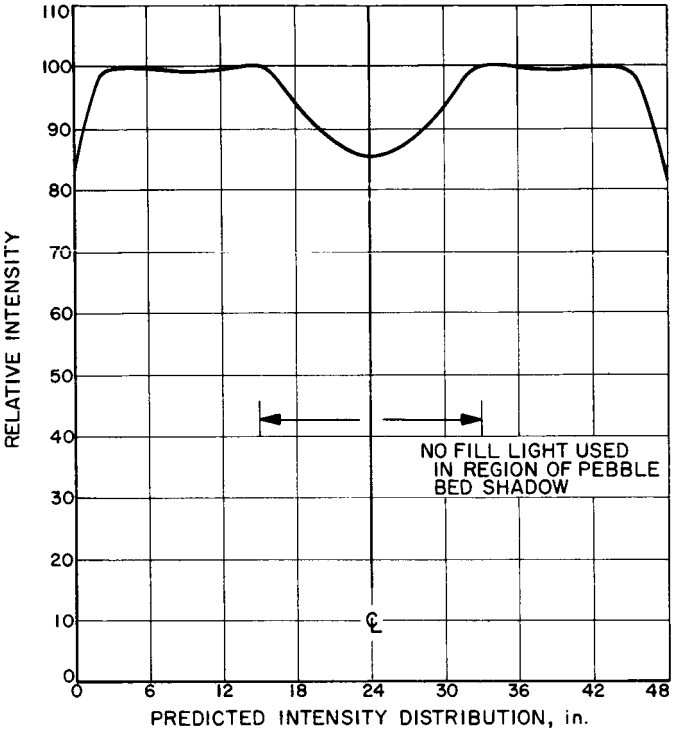

Figure 39. Simulator intensity distribution

PART FOUR
DEEP SPACE INSTRUMENTATION FACILITY

During the last 2 months a most successful experiment has been underway at the DSIF Goldstone station complex. Using the two 85-foot antennas at Goldstone as transmitter and receiver, respectively, contact was made with Venus by bouncing radio signals off the planet. To illuminate the planet between 10 to 13 kilowatts of transmitter power was employed. The receiver site used a newly designed low-noise maser amplifier feeding a parametric amplifier and a very narrow-band receiver; it was possible to obtain a signal-to-noise ratio as high as 18 db. Using a synchronous receiver, true doppler frequencies were measured and, using a ranging system, measurements were made which are accurate to better than 100 miles. Both techniques have generated measurements which make it possible to calculate the astronomical unit to greater accuracies than has ever been done before. One unusual and unexpected result of the tests was the high reflection coefficient of Venus. Preliminary measurements indicate it to be as high as 20% or over 10 times that of the moon. Also unexpected was the very narrow effective spectral bandwidth of 5 to 10 cycles. These two measurements have caused a great deal of speculation. Successful polarization measurements were also made. This issue of the *SPS* includes the first discussions on the equipment and tests which made this experiment successful.

As part of its long range plan to furnish adequate communication facilities to the Lunar and Planetary–Interplanetary Programs when these facilities are needed, the DSIF has contracted with four companies to make feasibility studies for a large antenna (approximately 240 feet in diameter). Such an antenna will be needed to communicate at interplanetary distances with reasonable signal bandwidths and at shorter distances when one or more real time television signals will be required. A synopsis of this project and reports on foundation studies and microwave optics which support this project are included in this *SPS*.

The DSIF furnished the Woomera and Goldstone stations in support of the NASA *Explorer X* (P-4) sounding rocket. These stations successfully tracked the probe during its lifetime and obtained much useful data.

I. Systems

A. Venus Radar Experiment

1. Cavity-Type Ruby Maser

A 2388-mc, cavity-type ruby maser has been constructed and installed at the Goldstone tracking station for use in the 1961 Venus radar experiment. The maser is similar in design to the 960-mc research and development maser (*RS 36-6* and *-7*). Based on experience with the 960-mc unit, various refinements have been incorporated in the 2388-mc maser to improve the general system performance. Figure 40 shows the maser prior to installation at the apex of the Goldstone HA-Dec antenna.

The dewar system performs as expected, with a useful life of 24 hours. Daily filling on the antenna maintains the maser in operating condition. The ion pump used to maintain the dewar vacuum has maintained the vacuum to better than 10^{-7} mm of Hg after 1 month of continuous operation. The unique design of this pump enables it to outperform ion pumps twice the volume and four times the weight.

The performance of the maser was checked after installation on the receiving antenna. The gain-bandwidth product (25 mc) and noise temperature (25 to 30°K) was substantially the same as measured in the laboratory. The presence of gain variations with antenna position was detected. The source of this gain variation is believed to be small changes in the magnetic field resulting from the mechanical shifting of the magnet system relative to the ruby crystal. Gain fluctuations observed are of the order of ±2 db when the antenna is rapidly scanned across

Figure 40. 2388-mc maser

the sky. When tracking a slowly moving object such as Venus, periodic adjustment of the magnet current allows the gain fluctuations to be kept under ± 0.5 db. Gain measurement of the maser is made by injecting known signals through directional couples fore and aft of the maser.

2. Feeds and Microwave Systems

The preparatory work for the Venus radar feeds has been reported in past issues of the *Research Summary* (*RS 36-7* and *-8*). The primary design objective was to obtain a circularly polarized 2388-mc feed that would produce the highest figure of merit (the quotient of gain and system temperature) for the 85-foot receiving antenna. In order to achieve this purpose three horns were provided. Two of these were conventional horns to produce edge illuminations of 10 and 14 db (and with fin loading to obtain equal E- and H-plane patterns). Also, a shaped beam feed horn was developed at JPL (*RS 36-8*). All three horns were designed to use the same waveguide phase shifter and transformer sections to achieve circular polarization.

During the installation period the three horns were tested for gain, ellipticity, antenna temperature, and secondary patterns. The shaped beam feed was found to have from 0.8 to 1.1 db more gain than the conventional feeds. The axial ratio of the elliptical polarization was 0.75 db for the shaped beam feed. The measured antenna temperatures with the antenna pointed at zenith (and with a quiet sky background) are shown in Table 4. The best estimate of the far field gain, based on measurements taken in the near field at 0.3 D^2/λ, is 53.5 for a matched polarization isotropic source. Because of its superior performance, the shaped beam was used in the Venus radar experiment.

A block diagram of the Venus radar feed and transmission line system is shown in Figure 41. Figure 42 is a photo of the antenna focal point with the feed system, maser, helium load, and parametric amplifier installed. Antenna temperatures are measured by comparing the recorded noise signal from the antenna to that from the liquid helium cooled load. A calibrated amount of additional noise is injected into the system to raise the apparent temperature of the helium load to equal that of the antenna.

To maintain the lowest possible system temperature, the feed and transmission line system up to the maser circulator was made entirely of waveguide. The input ports to the antenna feed and to the transmission lines joining the antenna feed, the helium load, and the circulator were all matched to apparent VSWR's = 1.02 after installation on the antenna. Because of residual errors in the measurement techniques, the real VSWR at these ports may be as much as 1.04. All flanges used in the system were lapped flat to improve measurement repeatability; wherever possible, MIL standard guide pins were used in the flanges.

Table 4. Measured antenna temperatures

Feed	Temperature, °K
Horn with 10-db taper	30
Horn with 14-db taper	16
Shaped beam feed	14[a]

[a]Absolute accuracy about 4°K.

The waveguide attenuator in use in the noise injection line is an FXR Model R-160 B that has been modified at JPL for precise control by a remote servosystem. The attenuator is a flexible vane type and is extremely well matched over the entire attenuation range. The apparent VSWR is less than 1.03 over at least a 20-db range. The minimum insertion loss was measured and found to be 0.08 db, the attenuation repeatability was excellent.

After the successful tests on the shaped beam feed for the receiver antenna, the test model of the shaped beam feed was temporarily mounted on the transmitting antenna. Gain tests again indicated at least 0.8 db more gain than for the other available transmitter feeds. After this, another shaped beam feed was fabricated for use with the 10-kilowatt transmitting system. The feed section was designed to attach to the standard circularly polarized phase shifter section.

A modified waveguide 90-degree phase shifter and square to rectangular transformer were fabricated, tuned, and installed at the same time that the newly fabricated shaped beam feed was installed on the antenna. The new phase shifter was installed to improve the ellipticity of the transmitter feed system. The old phase shifter provided broad bandwidth operation but the polarization axial ratio was 1.2 db at best. Both phase shifters are of the same basic design; five double waveguide irises spaced apart in a square waveguide section, with all sharp corners rounded to prevent corona arcing. After installation of the new shaped beam feed, phase shifter, and transformer, the ellipticity was measured for right hand secondary polarization and the axial ratio was less than 0.3 db. The present best estimate of the far field gain of the transmitter antenna, under the same conditions that apply to the receiving antenna, is 53.8 db.

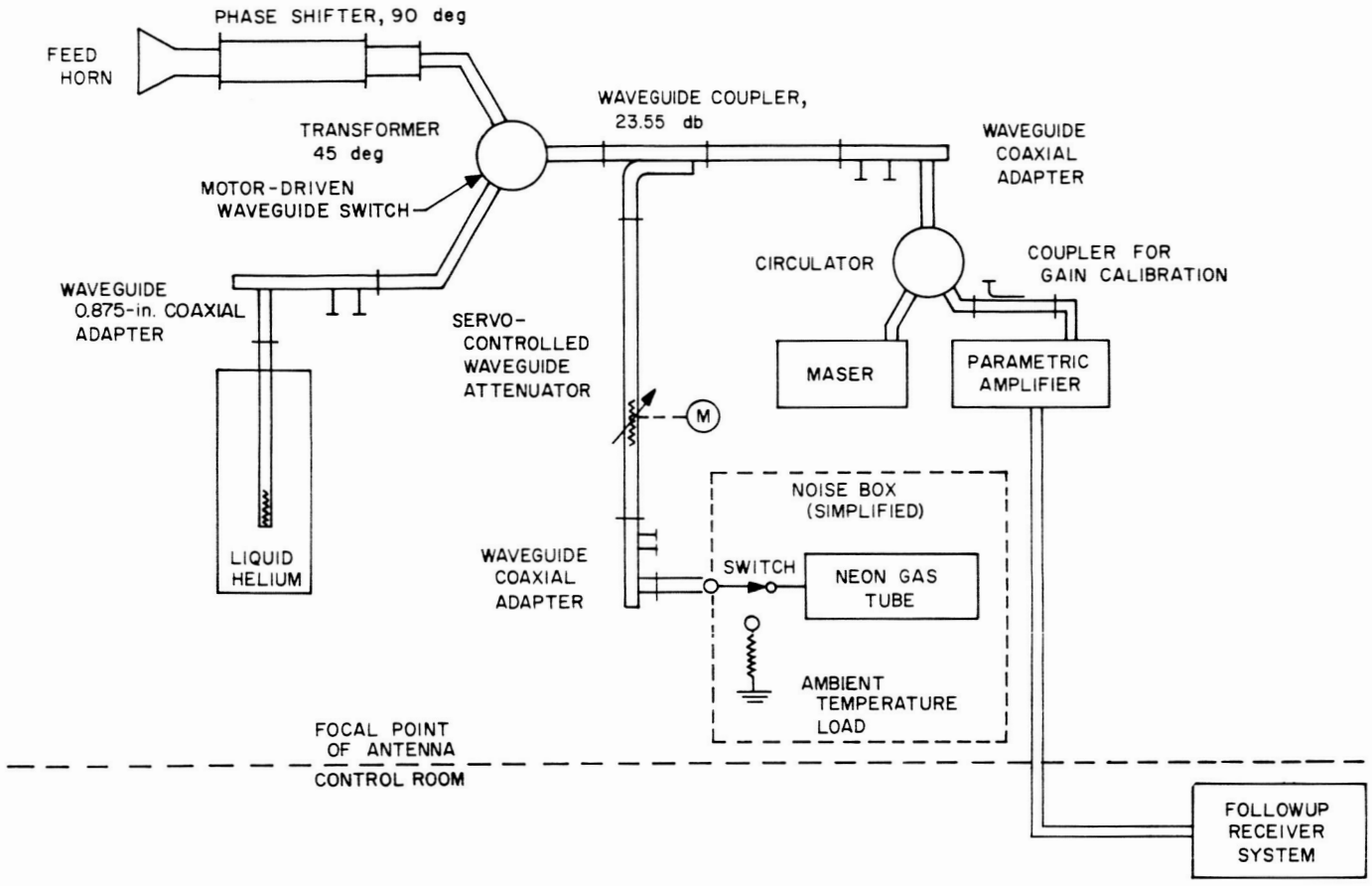

Figure 41. Feed system

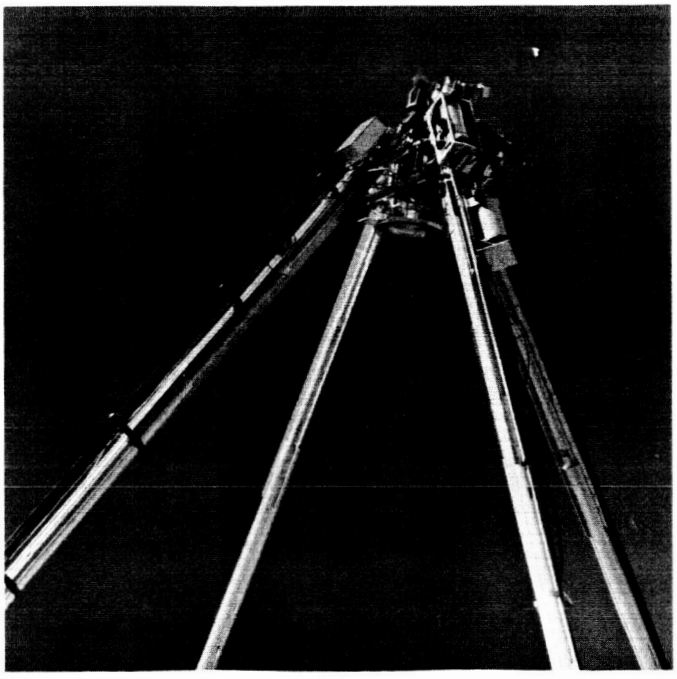

Figure 42. Maser and low-noise feed installation

The normal mode of operation during the Venus radar experiments has been to transmit right handed secondary circular polarization (CP) and receive left handed secondary CP. A diagram of the circular polarizer unit is shown in Figure 43. The signal comes from WR430 waveguide operating in the TE_{10} mode into a 45-degree rectangular to square transformer. This divides the power equally into the TE_{10} and TE_{01} modes in the square waveguide. Following the transformer is a square waveguide, iris loaded phase shifter. This phase shifter retards one mode 45 degrees and advances the other mode 45 degrees in phase.

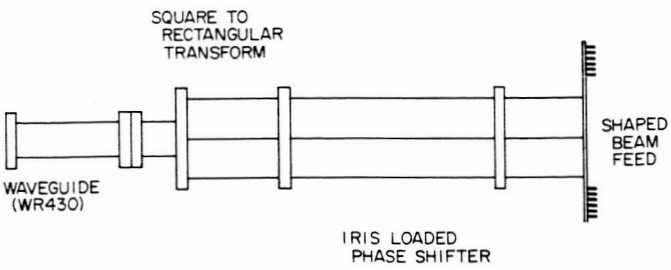

Figure 43. Circularly polarized feed assembly

The two components, therefore, have a 90-degree phase difference and a 90-degree space orientation so that they give rise to a circularly polarized wave. This wave is launched into free space through the shaped beam feed. To reverse the sense of rotation of the wave, the 45-degree transformer is rotated 90 degrees about the axis of symmetry with respect to the phase shifter.

On April 7, 1961, an experiment was performed in which the transmitter feed was converted to transmitting left handed CP and the receiver feed was unaltered. It was found that when transmitter and receiver both had left handed CP the signal strength was down approximately 11 db from the right to left hand case. For a perfectly smooth, conducting sphere one would expect all the incident left handed CP to be reflected as right handed CP.

On April 17, the four combinations of circular polarization were employed; a preliminary analysis of the results obtained is shown in Table 5.

Tolerances have not been established on the reflection coefficient determination as yet. In particular, the 0.08 reflection coefficient was the result of only one measurement. The difference between this and the 0.1 (normal) reflection coefficient should not be regarded as significant at this time. The ellipticities of these feeds are shown in Table 6.

Therefore, one would expect (on the basis of ellipticity) that the left to left signal would be down more than 18 db from the right to left case, and that the right to right case would be down more than 28 db from the left to right case.

Table 5. Preliminary results of depolarization experiments with Venus radar

Transmit	Receive	Reflection coefficient	Predetection filter bandwidth, cps
Right	Left	≈0.1 times reflection from an ideal, conducting sphere	—
Right	Right	13.4 ±2 db below 0.1	25
Left	Right	≈0.08 times reflection from an ideal, conducting sphere	—
Left	Left	12.8 ±2 db below 0.08	25
		11.7 ±2 db below 0.08	50

Table 6. Feed ellipticities

Polarization	Transmitter axial ratio, db	Receiver axial ratio, db
Right handed	0.4	0.2
Left handed	1.1	0.8

From the results of April 16 and 17, it was decided that an experiment which determined the ellipticity of the reflected signal might give a better understanding of the phenomena. A rotating linear receiver feed was constructed. It was employed at the receiver site in conjunction with the right handed CP feed at the transmitter. Venus was observed with the linear feed rotating in a stepwise manner employing 30-degree steps. The observation time of these steps varied from 2 to 20 minutes. The peak-to-peak step variations of the integrated receiver power in each step ranged from 1.5 to 2 db. It should be emphasized, however, that the signals were quite noisy and that analysis of this data can only be regarded as preliminary.

The most obvious explanation of depolarization phenomena is rough scattering by the surface. This is the same mechanism causing depolarization by the moon which has about the same magnitude for the cross polarized component. However, the ellipticity measured with the rotating linear feed on the moon was less than 0.9 db. A more thorough evaluation of the data is now in progress.

Rotating linearly polarized feed. The results of depolarization tests using circularly polarized feeds indicated that further information might be obtained by transmitting circularly polarized energy and receiving linearly. A rotating linear feed system was developed, tested, and then installed at Goldstone. A diagram of the feed system is shown in Figure 44. The shaped beam feed and square waveguide radiating elements, as well as the square to rectangular waveguide transformer, are the same as those used in the circularly polarized feed. The 16-inch section of square waveguide replaces an iris loaded quarter-wave plate so that the polarization remains linear. An end wall transition required for mechanical symmetry was used to go from WR430 to 1.625-inch rigid coaxial line. The end wall transition leads to a coaxial rotary joint. This joint had a VSWR of 1.10, an insertion loss of 0.04 db, and no measurable wow. From the rotary joint several 1.625-inch coax bends were used to go to a conventional coax to waveguide transition mounted on a waveguide switch. The waveguide switch permits selection of either the antenna or the liquid helium load; the common port leads to the circulator and maser. The unit, from the shaped beam feed to the rotary joint was mounted on two ball bearings supported in an aluminum angle frame; rotating members were turned by an electric motor through a reduction gear system at the rate of one rotation in 35 seconds.

The VSWR, as a function of frequency at the switch side of the rotary joint looking through the feed system, is shown in Figure 45. The narrow bandwidth is caused by the end wall coaxial to waveguide transition.

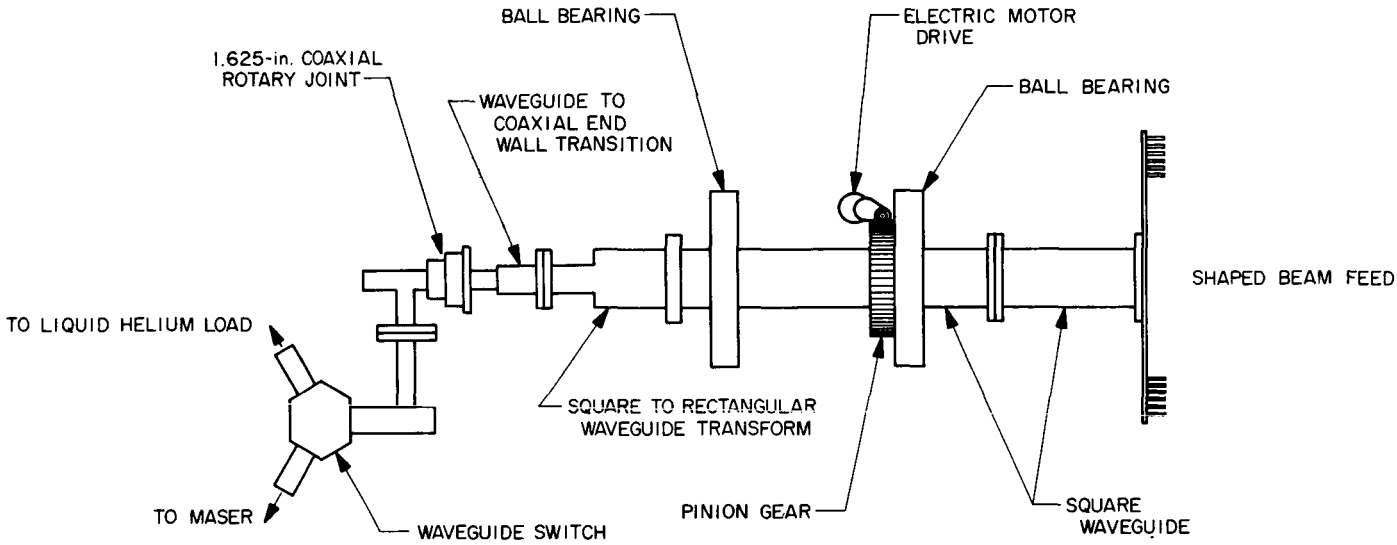

Figure 44. Rotating linear polarized feed

In evaluating the feed it was possible to separate two gain fluctuation mechanisms. The first was a maser gain change due to fluctuations of impedance with rotation. The second was a change of antenna gain with rotation. In Figure 46 the antenna was directed at the zenith and the noise tube was fired; then the feed was rotated. The system noise level was recorded. The system temperature with the noise tube on was approximately 110°K and the peak-to-peak temperature variation is approximately 1°K, giving less than 0.04-db amplifier gain change.

Through the use of drift curves, amplifier gain changes are cancelled to a large extent. The possible causes of temperature variations are: the radio source, the antenna background, and the antenna gain. It is difficult to see any mechanism to explain lunar polarization. It is probable, therefore, that these fluctuations of 0.2 db in amplitude are caused by antenna gain variation as a function of polarization angle. As part of the calibration procedure, the antenna was boresighted on the linearly polarized collimation tower antenna with several different polarization angles and showed no significant squint. When cross polarization was tested, the on-axis null was found to be down more than 36 db below the peak of the main beam for matched polarizations. One of the cross polarized sidelobes was tested and was 27 db down from the peak signal.

3. Antenna Temperature Measurements

An antenna system is optimized by illuminating as much of the reflecting surface as possible with the pickup or feed horn. Unfortunately, as the illumination is increased, there is generally an increase in the equivalent antenna temperature due to sidelobe effects. Thus, the two parameters which need accurate measurement are antenna gain and temperature. The discussion here is confined to the determination of temperature.

The equivalent noise temperature of an antenna is defined as the temperature to which a matching resistor

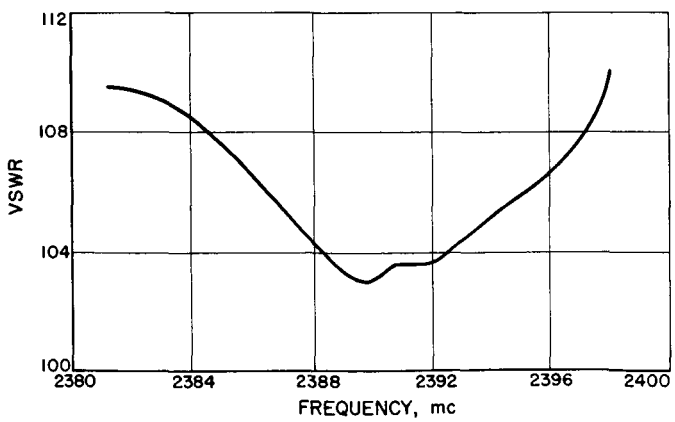

Figure 45. Rotating feed VSWR vs frequency

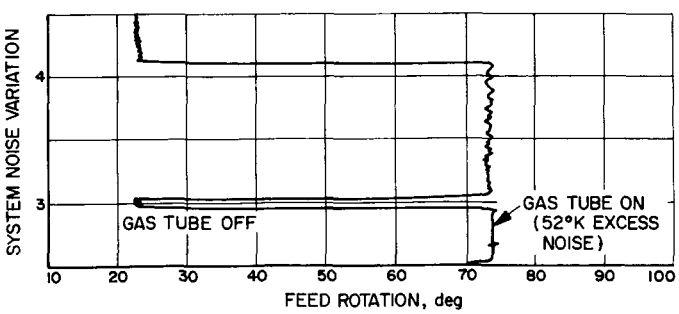

Figure 46. System noise vs feed rotation

must be raised in order that the thermal noise emanating from the resistor is equal to that from the antenna. This definition suggests immediately a possible way of performing the measurement: a receiver is switched alternately between the antenna and a resistor with adjustable temperature, T_0, and when the output is constant the antenna temperature $T_a = T_0$.

Two difficulties arise with this method: (1) The gain of the receiver does not necessarily stay constant during the measurement. (2) It is usually difficult to vary the temperature of the reference resistor in the region of interest; namely, 10 to 50°K (for good antennas in the S-band region).

An alternate procedure is to use a high temperature noise source with a precision attenuator and directional complex in place of the reference resistor. A neon discharge tube, for example, has a noise temperature of around 15,000°K and injects noise power into the maser input given by

$$T_{eq} = t\alpha T_N + tT_a$$

where

T_{eq} = equivalent noise temperature at maser input
t = transmission coefficient of directional coupler
α = attenuation of variable precision attenuator
T_a = noise temperature contributed by attenuator
T_N = temperature of noise tube

The advantage of this method is that the input impedance seen by the maser is fairly constant throughout the measurement; this requirement is important with masers because the gain is sensitive to impedance changes.

The actual mechanization for accurate antenna temperature measurement consists of the system as shown in Figure 47. The liquid helium cooled termination is used to obtain an accurate noise temperature of the receiver system. This is obtained from the power ratio

$$Y_1 = \frac{T_r + T_M + t\alpha T_N + tT_a + T_e}{T_r + T_M + tT_a + T_e}$$

which gives the power ratio for the system output when the noise tube is fired to that when the tube is not fired. In this ratio

T_r = equivalent noise temperature of helium cooled load
T_M = maser noise temperature
T_e = equivalent noise temperature of line losses

Another similar ratio is obtained by switching to the antenna:

$$Y_2 = \frac{T_2 + T_M + t\alpha T_N + tT_a + T_e}{T_a + T_M + tT_a + T_e}$$

The only unknown quantity remaining is the antenna temperature T_a.

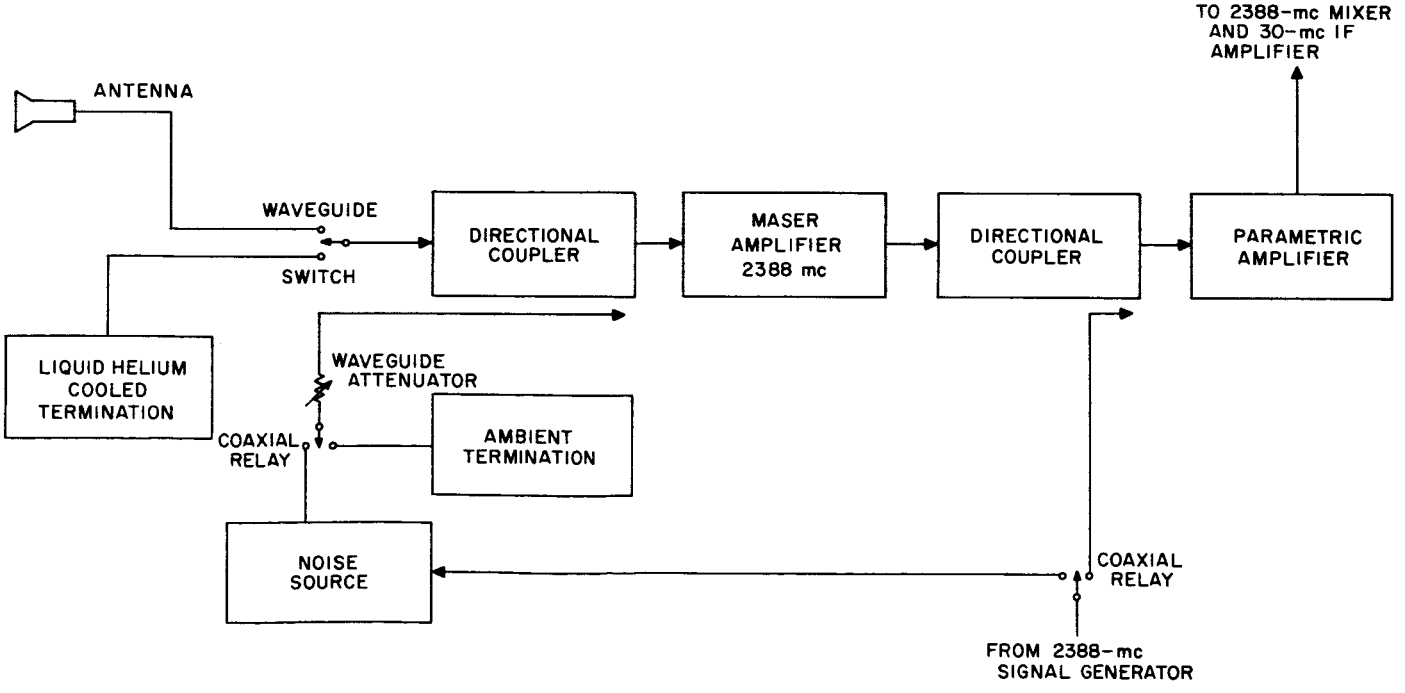

Figure 47. Venus radar receiving equipment

Utilizing this technique, measurements of maser system temperature, T_M, and antenna temperature, T_a, were made several times daily throughout the approximate 2 months of the Venus experiment. The results obtained will be summarized in a future issue of this report.

4. Black Body Radiation Measurements

To evaluate the use of radio stars as a calibration technique for the Goldstone antennas some radio astronomical measurements have been made, utilizing the Venus radar system receiving antennas and a low-noise amplifier. Since the system could only be operated as a continuous (i.e., unswitched) radiometer, its capability was dependent on gain stability. The effect of receiver gain instability may be readily explained as follows:

The minimum detectable radiation temperature for a radio source is given by

$$\Delta T = \frac{T_R}{(B\tau)^{1/2}}$$

where ΔT is the equivalent antenna temperature for the source, T_R is the receiving system temperature, B is the receiver bandwidth, and τ is the integration time at the detector output. This equation assumes a constant gain, G, in the receiving system during the observation. If the gain varies, as it inevitably does, the system sensitivity is degraded. This is seen as follows: The receiver output due to the observed source is given by $G\Delta T$; this is obscured by fluctuations in the amplified system noise, $T_R\Delta G$, where ΔG is the gain variation. A convenient criterion for the gain stability desired is given by equating the two quantities.

$$G\Delta T = T_R\,\Delta G$$

or

$$\frac{\Delta G}{G} = \frac{\Delta T}{T_R} = \frac{1}{(B\tau)^{1/2}}$$

This is an important parameter for a receiving installation used for radio astronomy measurements. If $\Delta G/G > 1/(B\tau)^{1/2}$, it may be desirable to use some form of compensation for gain variations. On the other hand, if $\Delta G/G \leq 1/(B\tau)^{1/2}$, it is of little advantage to employ gain stabilization. Indeed, it is often found that switched radiometer techniques can defeat their own purpose and degrade the system performance. This results from the fact that all radiometer techniques invariably sacrifice some of the received information. The foregoing remarks apply particularly to low-noise systems.

Good radio-astronomical results were obtained in a CW type of measurement using the maser and a stable mixer for maximum gain stability. Figure 48 shows a drift curve for M87, and Figure 49 shows the object, dependent on the night-time seeing conditions.

5. TV Tracking System

For the Venus radar experiment, the primary system of positioning the transmitter and receiver antennas onto Venus was by automatically slaving the antenna system to precalculated angles. A high reliability backup to the complex automatic system was necessary; therefore, the feasibility of using the existing antenna mounted TV system was considered.

A study was undertaken to determine the capabilities and limitations of the current DSIF TV tracking aid system configuration, particularly under daylight tracking conditions. Field tests were then carried out to empirically affirm the study conclusions. A summary of the results of that study and the associated empirical test

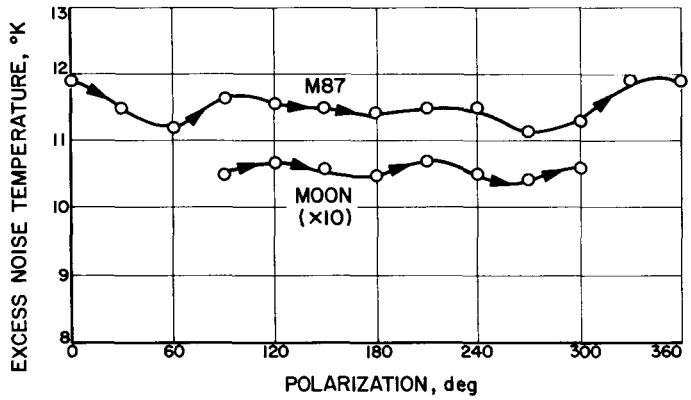

Figure 48. Radiation drift curve for M87

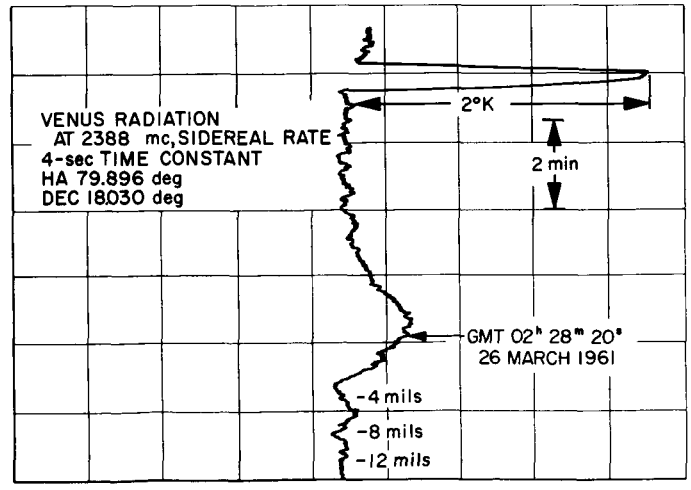

Figure 49. Radiation drift curve for Venus

data are presented in this report. The apparent system sensitivity exhibits rather broad boundaries due to such factors as the age and rating of the vidicon, personnel adjustment of controls, atmospheric attenuation, age of tubes and various electronic components, etc.

GTS–DSIF TV tracking aid system. The TV system configuration at Goldstone consists of a 40-inch focal length Zoomar, folded mirror, lens system with an effective aperture size of 5 inches. The closed loop TV system is a Kintel 1986 C system incorporating a Machlett 7351 vidicon tube. The spectral response of the 7351 vidicon tube is in the red end of the visible spectrum and peaks at 6200 to 6400 angstroms. The Machlett 7351 vidicon tube has an average sensitivity of 0.1 footcandles face illumination required to produce 650 lines resolution. The DSIF configuration 7351 vidicon tubes are selected tubes with an average sensitivity approaching 0.05 footcandles face illumination required to produce 650 lines resolution.

Figure 50 shows the capabilities of image tube-lens configuration. From this figure it can be seen that the GTS–DSIF system is sensitive to a +4 to +5 magnitude object, dependent on the night-time seeing conditions. Figure 51 shows the star magnitude versus the number of stars available. This data indicates that for night-time tracking there are approximately 700 to 1200 stars, dependent on seeing conditions, available to the DSIF TV system. A study of the problem shows that near the limits of the antenna horizon mask, the TV system capability is degraded by approximately 1 to 1.5 magnitudes. This still leaves approximately 300 to 700 stars, a number quite adequate to permit calibration of the antenna, via star track data, over its entire operating range. The spectral response peak of the vidicon tube is in a region of high atmospheric transmission (for the visible spectrum). In

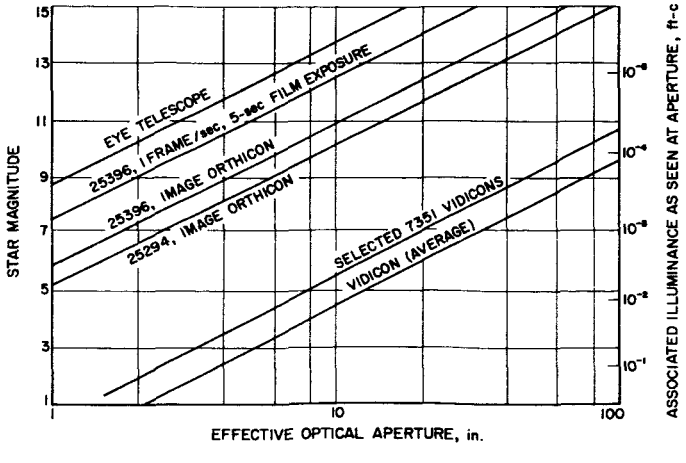

Figure 50. Sensitivity vs aperture size

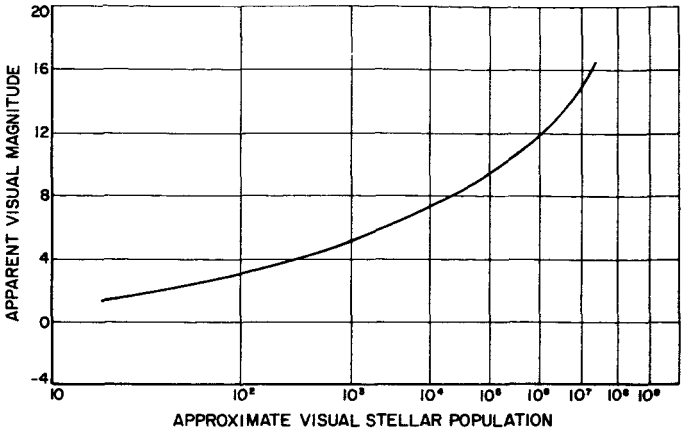

Figure 51. Stellar population

this spectral region scattering effects of the atmosphere are very small; attenuation is due largely to absorption by water vapor molecules. Figure 52 shows the apparent range of intensity of illumination on the earth due to the sun's energy. The night-time sky has an equivalent star magnitude rating of +22. The apparent range in intensities (day to night) is about 10^7. From Equation (1), for the difference in star magnitudes of two objects of intensities I_1 and I_2,

$$\Delta m = 2.5 \log I_1/I_2 \qquad (1)$$

it appears that the day-time sky brightness has an apparent star magnitude of +4.

It becomes evident from the preceding data that the GTS–DSIF TV system configuration should have the following capabilities.

(1) A night-time acquisition and tracking ability of +5 magnitude or brighter target, dependent on seeing conditions and angle from zenith.

(2) A day-time acquisition and tracking ability of about +3.5 magnitude or brighter target dependent on seeing conditions and angle from zenith. The day-time limitation is a result of the apparent sky brightness of about +4 magnitude and the inherent noise of the TV system.

(3) Since the loss of incoming light energy for the spectral response region of the 7351 vidicon tube is due largely to absorption by water vapor molecules with very little scattering loss, it would appear that the TV system should be capable of tracking through overcast or cloud coverage.

(4) Adequate for evaluation and calibration purposes as there are more than enough stars available for

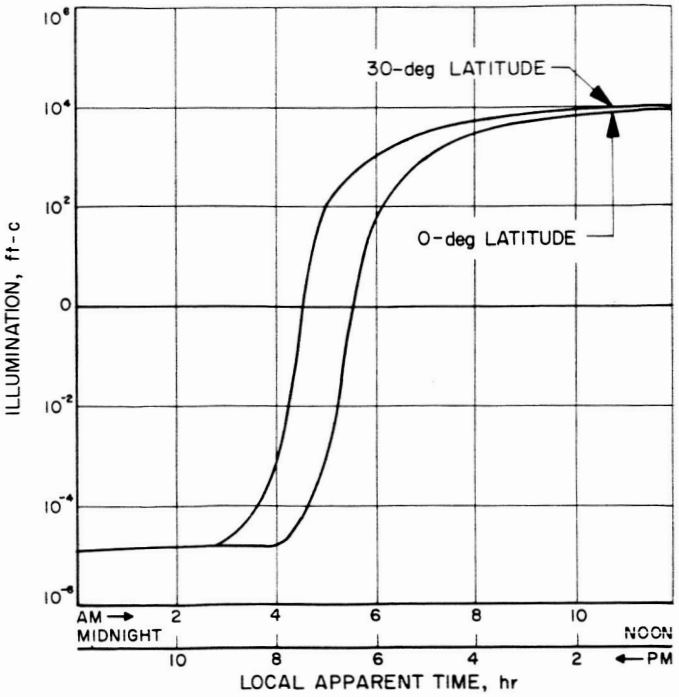

Figure 52. Earth illumination at summer solstice

both day- and night-time data acquisition (somewhere between 300 and 700 fairly evenly distributed across the sky).

(5) The ability to track Venus during the day-time. Venus has an apparent magnitude of about −4 as it approaches inferior conjunction (±3 months). However, the ability to track Venus very near inferior conjunction appears to be borderline, for at inferior conjunction, Venus is within about 7 degrees of the sun. The apparent brightness of the sun's aureole, at 7 degrees from its center, is about −3.8 magnitude.

To verify the predicted performance, field tests were made at the Goldstone tracking station.

On February 2, 1961, Vega was tracked (0.1 magnitude) into daylight (5 to 7:30 am local time) to determine proper TV system settings for day-time tracking. At 6:15 am the sky became overcast and depth of overcast increased until star was lost at 7:30 am. A check with the Edwards Air Force Base weather station disclosed that the depth of overcast, in the Goldstone area, was about 8000 ±2000 feet. At about 10:00 am Venus (−4 magnitude) was acquired in about 1 minute (which included tape drive and offset input time). The weather was heavily overcast, the signal was positive, and Venus was tracked until about noon. The cloud cover from the Edwards weather station data was base at 15,000 feet, top at 38,000±5000 feet, an average depth of 23,000 feet. Coverage composed of Alto-Stratus and Cirrus-Stratus merging (solid, no holes).

Vega was again acquired on February 3, 1961, at 6:30 am and tracked until 7:30 am with f/22 filter. Figure 53 shows Vega using f/8 filter. At 9:30 am Cygni was acquired (2.3 magnitude). At 10:00 am Venus was acquired (Fig 54) and was tracked until noon. At 12:00 pm Venus was acquired with the broad field of view (3-degree) acquisition TV.

On February 23, 1961, tests were run at the transmitter site. The transmitter site TV system has a capability of approximately one magnitude less than the receiver site, due to the RF screening in front of the lens aperture, required to prevent jamming of the TV system during

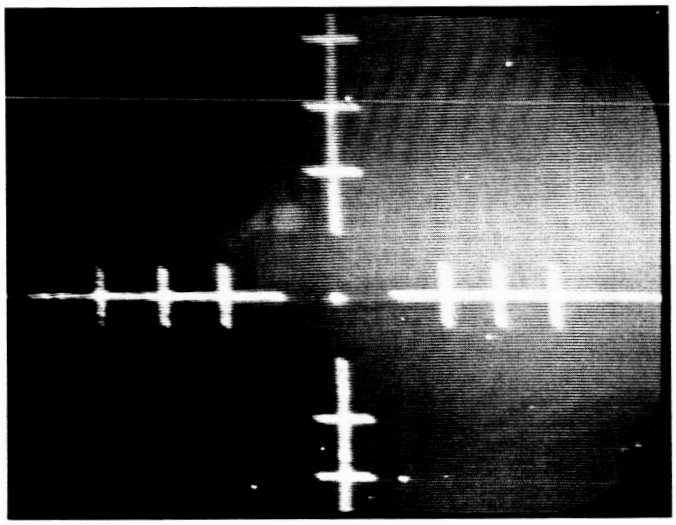

Figure 53. Morning track of Vega

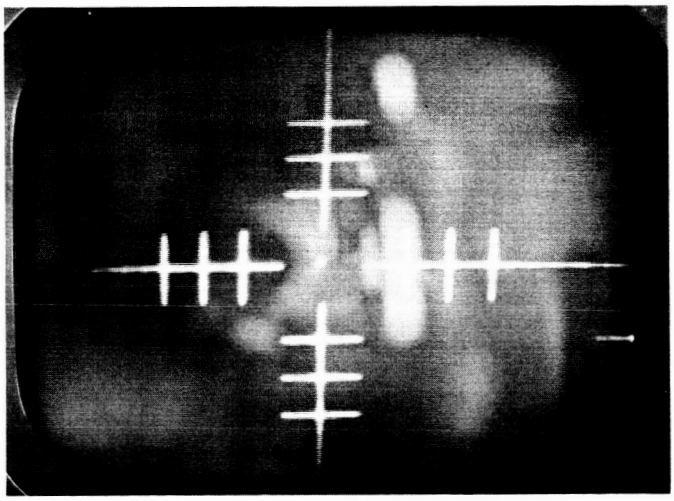

Figure 54. Day-time track of Venus

transmitting periods. A +0.9-magnitude star was acquired and tracked in the day-time; Venus was also tracked.

Based on the experimental results obtained and the approximate analysis, the TV system has the following capability: At night-time, a star of +5 magnitude or brighter can be acquired and tracked. In the day-time, acquisition and tracking capability in apparent star magnitudes at zenith is +3 magnitude or brighter at 30 degrees or more from the sun. The system is capable of seeing through some cloud coverage. Figure 55 is a presentation of the possible curve for this seeing capability for various star magnitudes. The system is apparently capable of tracking Venus to and through inferior conjunction with the aid of optical filters. The system is capable of acquiring and tracking a sufficient number of stars, day or night, to afford adequate calibration data for the DSIF antennas. If greater sensitivity is desired, this can be achieved by introduction into the system of more advanced tubes with increased sensitivities such as the Ebicon, Super-Ebicon, and Astracon tubes.

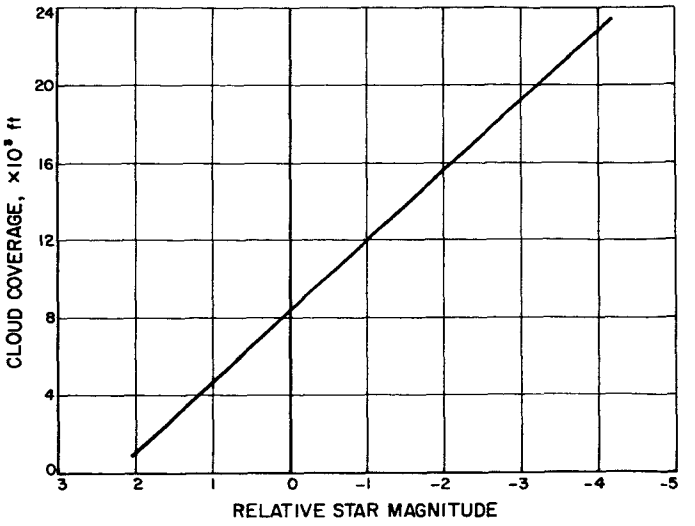

Figure 55. TV system seeing capability through cloud coverage

6. *Transmitter and Receiver Oscillators*

The 2388-mc receiver must be continuously and accurately tuned to maintain the doppler-shifted, Venus-reflected signal in the narrow passband of the receiver. This is accomplished during nonsynchronous reception by adding a synthetic doppler component to the receiver local oscillator frequency (*RS 36-7*, Vol I, pp 73–77). The added UHF doppler component is continuously compared with the computed UHF doppler data obtained from the Venus Ephemeris. Both are displayed on a digital readout in real time at 10-second intervals. If it is assumed that the computed data agrees to within a few cycles of the actual UHF doppler shift and that the reflected signal is specular and above receiver threshold, the receiver should automatically drop into lock when the operations switch is thrown to the synchronous receiver position. Thus, accurate programming of the receiver local oscillator provides a stable acquisition system for phase-coherent reception. Evaluation tests made with lunar-reflected signals, where the Ephemeris is accurately known, have confirmed this operation, and no difficulty has been experienced in switching from nonsynchronous to synchronous operation at signal levels near threshold.

a. Control operations. Closed-loop digital tracking has been planned for controlling the local oscillator frequency. However, since the digital equipment was not immediately available, a manually operated, aided-track system has been used initially for the Venus experiment. The problem of the operator attention required to control the local oscillator frequency so as to match the computed UHF doppler data continuously to within a few cycles has been alleviated by inserting rate information into the manually operated system by means of a motor-driven potentiometer. (The variable dc voltage from the potentiometer controls a 475-kc, voltage-controlled bias oscillator; see *RS 36-7*, Vol I, pp 75–77.)

The dc control characteristics of the 475-kc, voltage-controlled bias oscillator are shown plotted in Figure 56. The average slope is 10 cps/volt or 0.13 cps/deg rotation of the motor-driven potentiometer. The rotational speed of the motor-driven potentiometer is manually varied by changing the frequency of a 1-cps pulsed oscillator. The resultant control characteristic is shown in Figure 57. Two speeds are available, covering doppler rates from 1 to 40 cps/min. This range covers 95% of the expected doppler rates for any one transit of Venus. Slower rates may be accommodated by switching off the motor and matching the readouts at discrete intervals manually. Little difficulty has been experienced with tracking either Venus or the moon with a 1- to 2-cycle error, corresponding to a tuning accuracy of 1 part in 10^9.

b. Equipment and installation. The installation of the Atomichron at the Goldstone transmitter site is shown in Figure 58. The Atomichron has been installed in a shielded room to insure extremely low-leakage fields from the RF units that range over a band of frequencies from 100 kc to several kilomegacycles. An in-lock alarm signal informs studio personnel of the stability status of the 1-mc Atomichron reference signal from which is derived the 31.840000-mc synthesized LO signal. The 31.840-mc synthesizer and the transmitter oscillator, with the required

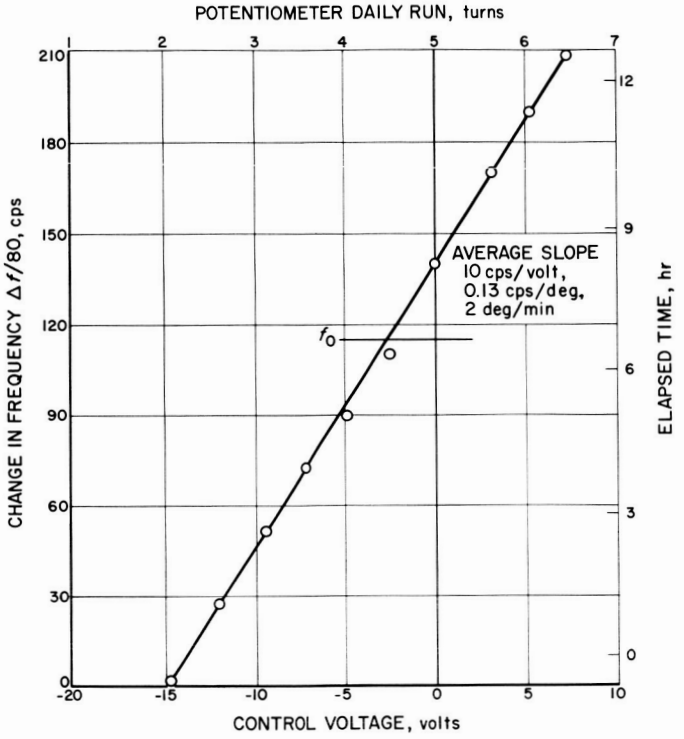

Figure 56. VCO characteristics

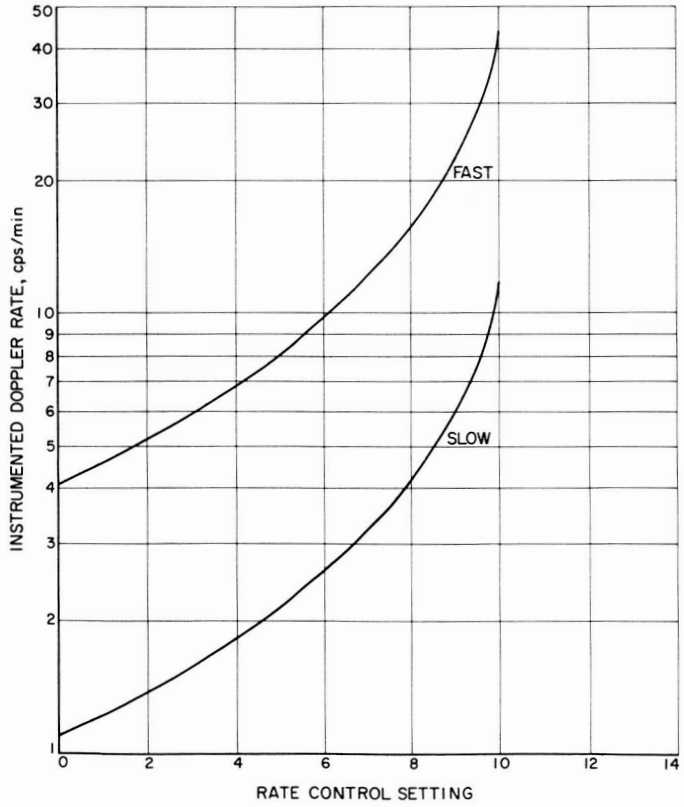

Figure 57. Pulsed oscillator rate control characteristics

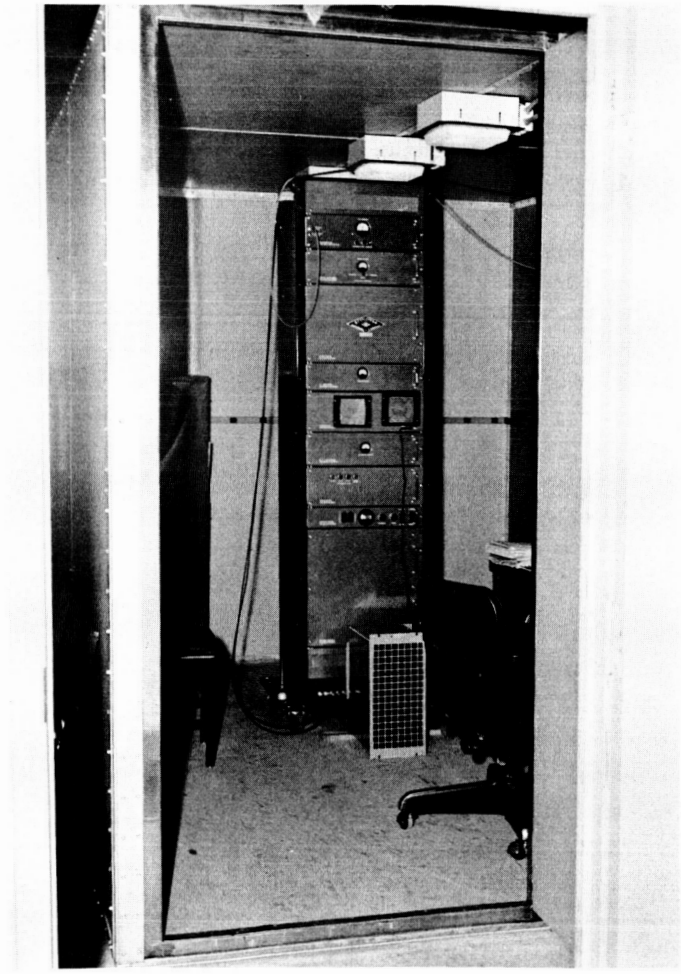

Figure 58. Atomichron installation at Goldstone

instrumentation for determining the lock status, are shown in Figure 59.

Figure 60 shows the two racks that contain equipment for programming and controlling the receiver local oscillator. The left-hand rack contains the local oscillator programming equipment and the filters for determining the bandwidth of the synchronous receiver (Fig 61). The right-hand rack includes the programmed tape-operated digital equipment and the digital readouts. Relay-operated switches permit synchronous or nonsynchronous receiver operation and receiver bandwidth selection from the control panel. The only serious difficulty experienced with the installation of the local oscillator equipment at Goldstone has been heat. Failures due to overheating of components ranged from a klystron failure in the Atomichron to transistor malfunctions in the digital equipment. A generous distribution of cooling fans solved this problem.

The oscillator instrumentation described above has demonstrated a technique for stabilizing the frequency of a UHF radio system with an atomic frequency standard. A technique has also been demonstrated for extremely accurate control of receiver local oscillator tuning to accommodate the time-varying doppler shift on a Venus-reflected VHF signal.

7. 2388-mc, Low-Noise Parametric Amplifier

The original 2388-mc receiver at the Goldstone tracking station has an effective noise temperature of 1580°K, which is typical of crystal mixers at the present state of the art. A fieldworthy low-noise, 2388-mc preamplifier was developed (*RS 36-6*, Vol I, p 42) and has now been installed at Goldstone, resulting in a receiver noise temperature of 300 to 400°K. This device can serve either as a principal low-noise amplifier or as the postamplifier following a 2388-mc maser amplifier. The latter configuration is used for the Venus experiment.

The amplifier is a one-port nondegenerate type utilizing a circulator in the signal port. The pump frequency of 9600 mc was chosen to make use of the extremely stable source already available at Goldstone as part of the 960-mc parametric amplifier system (*RS 36-4*, Vol 1, pp 45–47). The parametric element is a silicon varactor diode manufactured by Microwave Associates (Type MA450) and operated at zero bias. The signal port includes dual radial chokes; one is tuned to the 9600-mc pump frequency, and the other is tuned to the 7212-mc idle frequency. Separate controls are provided for impedance matching at the signal, pump, and idle frequencies. Impedance matching at the signal frequency is accomplished with a quarter-wave sliding transformer having a

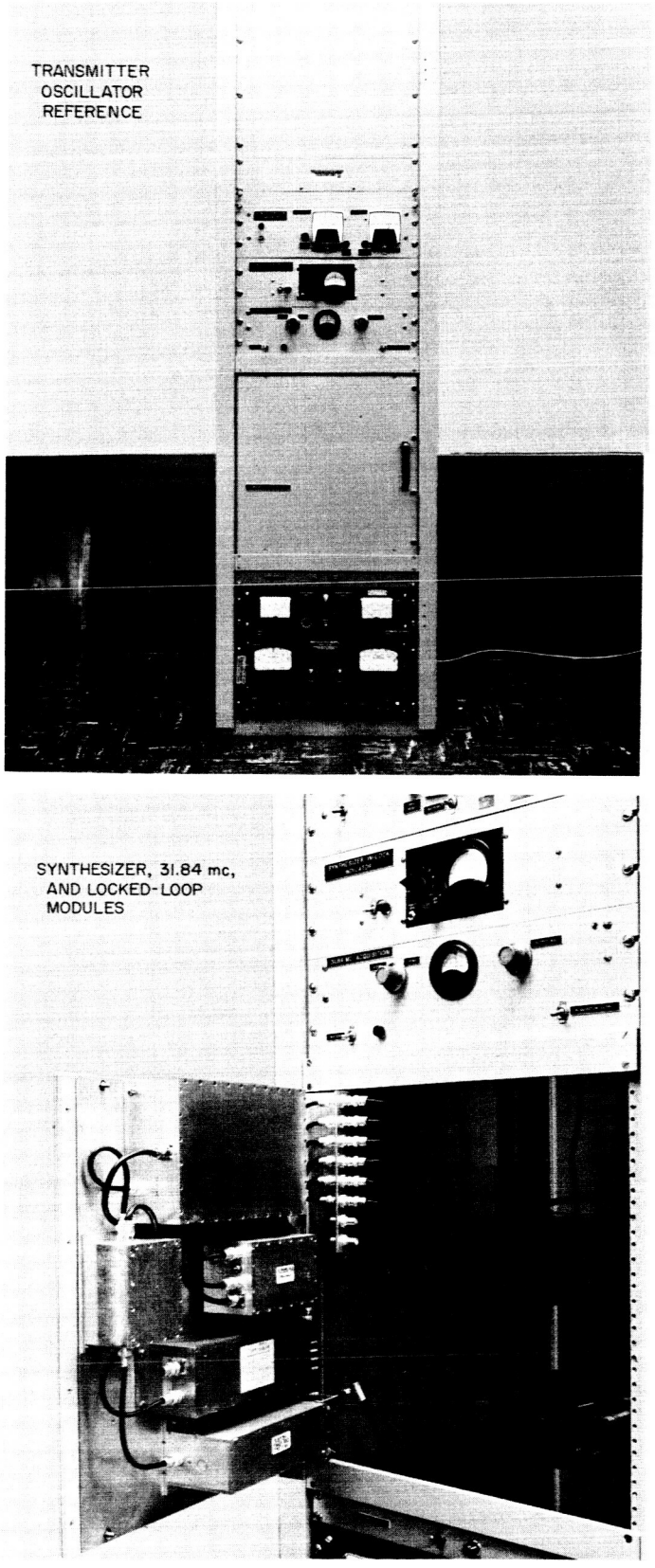

Figure 59. Transmitter oscillator

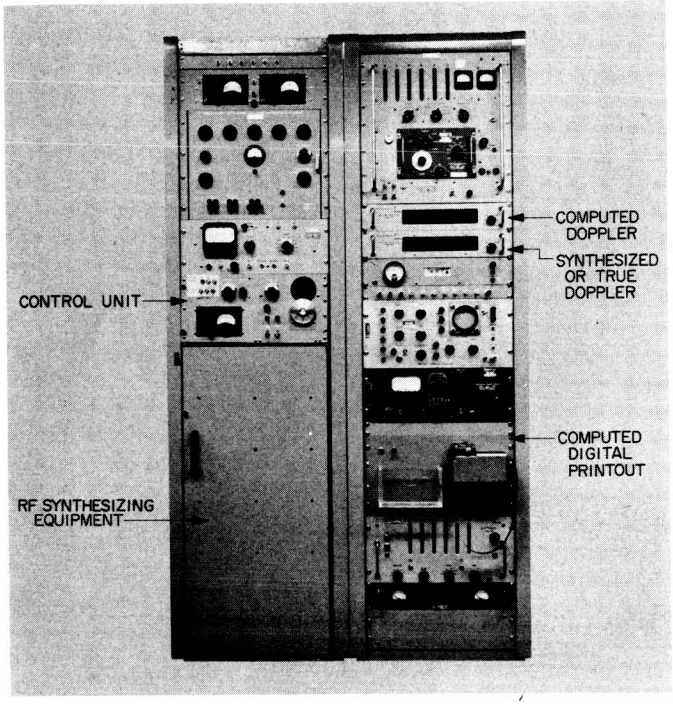

Figure 60. Receiver local oscillator

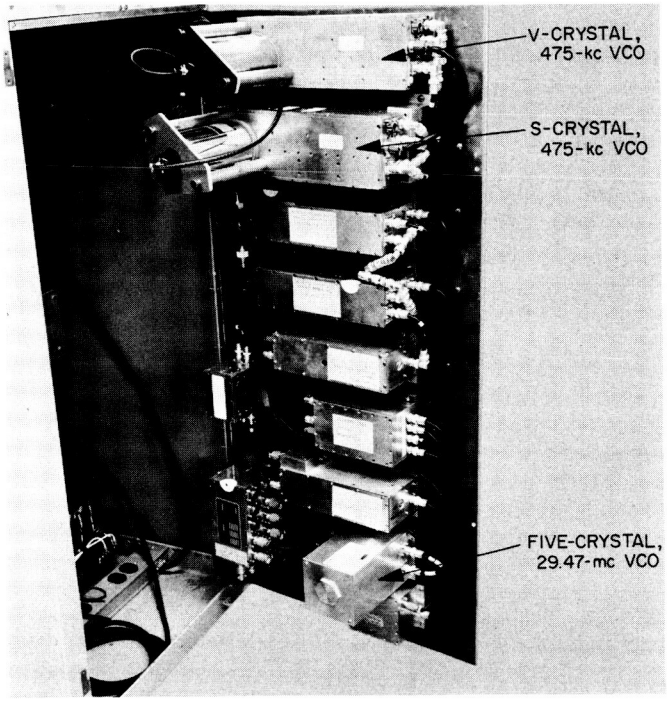

Figure 61. Modules for synthesized receiver local oscillator

characteristic impedance of 15 ohms in a nominal 50-ohm line. At the idle frequency, matching is done with an adjustable waveguide short; and at the pump frequency, with a ruggedized slide-screw tuner.

The amplifier is installed at the feedpoint of the Goldstone receiving antenna in a weather-tight enclosure, insulated from excessive heat loss, and thermostatically controlled to minimize detuning over the ambient temperature range encountered at the Goldstone site. A photograph of the box mounted at the antenna feedpoint is shown in Figure 62. A block diagram and interior photograph of the amplifier were presented in *RS 36-6*, Volume I, Page 42.

The pump source comprises a 32-mc, crystal-controlled oscillator, a $\times 5$ frequency multiplier, a 160-mc amplifier, a $\times 12$ UHF cavity frequency multiplier, a $\times 5$ microwave diode multiplier, and a 9600-mc klystron amplifier. A block diagram of the pump source is given in Figure 63. A photograph of the pump components mounted in a weather-tight enclosure is given in Figure 64. The pump box is installed in the west electronics cage at the rear of the antenna reflector on the 85-foot diameter Ha-Dec antenna along with a second box containing a ferrite current-controlled attenuator and pump power monitor. The pump power indication is repeated remotely in the control room and may be either manually adjusted or automatically maintained at the desired level at the

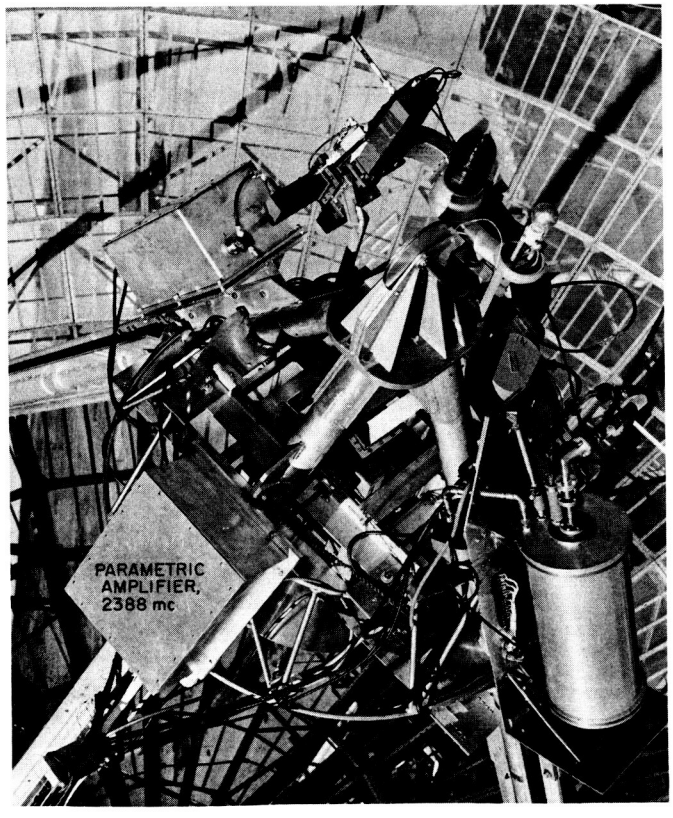

Figure 62. Parametric amplifier

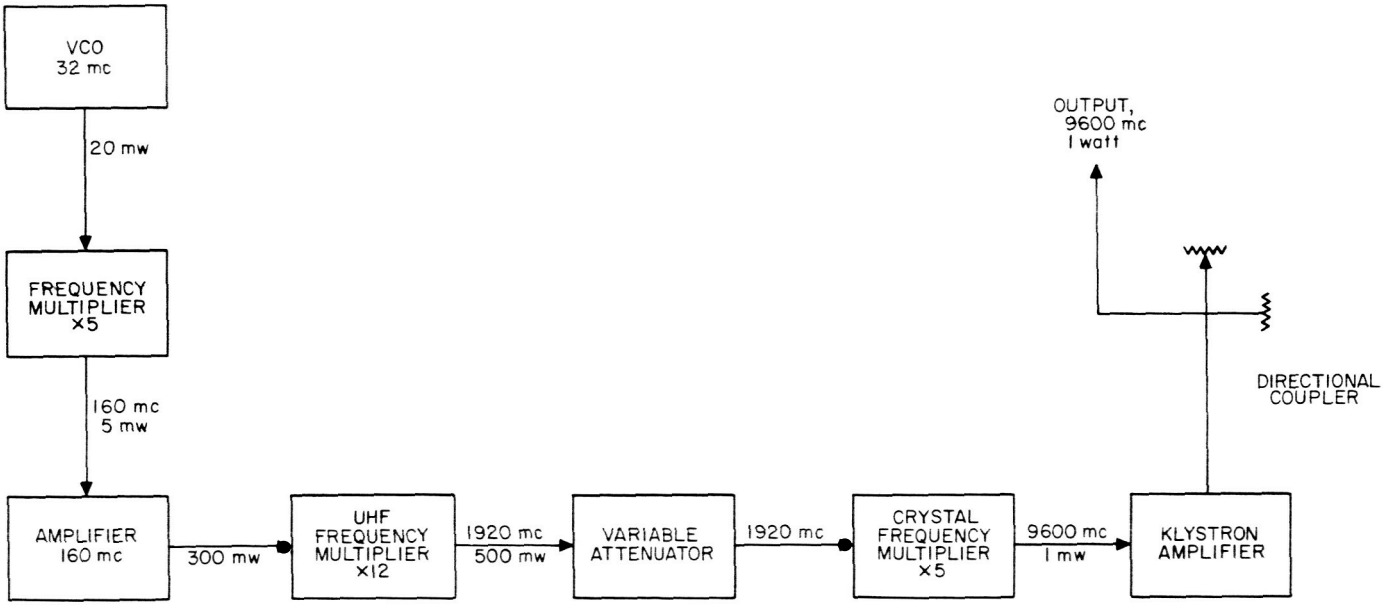

Figure 63. 9600-mc pump source

control room console. The pump power is transmitted from the west cage to the parametric amplifier at the feedpoint through X-band waveguide that is supported along the west quadripod leg.

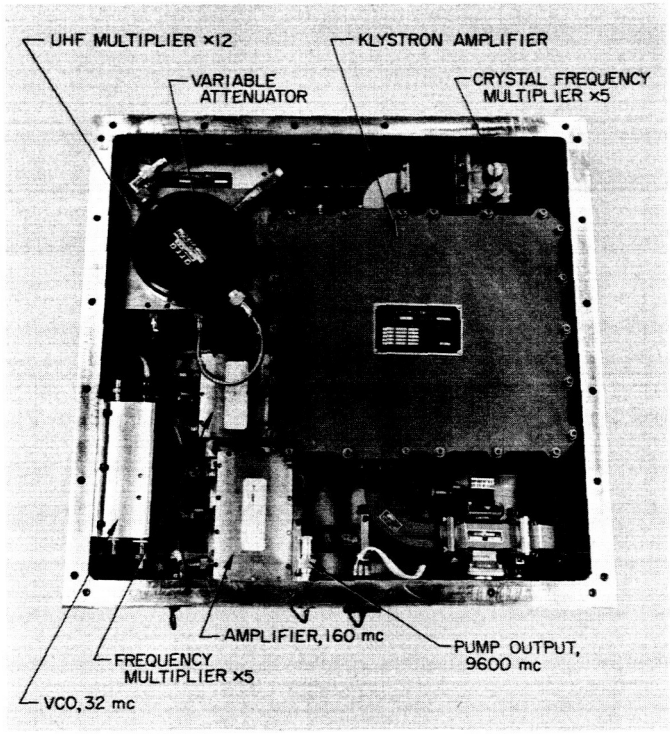

Figure 64. Pump source components

The measured noise figure of the Goldstone parametric amplifier and following system was 3.25 db at 20-db gain, referenced to the parametric amplifier input terminal. This indicates a noise temperature of 322°K. The bandwidth is 5 mc. A space path receiver sensitivity curve was made using the parametric amplifier as the principal low-noise amplifier. The results are given in Figure 65. It is noted that threshold of −159 dbm was obtained. Assuming an antenna temperature of 15°K, an input cable loss of 0.5 db, and a RF loop noise bandwidth of 20 cps, the theoretical threshold is −160 dbm; therefore, reasonable agreement with theoretical performance has been obtained.

Preliminary gain stability checks have been made on the parametric amplifier. The gain drift measured 0.2 db over a 15-minute period while the antenna was oriented in various positions. Less than 0.5-db gain drift was observed over a 45-minute period. It is anticipated that periodic checks of gain and noise figure will be made during the Venus experiment as frequently as operational experience proves to be desirable. The noise figure test equipment installed for the maser amplifier will be used for this purpose.

8. 2388-mc, CW Doppler Radar

a. Functional description. The 2388-mc doppler radar system for the 1961 Venus experiment consists of a highly stable 2388-mc, 10-kw transmitter feeding an 85-foot diameter transmitting antenna and a highly sensitive

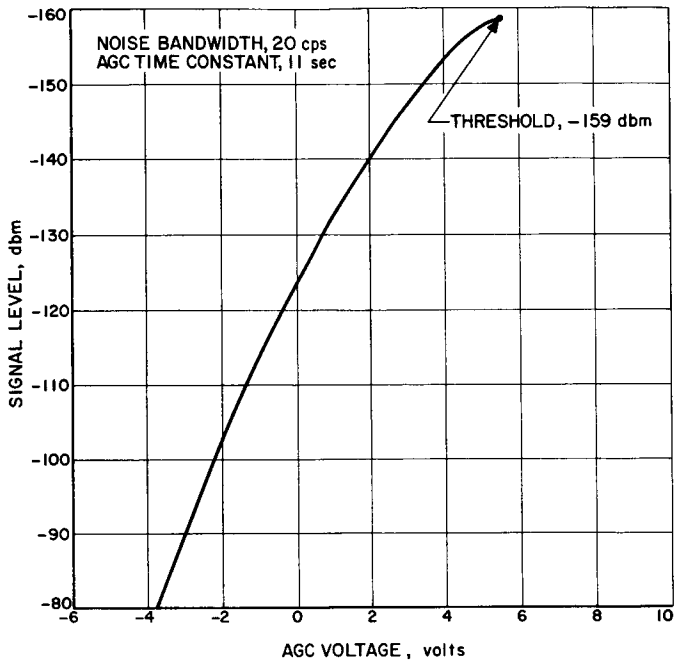

Figure 65. Receiver gain characteristic

receiving system fed by an 85-foot diameter receiving antenna. The function of the transmitter is to illuminate Venus and provide a Venus-reflected signal to the receiving system which is located some 7 miles from the transmitter.

A functional block diagram of the 2388-mc doppler radar is shown in Figure 66. A 31.84 ($31\frac{63}{75}$)-mc phase-stable, crystal-controlled oscillator is slaved to an atomic frequency standard to provide a frequency stability of 1 part in 10^9 or better for the transmitted signal (*RS 36-7*, Vol I, p 73). The oscillator frequency is multiplied to 2388 mc, amplified to a 10-kw power level, and fed to the 85-foot diameter transmitting antenna. At the transmitter site, the 31.84-mc frequency is coherently divided by 64, and the resultant 497.5-kc signal is sent via the microwave relay link to the receiver site to establish coherent reference signals for the 2388-mc receiver.

The synchronous receiver is a narrow-band, phase-coherent double conversion superheterodyne type which obtains its signal from the 85-foot diameter receiving antenna through a low-noise UHF amplifier. The low-noise UHF amplifier consists of a 2388-mc maser amplifier followed by a 2388-mc parametric amplifier. The coherent receiver consists essentially of an RF servo-loop operating at 2388 mc, an AGC loop, a UHF doppler detection system, and two auxiliary channels. One channel synchronously detects the Venus reflected signal and provides an input to the waveform measurement equipment. The second channel provides an input signal to the nonsynchronous receiver. This second channel is also utilized, during synchronous operation, to monitor receiver system gain and noise temperature. The output of this channel is detected (square-law diode detector) and recorded to provide a continuous record of system gain variation. Additional noise (55°K) is periodically introduced into the input of the receiving system from a calibrated noise source through a directional coupler (Fig 66) to provide a record of system noise temperature during coherent signal reception from Venus. During this mode of operation, the 29.85-mc IF amplifier and the second auxiliary channel are operated at fixed gain so that variations in received signal level do not produce corresponding variations in receiver gain due to AGC action. Acquisition of the Venus-reflected RF signal is accomplished by extremely accurate programming of the receiver local oscillator frequency (*RS 36-7*, Vol I, pp 75–77).

The 2388-mc CW doppler radar was originally designed to track the *Echo I* satellite. Waveform equations which describe the operations of the 2388-mc radar were presented in a previous *Space Programs Summary*. The angle error detection portion of the system and the coded ranging subsystem have been deleted since they are not being used in the Venus experiment. Detailed information relating to the various portions of the 2388-mc radar has been presented in earlier reports (*RS 36-1*, Vol I; *RS 36-2*, Vol I, Part 1; *RS 36-3*, Vol I, Part 1; *RS 36-4*, Vol I; *RS 36-5*, Vol I; and *RS 36-6*, Vol I).

b. System design parameters. The characteristics of the 2388-mc CW doppler radar are presented in Table 7. Assuming that the reflectivity of Venus is unity, the received carrier level at the point of closest approach to the earth (inferior conjunction on April 11, 1961) is −153.7 dbm. But 1 month prior to and 1 month following this time, the signal levels will be approximately 6 db less than the above value (*RS 36-7*, Vol I, pp 72–73). Threshold for the RF loop for a receiving system noise temperature of 57°K is −174 dbm for a receiver noise bandwidth ($2B_{L_0}$) of 5 cps. The AGC system has a closed-loop noise bandwidth of 0.03 cps at the 5-cps receiver bandwidth threshold, and the rms gain error is maintained to 0.3 db at threshold.

c. Preparation for experiment. Performance of the 2388-mc CW doppler radar was evaluated, prior to March 10, 1961, with closed signal path and space transmission sensitivity measurements. Closed path measurements were made by feeding a stable crystal-controlled 2388-mc signal to the receiver through the directional coupler normally fed by the calibrated noise source

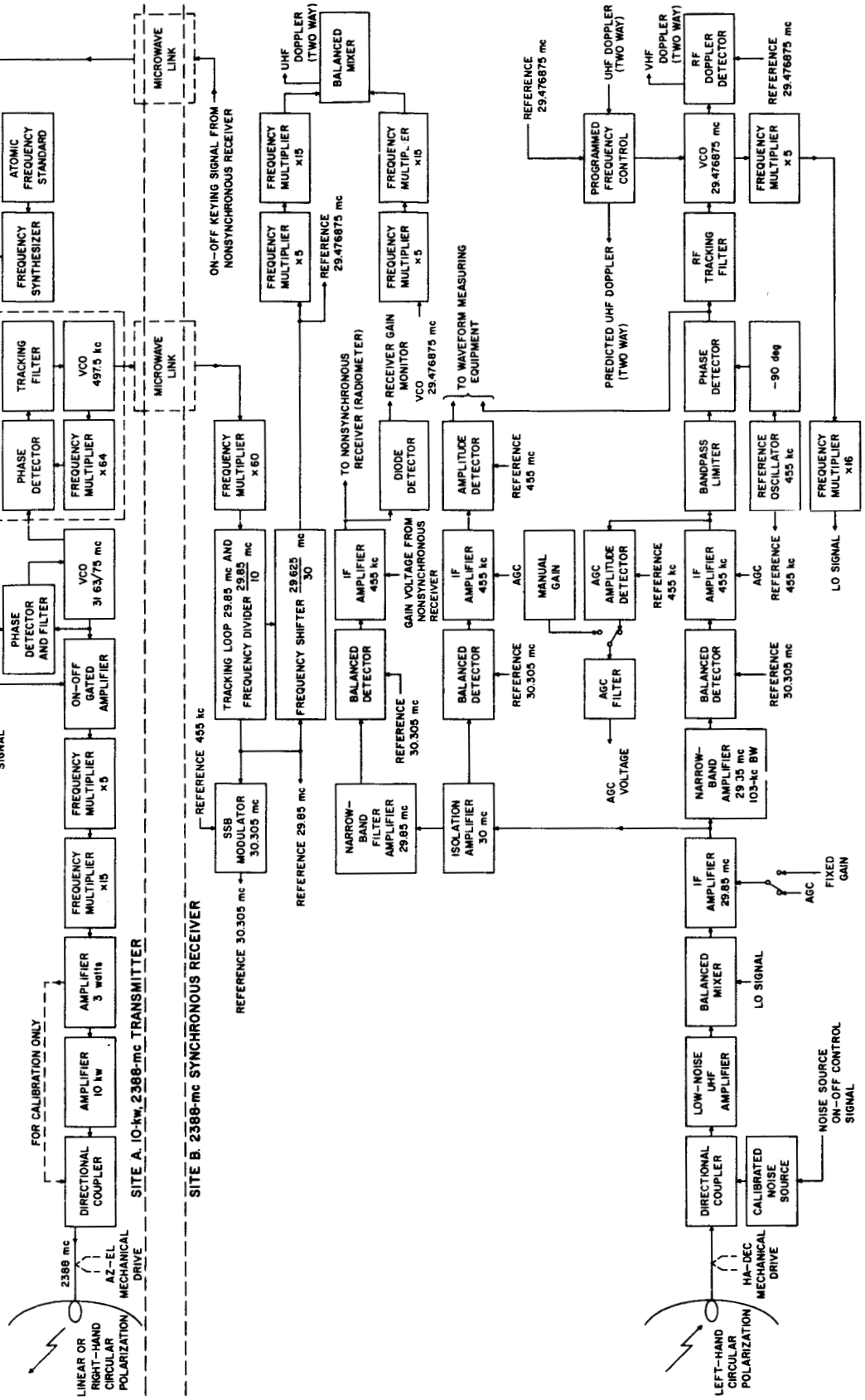

Figure 66. 2388-mc CW doppler

Table 7. Characteristics for 2388-mc CW doppler radar system

Characteristic	System values		
Transmitter carrier power, dbm	—	—	71.14 13 kw
Transmitter antenna gain, db	—	—	53.8
Transmission line loss, db	—	—	0.25
Reflection loss at 26.4 x 10^6 miles[a], db	—	—	−80.3
Space loss at 26.4 x 10^6 miles[b], db	—	—	−251.5
Receiver antenna gain[c], db	—	—	53.5
Transmission line loss, db	—	—	0.06
Receiving system noise temperature[d], °K	—	—	57
Receiver bandwidth $2B_{Lo}$, cps	5	10	20
Receiver threshold, dbm	−174	−171	−168
Receiver prediction bandwidth, cps	500	500	2000
AGC loop bandwidth $2B_{Lo}$, cps	0.03	—	—
AGC loop threshold, dbm	−191	—	—
At 26.4 x 10^6 miles range Received RF carrier, dbm	—	—	−153.7
S/N for RF loop, db	13.1	10.1	9.1
S/N for AGC loop, db	37.3	—	—

[a]Reflectivity of Venus assumed to be unity, diameter of Venus 7954 mi.
[b]Range to Venus at point of closest approach (inferior conjunction).
[c]Antenna gains are based on assumption that polarizations of the two antennas are matched.
[d]Typical measured value with receiver antenna pointed at Venus.

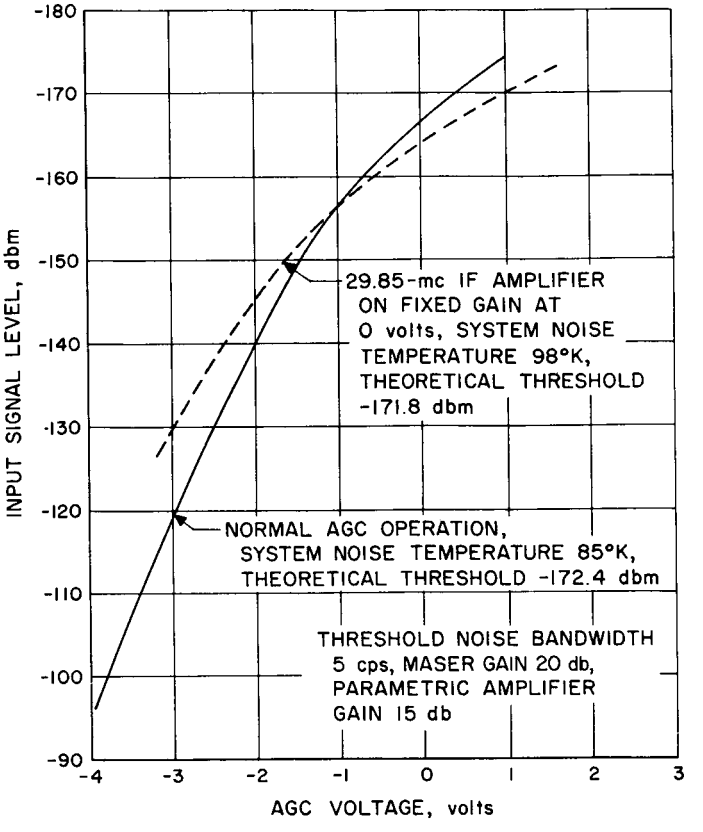

Figure 67. Synchronous receiver sensitivity

(Fig 66). Data of input signal level vs AGC voltage was obtained using precision attenuators between the signal source and the receiver. These closed path measurements provided preliminary data on system performance at signal levels well above threshold. Threshold measurements were not attempted because of the problem of spurious RF leakage.

Space transmission sensitivity measurements were of three types. The first type of measurement consisted of radiating a phase-stable, 2388-mc signal from a collimation antenna at a distance of 5400 feet from the 85-foot diameter receiving antenna. Precision attenuators were inserted in the transmission line between the signal source and collimation antenna to vary the received signal level. Figure 67 presents typical sensitivity curves of input signal level vs AGC voltage for the synchronous receiver. The IF amplifier was operated on normal AGC to obtain the results shown by the solid line. The curve shown as a dashed line was obtained with the 29.85-mc IF amplifier operating with a fixed gain voltage (0 volt). A second type of measurement consisted of illuminating the passive relay link (*RS 36-1*, Vol I) with the 85-foot diameter transmitting antenna to provide a signal to the 85-foot diameter receiving antenna. For this measurement, the 10-kw klystron amplifier was inoperative and the 3-watt exciter amplifier fed the power transmission line to the antenna. Precision attenuators were inserted in the transmission line between the 3-watt exciter amplifier and the antenna to vary the radiated 2388-mc signal power.

A third type of measurement was made with essentially the same equipment arrangement as described above for the second type. In this case, however, both the transmitting and receiving antennas were accurately pointed at the moon to provide a lunar-reflected signal to the synchronous receiving system. Earlier tests, during preparation for the *Echo I* passive satellite (*SPS 37-2*), had demonstrated that threshold measurements made with lunar-reflected signals were in very close agreement with threshold measurements made from the collimation antenna (first type of space transmission measurement). The sensitivity measurements made in preparation for the Venus experiment corroborated earlier measurements.

d. Preliminary performance. Reception of Venus-reflected signals with the nonsynchronous receiver, starting on March 10, 1961, provided data on receiver local oscillator tuning. Phase-coherent reception of a Venus-reflected signal was accomplished at approximately 00:02 GMT on March 23, 1961. The measured doppler shift on

the Venus-reflected signal was greater than the predicted doppler shift by approximately 1 part in 1600. Earlier attempts at synchronous reception of the Venus-reflected signal had been unsuccessful—possibly due to this discrepancy in doppler shift. Up to the time of this writing, phase-coherent reception of the Venus-reflected signal has been successful whenever it has been attempted. Successful phase-coherent reception has been obtained with threshold noise bandwidths of 5, 10, and 20 cps.

At the time of the first successful phase-coherent reception (March 23, 1961), the synchronous receiver was operating with a 5-cps threshold noise bandwidth, transmitter power was 12.8 kw, and the distance to Venus was approximately 49.7×10^6 km (30.88 million miles).

B. Digital Communications Techniques

1. Ranging Subsystem

a. History of ranging experiments. A series of radar ranging experiments was conducted at Goldstone during the period October 1960 through January 1961. The overall objective of these experiments was to combine the various parts into an operating system and to test the resulting system in actual ranging operations using convenient earth satellites. The *Echo* satellite was chosen for the first object to be ranged because it gave a large return signal and was often optically visible, making it easy to acquire. After some preliminary difficulties in getting the parts of the system to work properly together, the first successful ranging was performed on *Echo* Pass 1107 on November 11. After 1 minute and 20 seconds of range tracking, the range lock was deliberately broken and re-established. After an additional 2 minutes and 40 seconds of range tracking, RF lock was lost momentarily. When the RF lock was re-established, the ranging code was acquired again and another 30 seconds of ranging tracking obtained. Preliminary analysis and comparison of the data with the Ephemeris showed that actual ranging had occurred on all three acquisitions.

The following week, a successful ranging pass was obtained on November 17, followed by four consecutive passes on November 18. One of these passes had over 11 minutes in unbroken range tracking, and all four passes had the vernier operating for the entire time. However, in analyzing the data from these passes, it became evident that the range tally was counting the RF doppler with a wrong scale factor. Re-examination of the system showed that while the ratio of the RF VCO frequency in the receiver to the clock VCO frequency in the receiver was indeed 59¼ to 1, the ratio of the dopplers on these two frequencies was 60 to 1. The range tally had been designed using the 59¼ to 1 ratio.

Another set of four passes was obtained on November 23, this time without the vernier except for a short test section on the first pass.

It was desired that the vernier portion of the ranging system be tested, so the range tally, including the vernier, was redesigned and modified to include the correct ratio of dopplers, and another series of tests was run in January. By this time the *Echo* orbit was not being determined with sufficient precision for satisfactory acquisition, and the satellite was not often visible; therefore, another target was sought. The Goddard Space Flight Center was able to provide accurate Ephemerides for the *Courier* satellite, and the addition of a low-noise parametric amplifier had increased the sensitivity of the receiver by an amount sufficient to permit the tracking of a *Courier*-reflected signal; therefore, the *Courier* was selected as the target. Because of the low level of the returned signal, the operating procedures had to be refined; but after this was done, five successful ranging passes were obtained: one on January 30, three in succession on January 31, and one on February 1. The vernier was in operation on all of these passes.

b. Analysis of* Echo *ranging data. The *Echo* passes for which ranging data was obtained are listed in Table 8. These passes fall naturally into three groups, as shown in the table. In the following discussion of results, the data from each group is treated separately.

Passes 1107 and 1185. For these *Echo* passes, the experimental range r from the Ha-Dec site, in meters, was computed from the formula

$$r = \frac{R^2 - D^2}{2\left[R + D\cos\left(\Omega - z_1\right)\cos\beta_1\right]}$$

where D is the straight-line distance between the antennas of 10,705 meters (constant), Ω is the azimuth angle of the line between receiver and transmitter of 338.56583 degrees (constant), z_1 is the azimuth of the satellite in degrees, β_1 the elevation of the satellite in degrees, and R the range from the Ha-Dec site plus the range from the Az-El site in meters. The respective values of r were then compared with the Ephemeris prediction ranges r_E. The

Table 8. *Echo* passes ranged by Goldstone Tracking Station

Pass Group	Pass No.	Date	Greenwich mean time, hr: min	Ranging time, min: sec		Comments
				Without vernier	With vernier	
1	1107	11 Nov	10:40	01:20	—	First good ranging, isolated pass
				02:40	—	
				00:30	—	
	1185	17 Nov	11:54	02:00	—	Good ranging, isolated pass
2	1193	18 Nov	03:04	—	03:50	All of these passes have only vernier data and, because of the design error in the vernier, produced only non-reducible data
	1194	18 Nov	05:08	—	11:30	
	1195	18 Nov	07:14	—	01:40	
	1196	18 Nov	09:22	—	02:20	
3	1248	23 Nov	02:38	00:50	02:00	Resolution of ±1 clock cycle ambiguity possible because of three acquisitions on one pass
				01:40	00:40	
				01:20	—	
	1249	23 Nov	04:46	01:34	—	Good data except for possible ±1 clock cycle spurious count
	1250	23 Nov	06:54	01:56	—	
	1252	23 Nov	11:01	00:16	—	Data bad, apparent equipment malfunction
				02:22	—	
				02:56	—	

values of r and r_E have been plotted in Figures 68 and 69 for the ranging portions of *Echo* Pass 1107 and in Figure 70 for the ranging portion of *Echo* Pass 1185

It is apparent from these graphs that for each pass there is an appreciable error between r and r_E. However, it is equally apparent that the plots for r and r_E are in

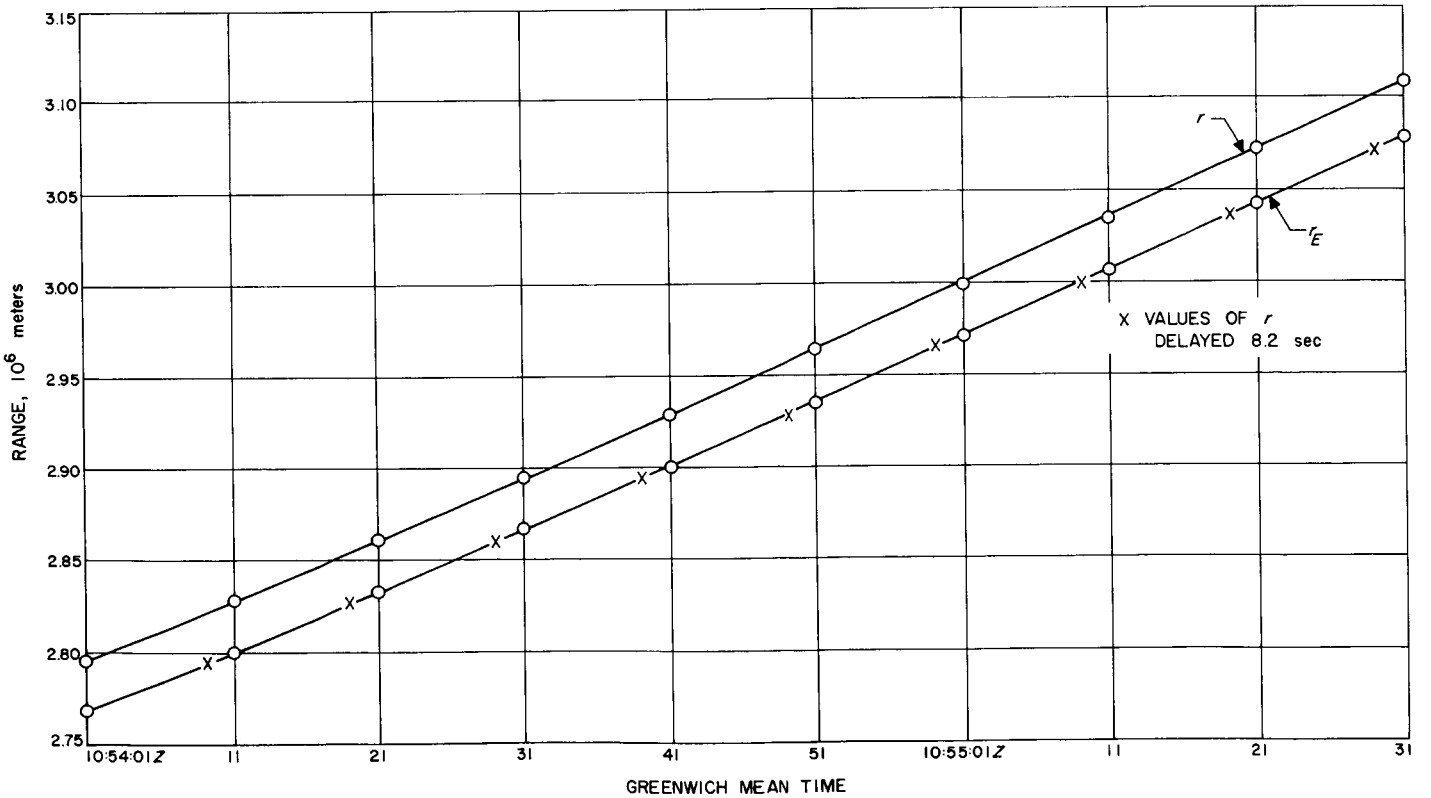

Figure 68. *Echo* Pass 1107, first ranging

essence parallel; i.e., the error is constant to a first approximation. This leads one to believe that a time discrepancy exists between the predicted and measured ranges. The fact that on more than one occasion, before and since, orbital predictions had been found to be off in time by as much as 42 seconds while being correct otherwise lends support to this belief.

Two ranging portions exist for Pass 1107, between which a new RF acquisition took place. The time displacement for the first portion was estimated graphically to be 8.4 seconds. The time displacement for the second portion was estimated graphically to be 8.0 seconds. Obviously, any time error for a given pass must be constant. Therefore, an error of 8.2 seconds was assumed for this pass. Values of r, delayed by 8.2 seconds, were then marked on the graphs by crosses and found to be in excellent agreement with values of r_E.

For Pass 1185, the time displacement was estimated graphically to be 1.6 seconds. Values of r, delayed by 1.6 seconds, were then marked by crosses and found to be in excellent agreement with values of r_E.

Passes 1193, 1194, 1195, and 1196. These *Echo* passes represent some of the best tracking that has been done. Unfortunately, it is not possible to reduce the data since only vernier data with erroneous weighting was obtained. This situation exists because the range measurement is made in essentially two parts. The first part is to acquire the range code and establish a reference range. The second part is to keep the range up to date by counting doppler. In these passes, the reference point was not recorded. It was correct when it was obtained, but it was not recorded. The increments obtained can be corrected for the erroneous scale factor, but the initial point is lost. Checks of the internal consistency of the data and checks against the doppler show that, except for the erroneous scale factor, the system was working well.

Passes 1248, 1249, 1250, and 1252. The first three of these *Echo* passes were good passes. While preparing for

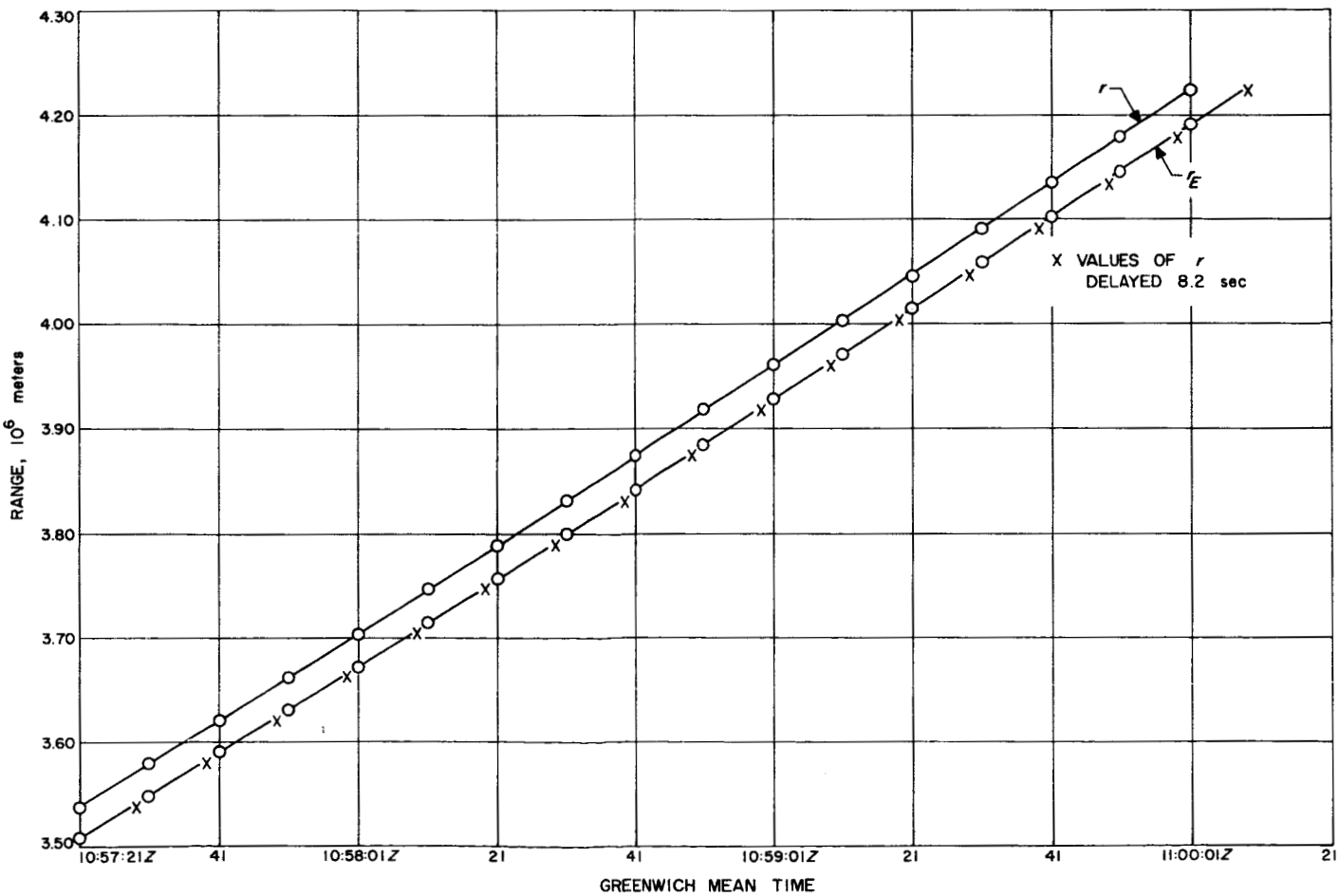

Figure 69. *Echo* Pass 1107, second ranging

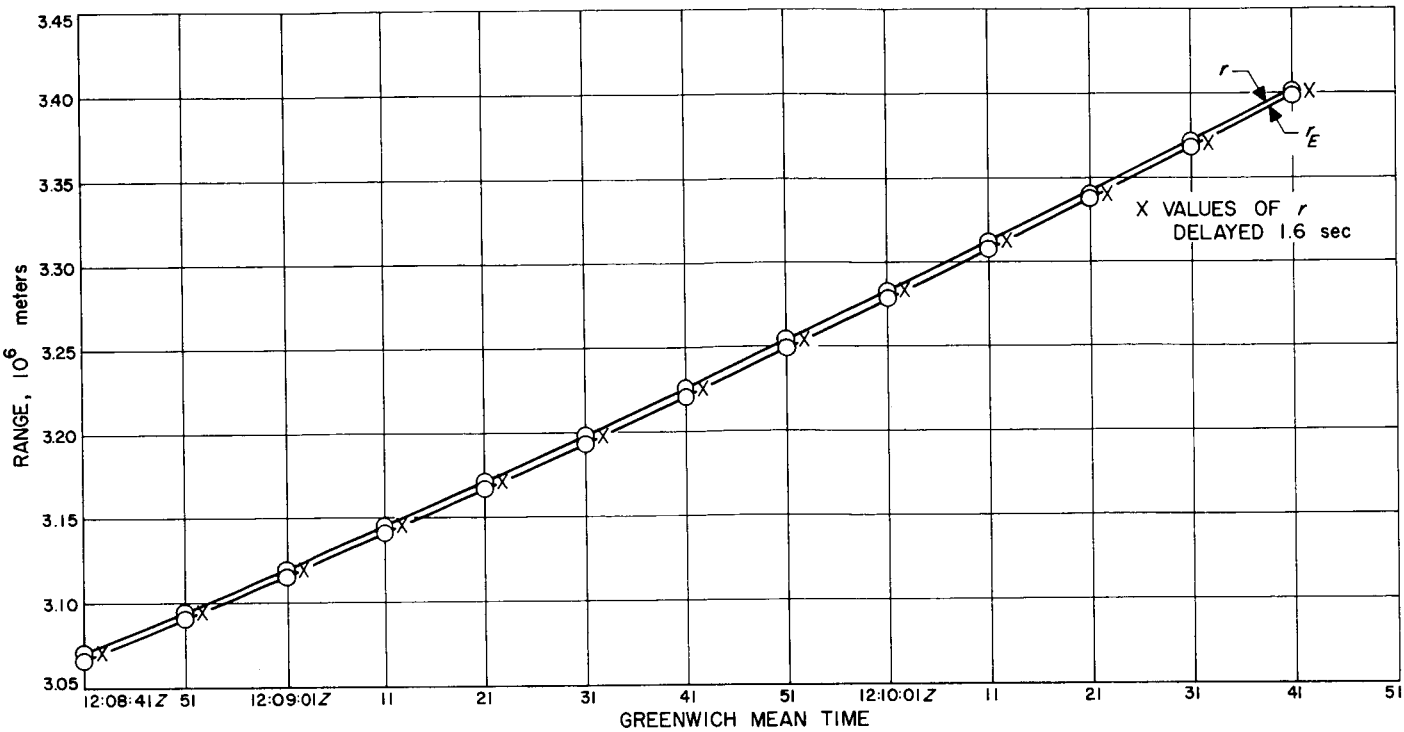

Figure 70. *Echo* Pass 1185

the fourth pass, something in the system changed drastically. Attempts were made to rephase, but the fourth pass was not ranged because it was not possible to acquire the range code over the passive link; only RF tracking was done during the fourth pass. By the time of the fifth pass, the situation (which was not, and still is not, understood) was rectified sufficiently so that the range code could be acquired over the passive link, but not reliably. The ranging of the fifth pass is not good, partly because of the unexplained difficulty already mentioned and partly because of what appears to have been a malfunction in the range tally. Because of these difficulties, the data reduction has been restricted to Passes 1248, 1249, and 1250

An orbit was fitted to the angle and doppler data from these passes, using the IBM 7090 computer. From the orbit, the range to each of the sites was computed. The range measurement was compared with these computed ranges for all times for which good ranging data was available. The error was computed for each point, and the means and standard deviations for each acquisition were determined. These are given in Table 9.

The comparison was made in terms of the average of the ranges to each of the two antennas, with the error being the measured quantity minus the computed quantity. The increment for the measured quantity is one clock cycle or 301.33 meters. Only two of the errors differed from the mean error by more than the increment, and they were differences of 304 meters and 303 meters. These are easily explainable as one increment plus a small error in the calibration. Checks were also made of the first and second differences of the ranges; it was found that they were in increments of 301 meters and smooth. The increments in the range number between each pair of points were compared with the average of the doppler for each pair of points and found to agree within less than the increment of the range number except for one pair where the error is slightly greater than one increment. This particular error is positive, while the errors for the two adjacent pairs are both negative, showing that this particular time interval just caught a count at either end.

Table 9. Results of *Echo* ranging passes

Pass No.	Acquisition No.	Error mean, meters	Error standard deviations, meters	No. of Points
1248	First	−2083	163	6
	Second	−2829	119	11
	Third	−2455	81	9
1249	First	−4152	122	46
1250	First	1677	146	46

The several computations indicate that the data is smooth and self-consistent for each acquisition. However, there is a bias between the measured range and that computed from the angles and doppler. Part of the bias is due to an error in the range tally.

After these tests were run, it was discovered that a wire had been omitted in the range tally, apparently during one of the modifications. This had the effect of introducing a logical error, such that an additional count of one clock doppler cycle might be made at the beginning of a run. This means that all of the range numbers in a given run may be in error by 301.33 meters in either direction.

In Pass 1248, if it is assumed that the first acquisition had a spurious count to make the range 301 meters too high and the second acquisition had a spurious count to make the range 301 meters too low, then the means for the three acquisitions became −2384, −2528, and −2455. If the points in the first and second acquisitions are corrected according to this assumption, the combined mean error is −2464 meters, and no corrected point differs from this amount by more than the increment. There is, unfortunately, no way to tell at this time whether the other two passes have this bias in them.

c. Analysis of Courier *ranging data.* The *Courier* passes for which ranging data was obtained are listed in Table 10. An orbit was computed on the IBM 7090 computer from the angle and doppler data taken in Passes B, C, and D. The computer then determined from this orbit the range to each of the two sites. The average of these two computed ranges was compared with the average of these two ranges as measured by the ranging system with the vernier operative and is given in Table 11. These data points for which the vernier were inoperative were omitted from the comparison. At first glance it appears that the vernier has not improved the measurement accuracy, because it should reduce the increment of range to 5 meters and give a standard deviation of less than 5 meters. An examination of the data shows it to be smooth and to agree with the doppler much better than the large standard deviation would indicate; but the curve of measured range is not just displaced with respect to the curve of computed range but is skewed. The agreement beween the range measurements and the doppler measurement indicates that the difficulty is probably in the computed range. It is known that the computed orbit does not fit the angle and doppler data as well as should be expected.

Table 10. *Courier* passes on which successful ranging was obtained

Ranging period	Date	Greenwich mean time, hr: min	Ranging time, min: sec	
			Without vernier	With vernier
A	Jan 30	22:51	00:02	02:58
B1	Jan 31	18:11	00:26	01:12
B2	——	——	00:08	——
B3	——	——	00:26	——
B4	——	——	00:12	01:40
C	Jan 31	20:05	00:26	02:48
D	Jan 31	21:55	00:06	03:46
E1	Feb 1	19:12	00:32	00:32
E2	——	——	00:16	00:06

Table 11. Results of *Courier* ranging passes

Ranging period[a]	Change in range	Mean error, meters	Standard deviation, meters	No. of points
B1	Decreasing	−6,483	152	35
B2	Increasing	−5,325	380	13
B3	Increasing	−6,002	199	76
C	Increasing	3,721,548	141	76
D	Increasing	−4,715	33	113

[a]Periods described in Table 10.

Pass C is obviously in error, apparently due to a malfunction in the range tally which at some point injected a large spurious number. The small standard deviation indicates that the tracking and vernier were operating well.

Passes A and E were compared briefly to the Ephemeris and found to agree within a few kilometers, although Pass A shows evidence of being skewed also.

d. Conclusions. From the foregoing discussion, the following conclusions may be drawn: (1) The experiments were generally successful in that they showed the basic ideas of the ranging system to be correct and workable. (2) The accuracy of the measurement appears to be good, although it is as yet uncertain just how good. The present uncertainties of a few kilometers in several thousand kilometers are fractions of 1% and may well be due more to uncertainties in the computed orbit than to uncertainties in the range measurement itself. More work is being done to try to obtain a better standard for evaluation of the ranging data.

2. Kineplex Data Transmission System

In the development of digital data transmission systems for use in spacecraft experiments, it is necessary to evaluate the performance of the various systems and make

comparisons which enable the designer to choose the system which best fits his particular need. The theoretical performance of digital systems has been discussed by several authors (Refs 2 through 7). In order to complete the evaluation it is necessary to determine the actual experimental performance of practical systems. An experimental investigation has been initiated at JPL for this purpose. As one phase of the investigation, a complete Kineplex transmit and receive laboratory test set was purchased from the Collins Radio Company. The initial tests of the Kineplex system have been completed and the results are presented in this report.

a. Summary of results. The performance of the ideal Kineplex system is shown by the graphs of Figure 71. The phase reference and bit synchronizing reference were wired directly from transmitter to receiver. The measured performance agreed with the theoretical curve with an average error of 0.23 db rms and a standard deviation of 0.3 db rms. The performance of the system when operating with a locally derived bit synchronization (square data points) appeared to be fully as good as the ideal system over the range of operation.

Normally, the Kineplex system uses a phase reference derived from the phase of the preceding data frame after storage in a resonator. The performance for this mode of operation is shown in Figure 72. The observed data agreed with the theoretical curves with an average error of 0.1 db rms and a standard deviation of 0.14 db rms for the ideal and derived bit synchronization methods.

The graphs of Figure 73 show the performance while utilizing a phase reference which was derived by a servo

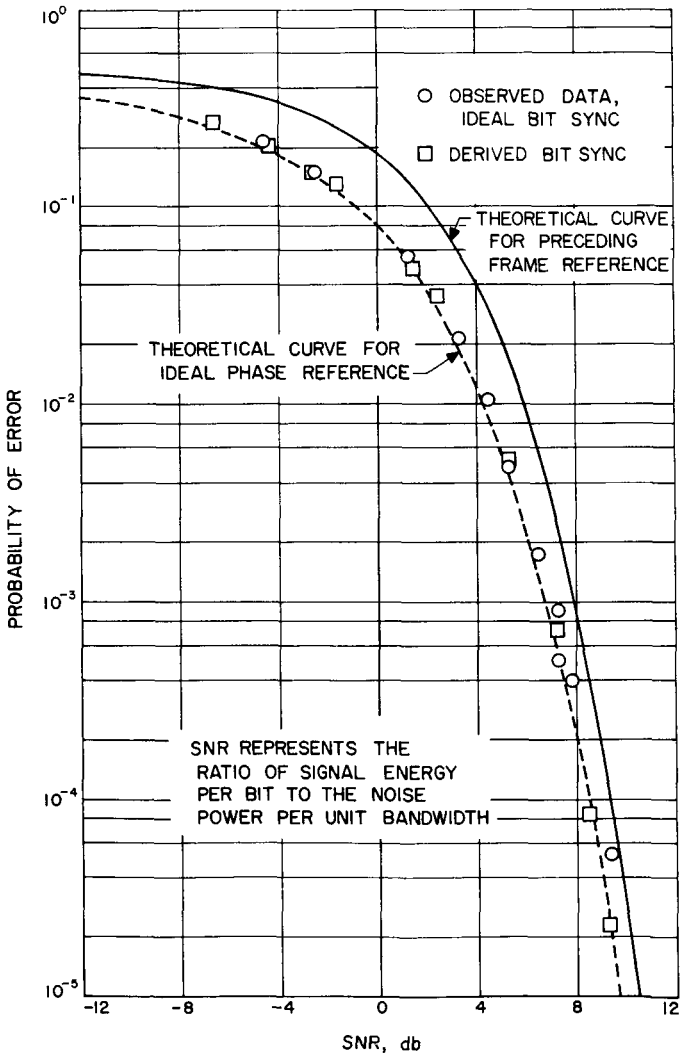

Figure 71. Probability of error vs SNR for the Kineplex system with ideal phase reference

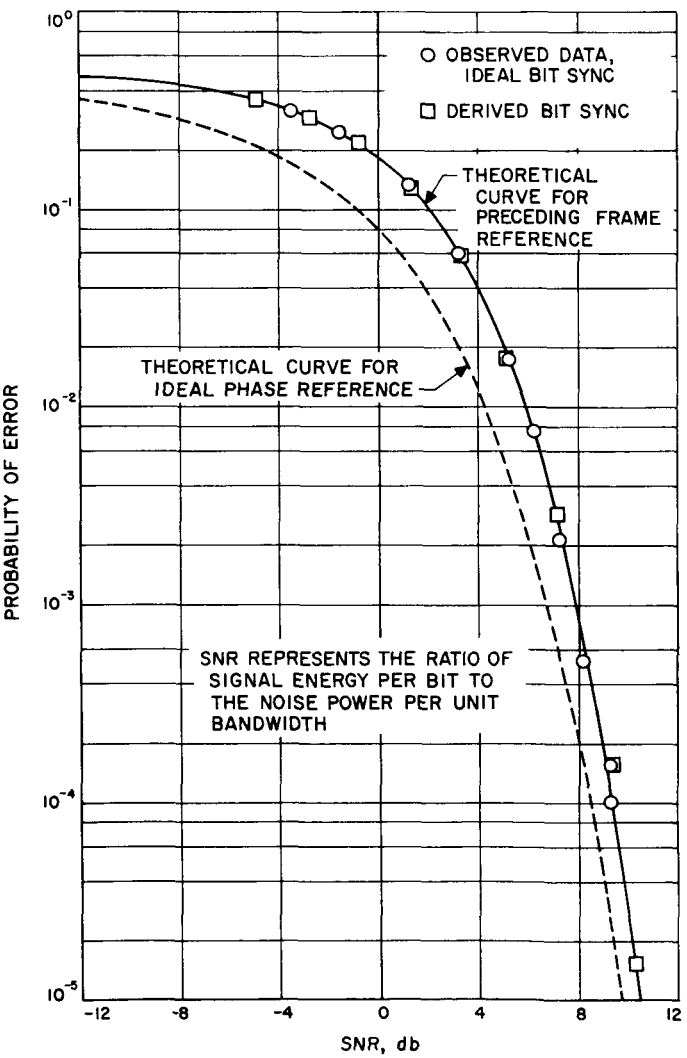

Figure 72. Probability of error vs SNR for the Kineplex system with preceding frame phase reference

in the receiver from the phase of the transmitted signal. For this mode of operation, the performance showed an improvement of about 0.5 db over that indicated for the preceding-frame phase reference system when the SNR values (ratio of signal energy per bit to the noise power per unit bandwidth) were 0 to 9 db. However, for SNR's less than 0 db, the observed data indicates a degradation of 1.5 to 2.0 db relative to the preceding-frame reference system.

b. Description of the experiment. The digital telemetry test system as described in *RS 36-7* was used in this experiment. A photograph of the test setup is shown in Figure 74. In order to provide synchronous data, the test unit data source was supplied with a 45.45-cps square-wave from the Kineplex transmitter. The message data was supplied to the transmitter in sequences of 131,071 bits at the rate of 45.45 bits/sec. In the transmitter, the phase of a 960-cps sine-wave was either advanced or retarded by $\pi/2$ radians in accordance with the *zeros* and *ones* of the input data. This output signal was passed through a precision noisy channel, which mixed the signal and noise with a calculated accuracy of 0.2 db rms, and then passed to the Kineplex receiving system. After detection, the message bits were compared with the original message suitably delayed to compensate for delays in the system. The errors were counted in a 15-stage binary counter. The signal energy per bit was maintained constant throughout the test, while the noise power was varied by means of precision attenuators.

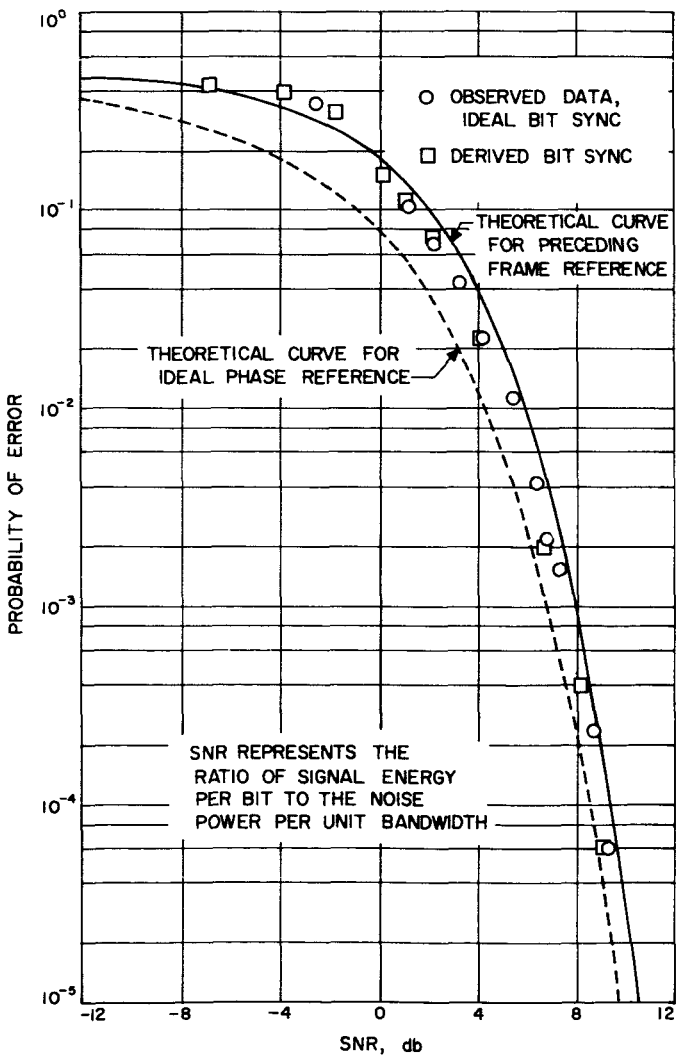

Figure 73. Probability of error vs SNR for the Kineplex system with local phase reference

Description of Kineplex system. The Collins Kineplex transmit and receive terminals designated, respectively, TE 290 A-1 and TE 290 B-1, comprise a single-tone, single-channel binary data transmission station. It uses a 960-cps carrier with ± 90-degree phase shifts representing data *zeros* and *ones*. The name Kineplex is derived from the detection technique which utilizes kinematic filtering and from the fact that the equipment is generally used for providing multiplex operation. Figure 75 shows a close-up of the receive terminal mounted in a standard rack. This shows the front panel with controls, input and output jacks, and indicator lights. The major proportion of circuitry is constructed on tiny modules which are mounted on plug-in panels. The photograph shows one of the panels extended by means of an extension plug which permits troubleshooting procedures while the equipment is operating.

The simplified block diagram of Figure 76 describes the functional operation of the system. In the transmitter, a 3840-cps, crystal-controlled oscillator drives a quadrature phase generator which provides four 960-cps, square-wave signals which are displaced in phase by $\pi/2$ radians. The output of the digital phase selector is a 960-cps square wave which is phase shifted either $\pi/2$ or $-\pi/2$ radians with respect to the phase reference at 22-millisecond intervals in accordance with the binary input data. When the system is operating in the ideal phase reference mode, the phase reference in the transmitter is shifted -90 degrees after each bit is transmitted (Refs 8, 9). When operating in the modes described as local phase reference and preceding-frame phase reference, the phase of the preceding bit is used as the reference. The encoded 960-cps square wave is then filtered and passed through the precision noisy channel to the receiver.

In the receiver, the encoded 960-cps signal is balanced modulated with a stable 20,975-cps reference to provide the 21,935-cps signal required to pass through the narrow-band, matched-filter system. The keyed filters are

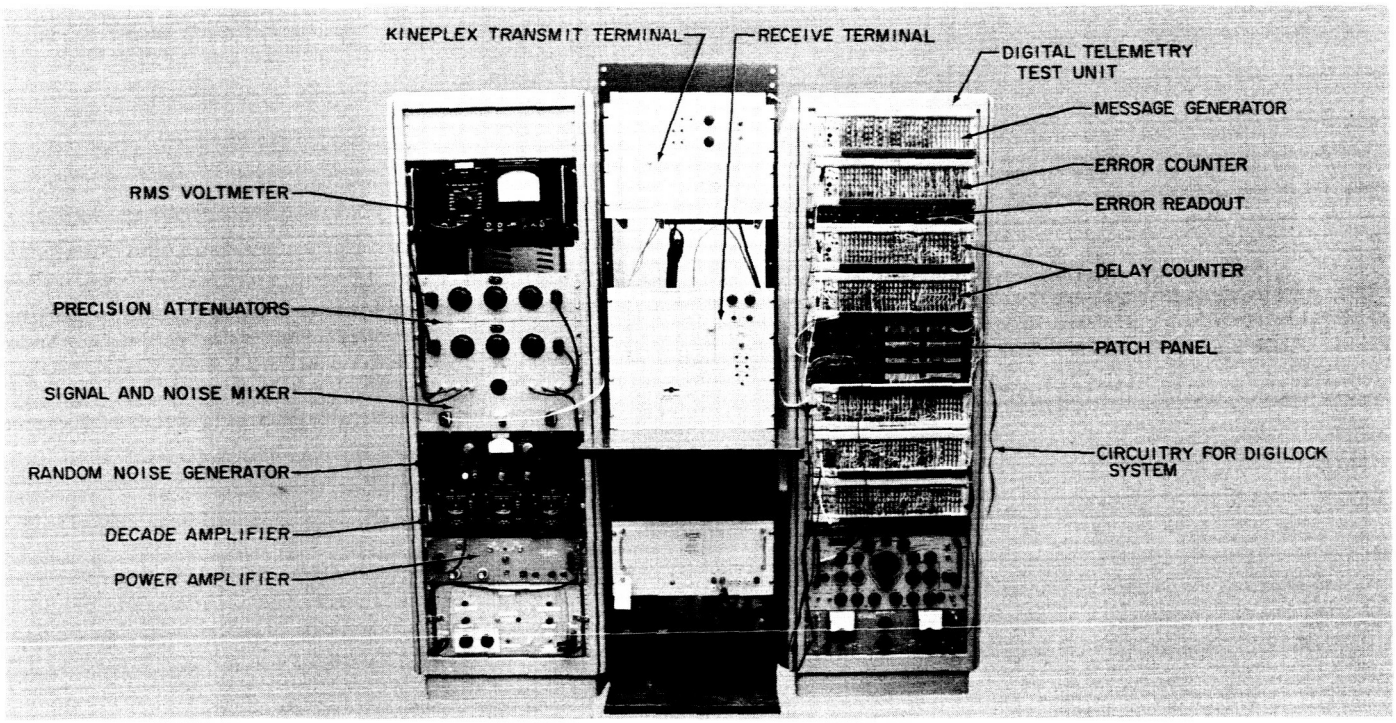

Figure 74. Instrumentation for testing the Kineplex data transmission system

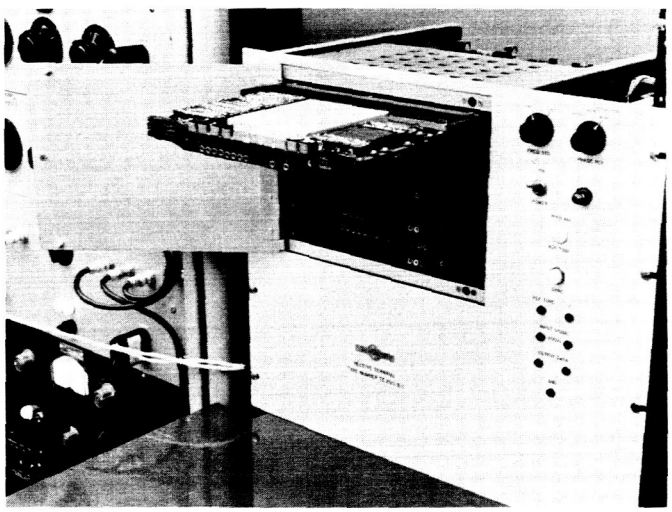

Figure 75. Kineplex receive terminal

driven on alternate data frames. During a drive period, one of the resonators builds up energy at the same frequency and phase as the input signal, while the other is storing the amplitude and phase information from the preceding frame. The lower trace of Figure 77 shows the input waveform to a keyed filter, and the upper trace represents the output waveform for the preceding frame phase reference mode of operation. The lower trace shows the sampling time, the quench pulse, the drive period, and storage. The upper trace shows the integration of the data tone, storage of amplitude and phase information, and quenching of the resonator. The output of one resonator is compared in a phase detector with the output of the other resonator which has been phase shifted 90 degrees. Immediately following the drive period, a sampling pulse gates the output of the phase detector into a shaper which converts the analog phase output to binary levels, thus indicating whether a 0 or 1 has been sent. After the sampling gate, the resonator which stored the amplitude and phase information of the preceding frame is quenched prior to receiving the next data frame. During this period, the other resonator stores the amplitude and phase information for comparison at the end of the period. The period of a data frame consists of the drive gate duration of approximately 18.18 milliseconds and the sampling and quench gate duration of 3.82 milliseconds.

In order for the detection process to be performed efficiently, the gating operation in the receiver must be timed synchronously with the 22-millisecond timing in the transmitter. This synchronization is accomplished in the receiver by determining the time of each phase transition in the 960-cps data signal. The bit timing reference is provided by the time base generator which is driven

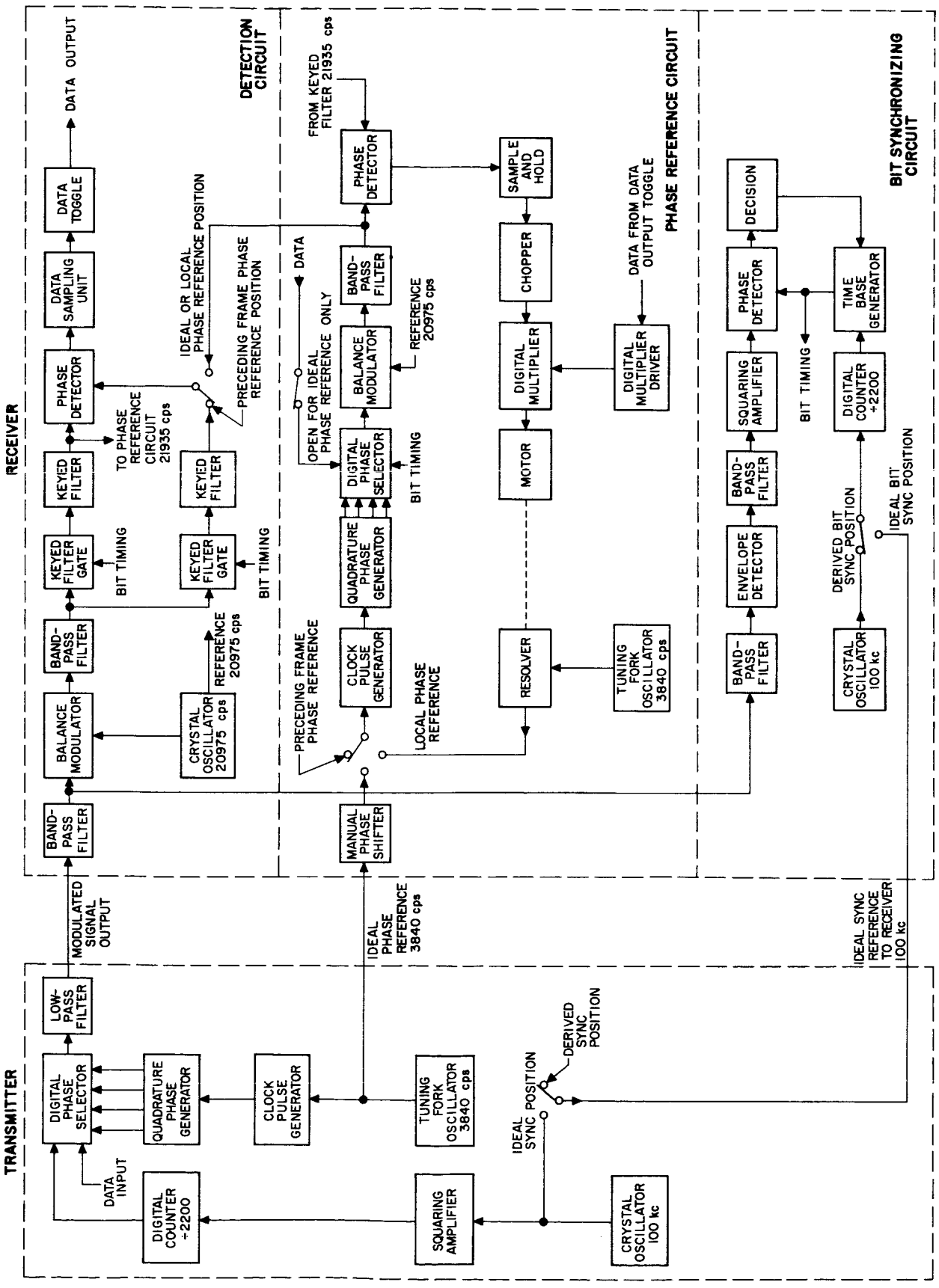

Figure 76. Kineplex data transmission system

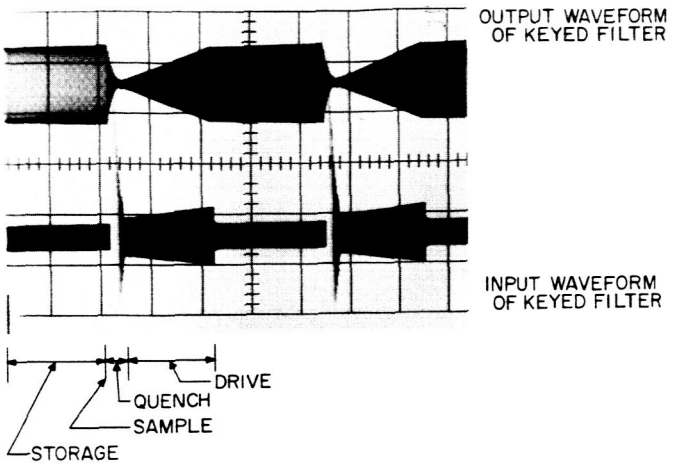

Figure 77. Keyed filter input and output waveforms

by a 45.45-cps square-wave derived from a 100-kc crystal controlled oscillator in the receiver. This reference is compared in a phase detector with a 45.45-cps square-wave derived from the 960-cps data signal. The bit timing error is applied to the time base generator causing it to run synchronously with the phase transitions in the 960-cps data signal.

In the detection process, it is also necessary for the system to have a phase reference corresponding to the phase reference in the transmitter. In the standard Kineplex detection system, the phase reference is determined from the phase of the preceding bit. An alternate method (Refs 8, 9) of deriving the phase reference from the preceding bit uses a servo-loop as shown in Figure 70. In this local phase reference mode, the output of a 3840-cps oscillator is phase shifted by the servo which locks the reference tone to the incoming data tone. The output of the servo-loop is phase shifted in response to the received data in order that it will always be in the proper phase to detect the next bit. One important weakness of this method should be noted. Since the preceding bit is used to set the phase reference for the following bit, an error in detection will result in a second error due to a false phase reference.

c. Conclusions. This report presents the results of an experimental investigation to determine the performance under noise conditions of the Kineplex detection scheme. The probability of error was measured for each of six operational modes as functions of the SNR (signal energy per bit/noise power per unit bandwidth). The theoretical curves (Refs 2 to 7) for ideal phase reference (coherent PSK) and preceding frame phase reference (differentially coherent PSK) are shown for comparison.

The performance for the ideal Kineplex system (Fig 71, circle symbols) shows very good agreement with the theoretical curves. The average error between experimental data and the theoretical values was 0.23 db rms. This is comparable with a probable error of 0.2 db rms predicted from the measuring equipment specification. Figure 71 also shows the performance obtained when the bit synchronization is derived from the transmitted signal (square symbols). This is in very good agreement with the performance of the ideal bit synchronization system shown in the figure.

The graphs of Figure 72 show the performance of the Kineplex system when the phase reference is derived from the phase information in the preceding data frame. The experimental data shows very good agreement with the theoretical curves with an average error of 0.1 db rms. This is well within the calculated accuracy of 0.2 db rms for the measuring equipment. It is again significant to note the good agreement shown in Figure 72 for the system utilizing the locally derived bit synchronization (square symbols).

The performance of the Kineplex system with a locally generated version of the phase reference is shown in Figure 73. This shows a slight improvement in noise performance relative to that indicated for the system using the preceding frame reference when the SNR values were in range of 0 to 8 db. A degradation of 1 to 2 db was noted for SNR's less than 0 db. The measured data shows an error rate which is two times the rate predicted for a coherent PSK system in the strong signal region. This indicates a tendency for errors to occur in pairs. While a theoretical analysis of the local phase reference system has not been performed, a study of the system block diagram shows that this double error rate should be expected intuitively. This is due to the fact that each bit is used to establish the phase reference for the following bit and an error in detection results in a false reference for detection of the next bit. For SNR's less than 0 db this result would not be expected. In order to complete the evaluation of the local phase reference system, it would be desirable to determine the experimental performance for SNR's less than 0 db and to calculate the theoretical performance for the entire range of SNR's.

In general, the observed data served to verify the calculated theoretical performance within the accuracy of the measuring equipment. It is significant to note the performance of the system when the timing synchronization was derived in the receiver for SNR's from -6.7 db (Fig 71, square symbols) to $+9$ db. The observed data

for error rates less than about 10^{-4} does not represent a good statistical average since the message length was only 131,071 bits.

The performance of the practical Kineplex system (preceding frame reference) shows a 3- to 5-db degradation relative to the ideal coherent PSK system for SNR values from 0 to −50 db. This difference approaches 2 db at an SNR of 4 db and decreases toward zero for higher values of SNR.

C. *Ranger* Program

During the months of June and July the DSIF stations will undergo a complete angle pointing accuracy evaluation in preparation for *Ranger* RA-1. Evaluation of these stations will begin as soon as feasible. Evaluation start times coincide with the completion of major modifications to the Goldstone station Az-El site and the Woomera tracking station and with the readiness dates for the Johannesburg tracking station and the Mobile tracking station. The evaluation tests will each have a specific function and will each be distinguishable primarily by analytical methods employed in reducing the test data.

Four types of evaluation tests will be performed:

(1) Multiple short star tracks.

(2) All-night (or horizon-to-horizon) star tracks.

(3) RF boresight static calibrations.

(4) RF dynamic tracking tests (helicopter and/or balloon tracking).

The multiple short star tracks will be used to determine gross errors in the angle tracking system (e.g., misalignment of code wheels) at the Woomera and Johannesburg tracking stations, and to evaluate the optical pointing of the antennas at the Goldstone Az-El site and the Mobile tracking station. To verify an already completed error analysis additional multiple short star tracks will be conducted at the Goldstone Ha-Dec site to allow for the possibility that the site might have to be used in its backup role for the Az-El site. The all-night star tracks will be utilized to evaluate the optical pointing error of the antennas at the Woomera and Johannesburg stations and the RF static and dynamic tests will be utilized to determine the RF boresight shift of the stations.

Data from the evaluation tests will be analyzed using the IBM 7090 computer and the results of this analysis will be published in a station calibration message. The data from the tracking tests is completely recorded, with the exception of the data from the RF boresight tests, on punched paper teletype tape and these data are introduced into the computer in this form. Data from boresight tests is either teletyped directly from the station in the case of static boresight tests or, in the case of dynamic tests, recorded photographically, shipped to JPL, where it is read, and the data entered into IBM cards for introduction into the computer. The station calibration message contains a description of both the random and systematic errors of the several DSIF antennas in a standardized format. The station calibration message format is:

Station calibration message

Date XXXXXXZ

Station No. X

S_{1k}	$E_k(x)$	S_{1k}	A_{00}	B_{00}
S_{2k}	$E_k(y)$	S_{2k}	A_{10}	B_{10}
$\sigma^2(S_{1k})$	$E_k(z)$	$\sigma^2(S_{1k})$	A_{01}	B_{01}
$\sigma^2(S_{2k})$	$E_k(cy)$	$\sigma^2(S_{2k})$	A_{11}	B_{11}
	$E_k(cz)$		A_{20}	B_{20}
	$E^2(\theta_{1k})$		A_{02}	B_{02}
	$E^2(\theta_{2k})$		θ_{1k}	$E^2(\theta_{2k})$

The quantities given in the station calibration message are the parameters of the equations defining the systematic errors and the random errors.

Systematic errors may be defined by one of two sets of equations:

$$\Delta\theta_{1k} = S_{1k} + E_k(x)\frac{\tan\theta_{2k}}{\cos\theta_{1k}} - E_k(z) + \left\{\frac{\cos\theta_{2k}\tan\theta_{1k} + E_k(cy)\sec\theta_{1k}}{[\cos^2\theta_{2k} + 2E_k(cy)\cos\theta_{2k}\sin\theta_{1k}]^{1/2}} - \tan\theta_{1k}\right\}$$

$$\Delta\theta_{2k} = S_{2k} - E_k(x)\sin\theta_{1k} - E_k(y)\cos\theta_{1k} \times \left\{\frac{\tan\theta_{2k} + E_k(cz)\cot\theta_{2k}}{[1 + 2E_k(cy)\cos\theta_{2k}\sin\theta_{1k} - 2E_k(cz)\sin\theta_{2k}]^{1/2}} - \tan\theta_{2k}\right\} \quad (1)$$

$$\Delta\theta_{1k} = S_{1k} + A^k_{00} + A^k_{10}\theta_{1k} + A^k_{01}\theta_{2k} + A^k_{11}\theta_{1k}\theta_{2k} + A^k_{20}\theta^2_{2k} + A^k_{02}\theta^2_{2k} \quad (2)$$

$$\Delta\theta_{2k} = S_{2k} + B^k_{00} + B^k_{10}\theta_{1k} + B^k_{01}\theta_{2k} + B^k_{11}\theta_{1k}\theta_{2k} + B^k_{20}\theta^2_{1k} + B^k_{02}\theta^2_{2k}$$

where k = station identification code, i.e, $k = 1$ for Mobile tracking station, $k = 2$ for the Goldstone Ha-Dec site, $k = 3$ for the Goldstone Az-El site, $k = 4$ for the Woomera station, and $k = 5$ for the Johannesburg station

$$\theta_{1k} = \begin{cases} \text{measured azimuth; } k = 1, 3 \\ \text{measured local hour angle; } k = 2, 4, 5 \end{cases}$$

$$\theta_{2k} = \begin{cases} \text{measured elevation; } k = 1, 3 \\ \text{measured declination; } k = 2, 4, 5 \end{cases}$$

$$\Delta\theta_{ik} = \{\theta_{ik}\,(\text{measured or observed}) - \theta_{ik}\,(\text{true or correct})\}$$

The two sets of equations correspond to two analytical procedures for determining systematic error. Equation (1) consists of recently developed equations whose parameters have physical significance as rotations in the coordinate system used to evaluate the antennas. Equation (2) consists of polynomials which have been used previously in the analysis of the antennas and whose coefficients have no easily discernible physical significance in terms of antenna errors. Equation (1) will be used for the evaluation of the Ha-Dec antennas since considerable experience has been had in using these equations. Equation (2) will be used in evaluating the Az-El antennas. Since this is the first instance in which the Az-El tracking systems will be completely evaluated, no experience has been gained in using Equation (2). Equation (1) provides the advantage of containing quantities having physical significance in the antenna evaluation. The parameters of the set of equations not determined for an antenna will be listed as zero in the station calibration message.

The antenna random errors for all stations are given by:

$$\sigma^2(\theta_{1k}) = E^2(\theta_{1k}) + \sigma^2(S_{1k})$$

$$\sigma^2(\theta_{2k}) = E^2(\theta_{2k}) + \sigma^2(S_{2k})$$

The quantity $\sigma^2(\theta_{ik})$ is the total rms tracking error observed during calibration and $\sigma^2(S_{ik})$ is the RF tracking jitter.

D. *Explorer X*

With the tracking of *Explorer X*, the Woomera and Goldstone DSIF stations participated in the first mission in which the DSIF operated as a net. *Explorer X* (P-14) carried a rubidium magnetometer similar to the one to be carried by the *Ranger* spacecraft and had as its prime function the measurement of the earth's magnetic field intensity. *Explorer X* was launched on March 25, at 1517 GMT and the DSIF stations, using their 108-mc tracking system, began a program of tracking and telemetry recording as soon as the probe rose above their respective horizons. This program was continued for approximately 60 hours, when the probe batteries failed.

Goldstone tracking station. Three tracking and recording periods were undertaken at the Goldstone Az-El site. During all three periods the station was plagued by high winds which made auto-tracking impossible. This difficulty was complicated by the fact that this mission occurred in the middle of the Venus radar experiment and was the first tracking mission in which the tracking receiver at the Az-El site was used. System checkout time was limited and there was not sufficient to optimize the 108-mc tracking system. An additional complication was added by the probe elevation angles being low (at most about 25 degrees) and the resulting multipath effects made it difficult to determine the proper antenna pointing angles for tracking. Tracking at the Goldstone station was done manually by monitoring the servosystem error meters and positioning the antenna for a maximum signal strength reading. No difficulty was experienced in recording the telemetry signals from the probe during the first two visibility periods. Only during the third period when the probe batteries were weak and the high winds (average wind velocity of 30 mph with gusts of 40 mph) made antenna motion almost impossible at the low probe elevation angles was the recording of telemetry unsuccessful. At this time the probe signal could only be locked onto momentarily and then the signal strengths were −145 to −150 dbm as compared with signal strengths of approximately −120 dbm during the previous recording periods.

Woomera tracking station. Tracking at the Woomera station was much more successful than at the Goldstone station. Table 12 summarizes the periods of successful auto-tracking and of telemetry recording. For the first two tracking periods the Woomera station successfully auto-tracked the probe from horizon to horizon and was able to record telemetry data for at least one-half hour before and after the periods of automatic tracking. At acquisition for the third tracking period the probe bat-

Table 12. Woomera tracking summary

Date	Auto-track		Telemetry recording		Maximum signal strength, dbm	Minimum signal strength, dbm	Peak-to-peak tracking jitter, deg
	Start	Stop	Start	Stop			
March 26	0719	1821	0550	1910	−118	−130	0.1
March 27	0646	1847	0612	1927	−123	−136	0.2
March 28	0700	0716	0650	0937	−149	−153	2.0

Note: All time in GMT.

teries had degraded to the point where the maximum received signal strength was −149 dbm and auto-tracking was possible for only 16 minutes. The last definite contact with *Explorer X* occurred at 0728 GMT, twelve minutes after the conclusion of auto-tracking.

E. Communications

The DSIF, because of the extreme distances between stations, requires an effective communications network. This communications network is used for transmitting administrative and technical traffic and consists of telephone links, used during a tracking mission, and teletype links, used both for passing technical traffic and data originating during a tracking mission. All these links pass through the communications center at JPL where, during an operation, they are monitored and the operation controlled from the adjacent Tracking Director's Office; during a Goddard Space Flight Center (SPACON) operation communications links are monitored and patched through to SPACON.

Teletype links. The teletype links are the primary links between the DSIF stations. Each station has at least one full time teletype circuit and an additional backup circuit available for communication with the communications center. The Goldstone station has three full-period 60-wpm lines and will in the near future be equipped with an experimental 100-wpm line. The routing of the lines from the overseas stations to the communications center is shown in Figure 78.

Long-distance teletype transmissions are done using carrier systems and radio links in the same manner as for telephone transmissions. The teletype information is transmitted by making or breaking a 60-milliampere current loop in a series of fractional second pulses. If the line is of sufficient length to introduce capacitance effects regenerators are placed in the line at intervals to reshape the pulses to their original waveform. These regenerators reduce the distortion of the teletype signals and thereby reduce both the resultant erratic operation of the teleprinter and the garbling of the printed output. The dc pulses are routed to the local telephone exchange where they are transmitted over a carrier system. The carrier system allows many transmissions to be carried over a single pair of lines to a local telephone office where the signals are separated and demodulated before being routed to their destinations. In the case of communications between JPL and the DSIF stations overseas the signals are routed to the overseas radio or cable links for transmission to another carrier system. The other carrier system routes the signals to the local telephone office. At the local telephone office the signals are demodulated, regenerated, and transformed into dc to be transmitted to their destination.

Telephone links. The telephone circuits to be used by the DSIF will be supplied by NASA and will consist

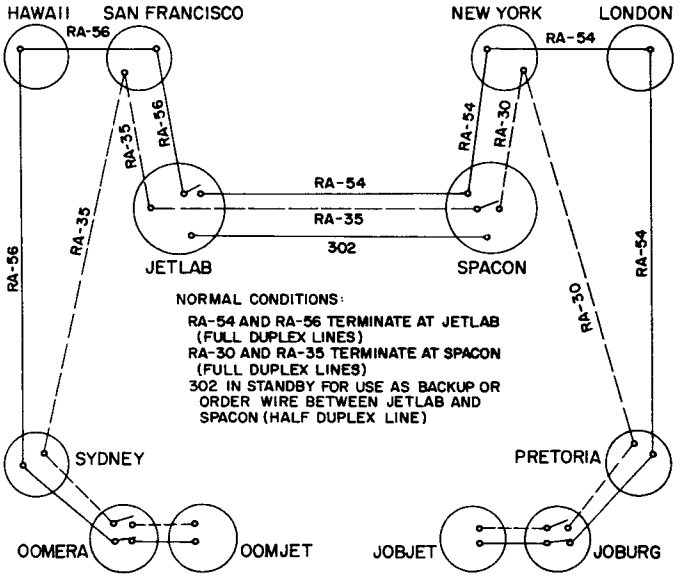

Figure 78. Routing of overseas teletype lines

primarily of four-wire carrier circuits. The messages using these circuits will leave the originator (either the communications center or a DSIF station) and travel by two-wire circuits to the local telephone office where they will be routed to the four-wire carrier circuits for transmission to the overseas radio link. The circuits which NASA will supply will consist of commercial links and, when there is no conflict of operations with JPL programs, the circuits of the Mercury net. Usage of the Mercury net is preferred because these circuits are all four-wire circuits. The disadvantage of commercial circuits is: two-wire circuits are used in these communications links both where the message words are switched to or from the radio link and where the messages are routed from long distance circuits to the local circuits. These two-wire circuits degrade the communications system quality.

Communications center. The JPL communications center (Fig 79) for the DSIF provides a centralized location for the monitoring and reception of messages pertinent to the operation of the DSIF. Teletype lines from each of the DSIF stations, from SPACON, from the JPL computer, and from the teletypewriter exchange board all terminate at the communication center. Figure 80 shows the lines which will terminate at the communication center during the *Ranger* mission and Table 13 gives the teletype call signs of the various stations. The commercial machines (teletypewriter exchange machines) are available to contact similarly equipped installations anywhere in the world. The lines from the DSIF stations, the lines from the JPL computer, and the lines from SPACON may all be patched into a communication net tailored to the operation in progress. A telephone patching system allows the four-wire talking and listening circuits entering the communications center to also be patched into a convenient voice net. These four-wire circuits originate at Goldstone, other DSIF stations, and the JPL computer. Capabilities also exist for conferencing as many as three voice nets at the communication center.

Figure 79. Communications center

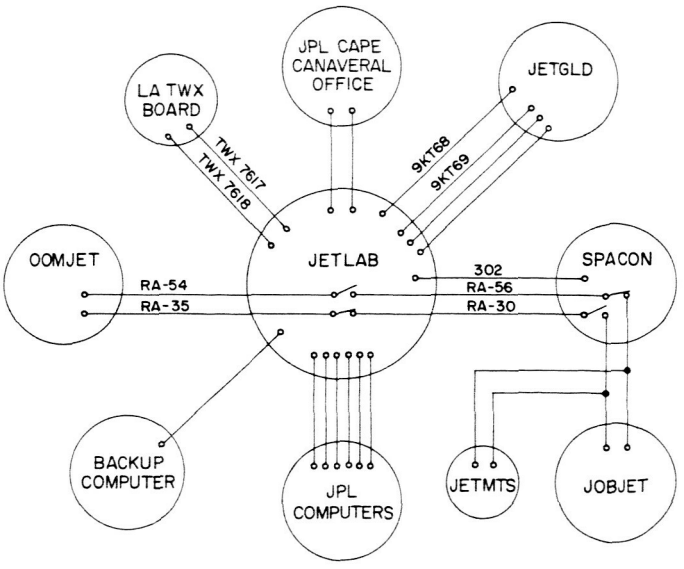

Figure 80. Communications center for *Ranger* RA-1

Table 13. Teletype call signs

Call sign	Station
JETLAB	JPL communication center
SPACON	Goddard Space Flight Center
JETGLD	Goldstone DSIF station
OOMJET	Woomera DSIF station
JOBJET	Johannesburg DSIF station
JETMTS	Mobile tracking station
OOMERA	Woomera Minitrack station
JOBURG	Johannesburg Minitrack station

A high frequency single sideband radio system is also located at the communication center (Fig 81) for use as backup for the communications link to the Goldstone station and the overseas stations. This equipment will be utilized to augment the phone circuits and will be available when no operation is in progress or when equipment failure occurs. For teletype transmission frequency, shift keyers may be coupled into this equipment and the teletype information (e.g., antenna pointing predictions) transmitted to a duplicate system at a DSIF station. At this station the signals are demodulated and transposed into a 60-milliampere loop which is switched into the local teletype system. By a similar method, using the radio

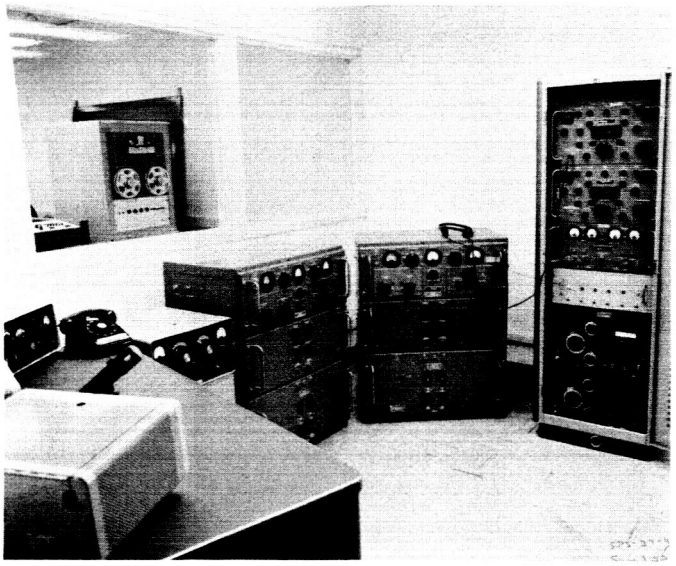

Figure 81. Backup radio equipment

receiving equipment at the communication center, teletype information (e.g., tracking data) may be received from the DSIF stations.

Located immediately adjacent to the communication center is the Tracking Director's Office. During an operation the Tracking Director and other cognizant personnel are able to monitor the various communications links from this location. This enables these cognizant personnel to be aware of occurrences in the various facilities participating in a tracking mission and to be able to communicate with these facilities with a minimum of delay.

F. Proposed Overseas Transmitter Installation

A recommendation has been made that a 10-kw, 890-mc transmitter with command capability as well as doppler capability be installed at the earliest possible date at an overseas station. Reasons for this installation are:

(1) In the determination of precise orbits at interplanetary distances, and in the determination, possibly, of lunar orbits, from earth-bound tracking stations, it is extremely desirable that two way doppler data be available from more than one station. Aside from the Goldstone station the only station presently equipped for two way doppler is the mobile tracking station which has a limited capability because of its low power and smaller antenna gain.

(2) Command and operational requirements may not always be possible within the tracking periods of a single station such as Goldstone. The availability of a second station with command capability will permit sending a lengthy command or one that has a lengthy reaction time in the spacecraft. In certain instances, the command from one station will set the situation for the next station in the tracking sequence.

(3) Mission reliability makes it desirable to have the flexibility of two command systems to permit handling nonstandard situations.

It has, therefore, been decided to accelerate the schedule for the installation of a transmitter overseas. The installation schedule is most sensitive to the main transmitter element, the high-power subsystem. The fabricators of the Goldstone transmitter, Varian Associates of Palo Alto, California, were contacted in March and again in April to establish a schedule and job requirements. Authorization for Varian to proceed was given in April and a schedule for the program agreed upon (Fig 82). Additional items for the transmitter exciter, reference generator system, and precision two way doppler system will be procured and installed within this schedule and the transmitter will be operational for the *Ranger* RA-4 mission.

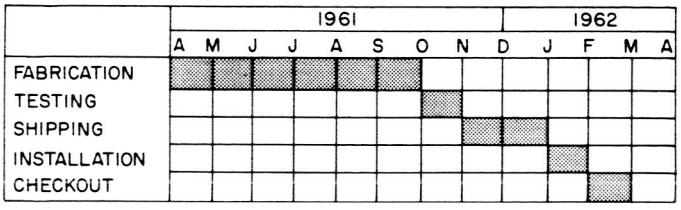

Figure 82. Transmitter installation schedule

II. Goldstone Tracking Station

A. Star Tracker

An optical star tracker system, utilizing a photoelectric tube sensor, has been purchased from Texas Instruments, Inc. The tracker is to be used as instrumentation for evaluating the tracking accuracy and structural deformation of the 85-foot diameter antennas at the Goldstone tracking site; also, the tracker with its tracking error signal outputs may be used for automatic tracking of visual targets.

The tracker consists of an f/8 refractive objective lens system with a 32-inch equivalent focal length, and associated electromechanical equipment necessary to supply signals proportional to the position of a target within the field of view.

It is expected that the tracker will be capable of detecting the following objects and supplying a signal proportional to the position of the object in the field of the tracker:

(1) A visual target on a collimating tower.

(2) A visual source carried on a helicopter or blimp.

(3) The planet Venus to within 5.5 degrees from the sun.

(4) Satellite balloons and cases which have optical properties.

(5) Collimating instruments.

(6) Stars during both day and night.

Quantitatively, the tracker shall function when the above objects have apparent visual magnitudes equal to or brighter than that shown in Table 14.

The tracker will be capable of operating satisfactorily under the following conditions:

(1) Elevation angles, all above a cone 3 degrees below the horizontal.

(2) Winds, 70 mph.

(3) Temperature, 10 to 140°F.

(4) Vibration, 0.5 g.

(5) Rain and ice.

(6) Sand and dust.

To increase the utility of the instrument for research and development type work the following auxiliary features have been provided: a self calibration unit which will permit predetermined angular offset checks of tracker; a reflex system to permit through-the-aperture viewing of a target; a retro-director to permit tracking

Table 14. Performance capability of star tracker

Operating conditions	Star magnitude
Night, cooled detector (−150°C)	9
Night, uncooled detector (20°C)	7
Day, cooled detector (−150°C)	4
Day, uncooled detector (50°C)	4

of a corner reflector at a range of at least 7000 feet; mounting rings for the unit concentric to the optical axis within ±0.002 T.I.R. (there is provision for adjusting the optical axis over an eccentricity of 0.015 inch); a set of field stops to permit changing the field of view; a set of filters to permit operation under all light conditions; and a set of error signal meters.

The tracker is currently undergoing subsystem tests and evaluation. After the completion of these tests the tracker will be installed on one of the antennas at the Goldstone tracking site and its error signal outputs mechanized for direct driving of the antenna via its servosystem.

B. 960-mc Maser

A 960-mc maser will be installed at the Goldstone tracking station for use in the 1962 *Ranger* and *Mariner* missions. The maser will be based on the 960-mc research unit which was tested at GTS in October 1960. Several modifications will be made to improve the field performance of the unit.

A new dewar is being considered for the maser; this dewar would contain a reference load at liquid helium temperature for noise-figure measurements. A reference load of this type (but in a separate dewar) was found to be very useful in the Venus radar maser system. By careful design it is hoped to be able to retain the desirable feature of at least 24 hours of operation per fill of cryogenic liquids. Based on the experience gained from the Venus radar experiment a modified pump power package is also being planned. This package will be unitized construction for easy installation and removal. In order to evaluate the klystron for the pump application it is planned to life test the tube as soon as possible.

A new low-loss circulator will be used in the maser. This, together with a copper plated coaxial transmission line, should yield a maser system noise temperature of around 30°K as compared with 40°K for the previous 960-mc system. Installation of the laser at GTS will be in the Fall of this year.

C. Antenna Structure

The operation history of the Az-El antenna has demonstrated a serious need for engineering improvement in the axis drive systems. Specifically, improvement is needed sorely in the areas of safety, performance, reliability, and freedom from maintenance.

In recognition of these needs, some months ago a program for improvement was developed. In formulation the program drew heavily on the talents and experience of many people and particularly on those familiar with the operation and service experience of the antenna.

The approved modification program is a two part plan. Part One, now in its closing days, has provided the design procurement, and planning in preparation for Part Two, the period of physical modification of the antenna to be accomplished in May and June of this year.

1. Drive System

a. Azimuth drive system. The primary element of the azimuth drive system is the large external-tooth ring-gear which provides the means of rotation of the steerable structure about the azimuth axis. Power for azimuth rotation is obtained from four drive unit assemblies, each comprising a hydraulic motor, a two-speed speed reducer and an output pinion, meshing with the ring-gear. The drive units are attached to the pedestal structure at equally spaced positions around the ring-gear. A portion of the ring-gear and one of the drive units can be seen in Figure 83. The present drive units are the principal

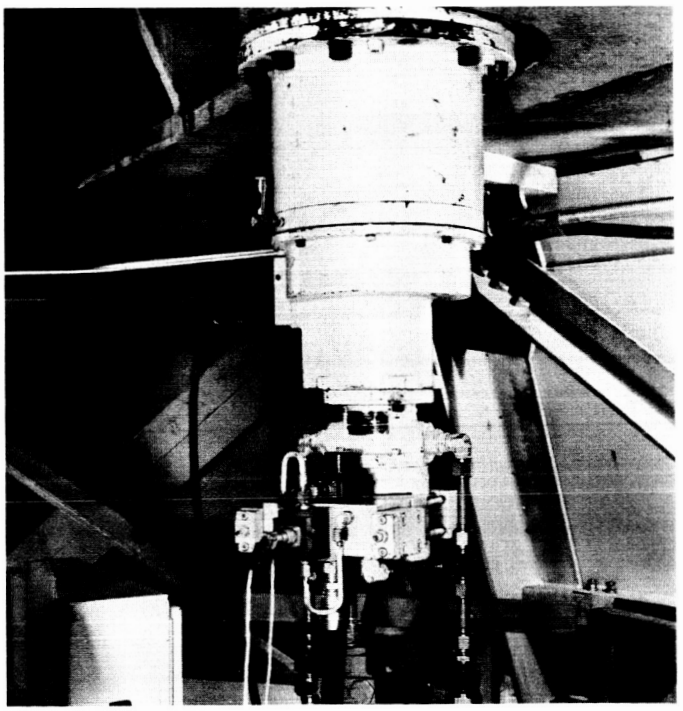

Figure 83. Azimuth ring-gear and drive units

offenders against acceptable standards of performance, reliability, and maintenance.

Replacement drive units have been obtained. Each of the four units comprises a large speed reducer with an output pinion on the low-speed end and a magnetic brake on the high-speed end. These reducers will be interchangeable with the present units. In connection with each speed reducer, additional gearing, a magnetic clutch, and two hydraulic motors will provide a two-speed drive with torque compatibility. One of the assemblies is shown in Figure 84.

A notable departure from present practice will be made in the hydraulic system for the new drive units. A single servovalve will serve the four hydraulic motors instead of the present arrangement of one valve for each motor. The single valve concept was adopted for reasons of favorable load distribution and electrical control system simplification.

Improvements of a secondary nature such as improved filtration, hydraulic manifolds to mount the maximum number of components, maximum use of rigid piping, welded fittings and flanged unions, and provision for pressure taps for monitoring purposes will be made. Basic modification of the electrical control system has become necessary because of the adoption of the single servovalve concept. Other performance-reliability-maintenance revisions will be made such as the use of stabilized amplifiers to minimize drift and the consolidation of service, test, checkout, control, power and signal equipment into a single new junction box.

b. Elevation drive system. Changes planned for elevation are very minor. The more important changes are: a new hydraulic control panel, a revised hydraulic manifold to consolidate components, and a new junction box.

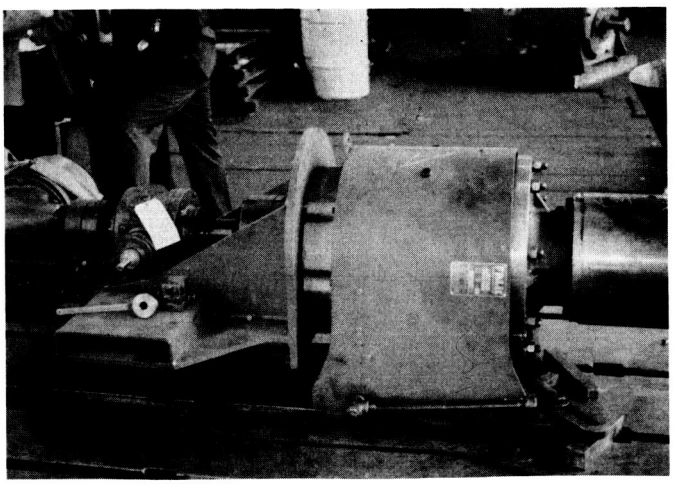

Figure 84. New azimuth drive unit

c. Az-El hydraulic system. Revisions planned for the hydraulic system are intended to reduce maintenance, improve the life of components and system reliability. The physical changes would eliminate pressure shock, provide improved filtration, use welded circuits, and provide separate hydraulic supply systems for azimuth and elevation. Hydraulic power adequate to implement the original servodrive performance specifications was not provided in the initial antenna installation.

A review of drive performance criteria indicated that some relaxation in the original specifications was in order in the interest of component life, reliability, and maintenance. The following servodrive performance aims were considered reasonable and were established for the modified drives: axis rates of 2 deg/sec in elevation and 4 deg/sec in azimuth, acceleration rates of 0.5 deg/sec^2 in elevation and 3 deg/sec^2 in azimuth, full drive performance with wind velocities up to 45 mph and stow capability in a 60-mph wind.

To implement this specification, the existing 100-hp pumping unit will be applied to the azimuth drive system. A new 125-hp pumping unit will supply the elevation system from the existing tank. A new oil air heat exchange will have sufficient cooling capacity for both systems.

d. Azimuth drive simulation tests. Although the single servovalve concept seems theoretically sound, there could be problems in the specific application to the azimuth system because of the geometry of the motor arrangement. Rather long runs or piping are required between the servovalve and the motors and, if the choice were open, of unequal lengths. Quantitatively, the effect of large trapped oil volumes (equal or unequal) on the dynamic behavior of the servovalve hydraulic-motor loops was unpredictable. It became evident that some experimental work was needed in verification of the specific use.

As Phase I of the major modification contract, a study and simulation program for high-speed azimuth drive was carried out. The experimental simulation of the azimuth drive system is shown in Figure 85. Even cursory thinking turns up the necessity for a full scale simulation. The simulator is essentially full-scale. Full-scale hydraulic motors and other electrical and mechanical control system components are used. The hydraulic piping is full-scale, the runs being unequal in length. The larger mechanical elements are represented by components having equivalent dynamic characteristics such as spring compliance, inertia, and backlash.

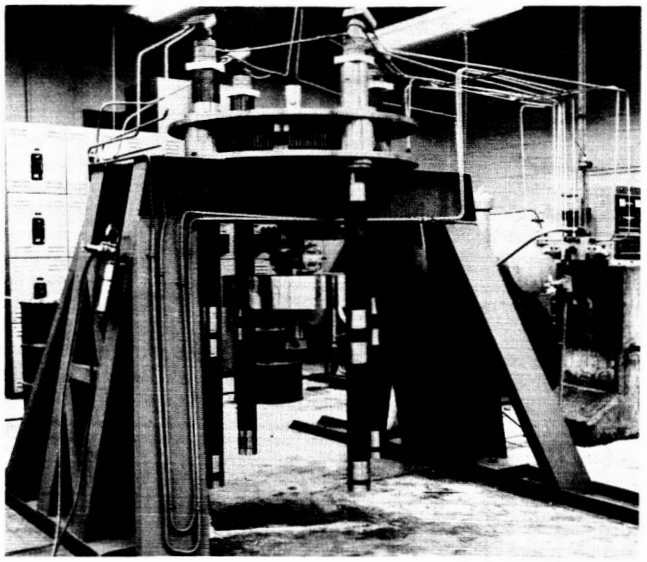

Figure 85. Azimuth drive simulator

The simulation testing has accomplished several things:

(1) It has verified the feasibility of the specific single servovalve configuration for azimuth with unequal line lengths.

(2) It has demonstrated the necessity for a pressure replenishing system to prevent cavitation in the motor lines when the drive is under oscillatory command. Such a system was applied to the simulator, and required pressure level and flow requirements were determined. This information should apply to the full-scale system.

(3) It has demonstrated the need for an antibacklash provision. Antibacklash was provided on the simulator by introducing a low-level directional pressure bias in the hydraulic motor lines. Within the limit of the bias pressure two motors are driving and two are driven. This scheme has been used very successfully on the Goldstone polar antenna. Again the components and settings should apply full-scale. The load sharing of the four hydraulic motors in the parallel drive arrangement has been a matter of great concern. The clear-cut prominence of the backlash when the drive is oscillating without the antibacklash provision offers qualitative evidence that the load sharing is good.

(4) It has provided essential information for the design of the azimuth drive electrical control system. The availability of this information should reduce the level and amount of corrective work required to make the real system operable.

2. Structural Modification

Operational experience with the Goldstone 85-foot diameter Az-El antenna has indicated the desirability of certain modifications to the structure in the interest of increased reliability, safety, ease of maintenance, and improved performance.

Blaw-Knox, the manufacturers of the antenna, studied the feasibility of the following proposed modifications:

(1) The addition of counterweights to balance the antenna about the elevation axis.

(2) The addition of sails to the structure in order to minimize wind torques about the azimuth axis.

(3) The addition of an electronics cage capable of supporting approximately 7000 pounds of additional electronics equipment.

(4) Modification of the support attachments of the ball jack screws to facilitate assembly and disassembly.

A brief summary of the results of the design study for the four proposed modifications follows.

a. Counterweights. The addition of counterweight arms projecting behind and below the dish box girder is the desirable method of balancing the antenna about the elevation axis, and at the same time providing ample space in the two arms for electronic equipment.

On the existing antenna, that portion of the dish above the ball screw connection acts as a cantilever. The addition of counterweight arms, which connect to the square girder, increases the girder stiffness thereby reducing deflection. Therefore, the addition of counterweights will not deteriorate the dish but rather will improve its deflection characteristics.

b. Sails. Sails might well be installed on the antenna which could very nearly completely balance the wind torque under the worst conditions. However, this is not a practical arrangement because major structural reinforcement to the trusses and square girders would be required to prevent serious deterioration of the dish. This is felt to be much too costly to be justified. In addition, benefits are negligible at certain elevation angles.

The practical size sail that could be installed without major structural alterations would balance approximately 50% of the wind torque with a 45-degree wind acting on the dish when pointed to the horizon. In a quartering wind, as the dish is elevated from the horizon to an angle of approximately 30 degrees, the sails reduce the wind torque. However, as the dish is elevated beyond the 30-degree position to the zenith, the sails increase the wind

torque. As a result, the addition of sails would be beneficial only for dish positions between 0 and 30 degrees elevation.

It is, therefore, felt that the addition of sails to the Az-El antenna is impractical.

c. Electronics cage. Incorporating the electronics cage within the counterweight arms offers a number of advantages:

(1) The weight of equipment installed in the arms would act as counterweight.

(2) Ample room could be provided within the two arms for equipment.

(3) The electronics area would be readily accessible from the top of the alidade.

(4) Installation or removal of equipment would be relatively simple using a lift and tilt method.

(5) The floors of the cage could be made level when the dish is directed toward the collimation tower.

(6) The arms could be enclosed with perforated plate for safety to personnel.

d. Ball jack screw supports. The suggested method for modification of the support attachments of the ball jack screws is the addition of bearing caps to the ball jack screw support bearing housings. This feature is certainly a desirable one but it appears that field modification of the existing antenna is too costly to be presently justified.

e. Revisions to be accomplished. The following modifications to the Az-El antenna are scheduled to be accomplished during May and June 1961:

(1) Counterweights to balance the antenna about the elevation axis.

(2) Electronics cages integral with the counterweight support structure.

D. Building Program

Because of the increase of diversified activities taking place at Goldstone, it has been found necessary to improve the facilities available to the personnel. A one million dollar building program is now in progress to provide new buildings and additions to existing buildings. These buildings and building additions are either of concrete block construction or prefabricated insulated steel. Air conditioning is provided in all buildings which house personnel.

1. Az-El Site

Figure 86 shows the plot plan of the Az-El site. The new buildings and building additions are:

a. Dormitory building. This building will provide sleeping quarters for transient personnel. Six rooms with

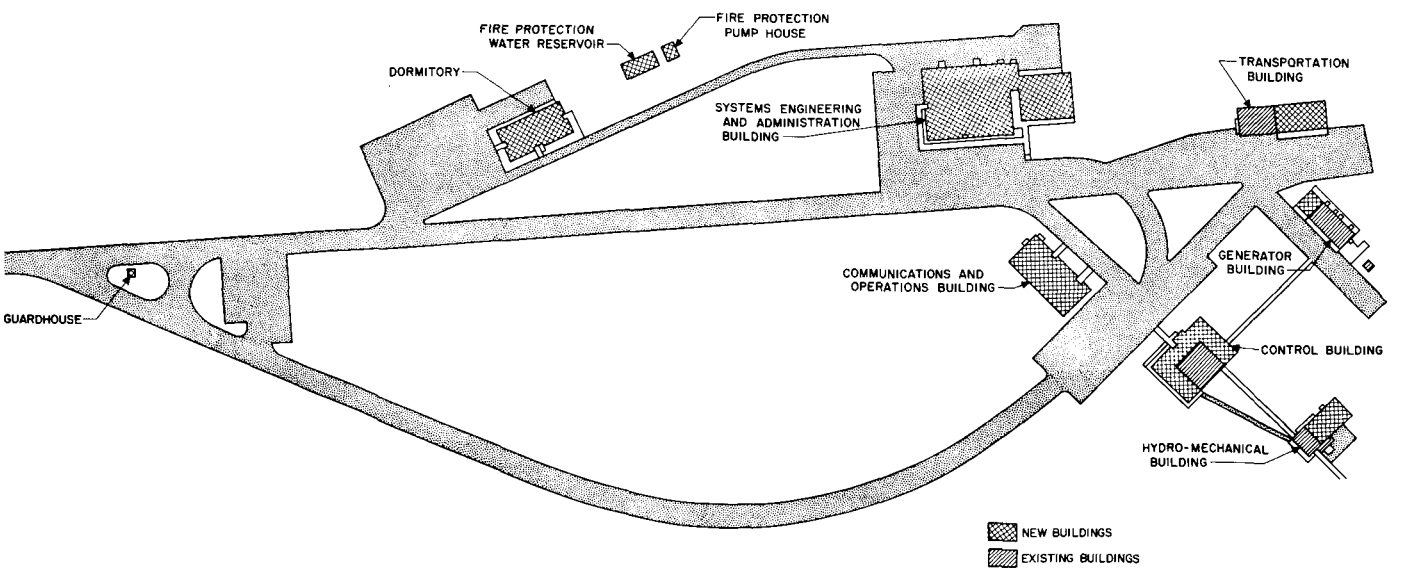

Figure 86. Az-El site

a total capacity of 30 persons and a separate VIP room will be available. Complete toilet and shower facilities will be provided.

b. Systems engineering and administrative building. This building will provide laboratory, technical, and administrative office space. The laboratories will be for research and advanced development groups, the engineering development group, and the operations group. Attached as a wing to the main building will be a self-service cafeteria and lounge area.

c. Transportation building addition. This building addition will provide storage space and a receiving area. All general maintenance and repair parts will be stored at this location.

d. Generator building addition. An addition is being made to this building to provide space for the two new generators being installed. The additional generator capacity will be required because of the lighting and air conditioning equipment in the new buildings and the additional technical equipment being installed for the *Ranger* program.

e. Hydromechanical building addition. An addition is being made to this building to provide space for the new atomichron, for the 100-kw transmitter, and for the new hydraulic test bench. A feed storage and maintenance area and a storage area for the hydraulic equipment will be provided.

f. Control building addition. An addition is being made to this building to provide operational space for the research and advanced development group activities in the transmitter area. One wing is to be devoted to the installation of advanced digital recording equipment; several engineering offices will also be provided.

g. Communications and operations building. This building will provide an operational control room for the Goldstone complex during a tracking mission. In addition, a communication room will be provided which will eventually become the complex teletype center. An equipment room will be provided to permit contractors to install special equipment required for future tracking operations. Several offices will also be available.

2. HA-Dec Site

Figure 87 shows the plot plan of the HA-Dec site. The new buildings and building additions are:

a. Laboratory building. This building will provide additional technical office laboratory space. The research, development, and operation groups will share this facility.

b. Hydromechanical building addition. An addition is being made to this building to provide space for feed maintenance and storage.

c. Control building addition. An addition is being made to this building to provide operational space for the research and advanced development group activities in the receiver area. One wing is to be devoted to the installation of advanced digital recording equipment. Several additional engineering offices have also been added.

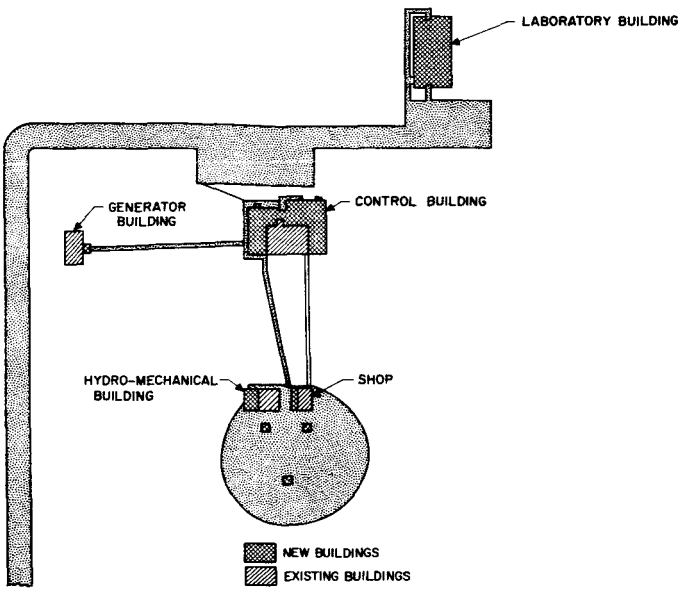

Figure 87. Ha-Dec site

III. Woomera Tracking Station

System Evaluation

During the months from October 1960 through March 1961, a series of all-night star tracks was performed at the Woomera, South Australia, tracking site. The purpose of these tests was to provide data for use in a quantitative evaluation of the tracking performance capability of the Woomera DSIF. Twenty tracks, ranging in declination from 290.4 to 42.1 degrees and covering a 165-degree range in hour-angle, were performed.

The star track data was analyzed by the JPL star track reduction program. This program may be divided into two parts: (1) raw-data reduction and (2) fitting and statistical analysis of residuals. The raw-data reduction portion of the program accepts as input observed local hour angle, LHA (O); observed declination, Dec (O); apparent local hour angle, LHA (A); apparent declination, Dec (A); and the Greenwich Mean Time (GMT) of each observation. LHA (A) and Dec (A) are calculated from the appropriate catalogued postions of the stars. The program output's two quantities of interest were, Δ (LHA), and Δ (Dec). They are defined as follows:

$$\Delta(\text{LHA}) = \text{LHA}(\text{O}) - \text{LHA}(\text{A}) \quad (1)$$

$$\Delta(\text{Dec}) = \text{Dec}(\text{O}) - \text{Dec}(\text{A}) \quad (2)$$

This output from the raw-data-reduction portion of the program forms the input for the fitting and statistical analysis portion. The latter portion of the program is presently capable of least square fitting a straight line to a designated portion of the Δ (LHA) and Δ (Dec) data for a given star. The program then calculates the standard deviation of the fit. The outputs of interest are:

E_α and E_δ = standard deviations of the data from the linear fit.

A_0 and B_0 = constant terms of the linear fit to Δ (LHA) and Δ (Dec) for a given star, respectively.

A_1 and B_1 = rate terms of the linear fit to Δ (LHA) and Δ (Dec) for a given star.

The program, as presently mechanized, uses LHA(O) as the independent variable in all calculations. The Δ (LHA) and Δ (Dec) for each star are plotted vs LHA (O); a range of LHA (O) is chosen, if it exists, for which Δ (LHA) and Δ (Dec) are approximately linear functions of LHA. The Δ (LHA) and Δ (Dec) data corresponding to the chosen LHA range is then used in the fitting and statistical analysis portion of the program.

1. Declination Analysis

The plots of Δ (Dec) vs LHA (Fig 88) indicate that Δ (Dec) is dependent both upon declination and hour angle. The large (0.012 deg maximum) jumps in Δ (Dec) observable in these star tracks are almost certainly because of operator adjustment of the pointing of the

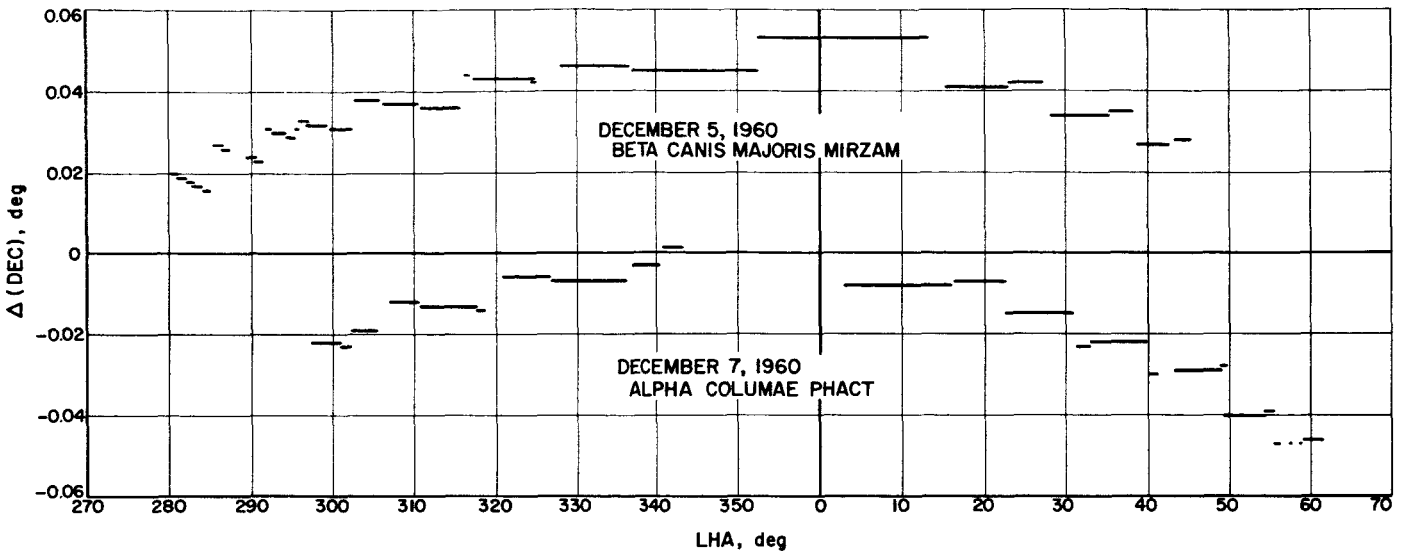

Figure 88. Δ (Dec) vs LHA

antenna in declination. Small jumps (0.001 deg) are due to roundoff error in the refraction correction. The slightly larger jumps (approx 0.002 deg) are due to a combination of refraction correction roundoff and the truncation error of the angular encoders. The characteristic inverted bowl shape of Δ (Dec) vs LHA plots indicates the presence of a systematic pointing error in declination. The shape of the error curve varies with declination, becoming less bowl shaped at large positive declinations. This error curve can be explained as a rotation about the X-axis of the antenna reference coordinate system with respect to the true coordinate system. The antenna reference coordinate system is an orthogonal Cartesian coordinate system originating at the intersection of the hour angle plane and the polar shaft. The X-Y plane is a plane parallel to the equator; the X-Z plane contains the station meridian.) The rotation angle θ must be a function of both LHA and Dec to explain the observed results. Consultation with the antenna structures group led to the hypothesis that the observed error is due to structural deflection of the Dec shaft as the antenna rotates in LHA. This hypothesis is corroborated by orthogonality measurements performed on the antenna.

One seeming anomaly is the nonsymmetry of a given error curve about the meridian. An antenna alignment procedure which utilizes the orthogonality measurements is designed to minimize nonsymmetry; however, these measurements and adjustments were performed before the electronics cage in the dish was equipped. The observed nonsymmetry is neatly explained in terms of the weight unbalance introduced into the structure by the fully equipped electronics cage.

The equator for Δ (Dec) due to θ is given by:

$$\Delta\,(\mathrm{Dec}) = B_0 + B_1\,(\mathrm{Dec}) + \theta\,(\mathrm{Dec}, \mathrm{LHA}) \sin\,(\mathrm{LHA}) \quad (3)$$

At a given Dec the functional form of θ is assumed to be K (LHA) and the values of B_0 and B_1 are used from the equation for Δ (Dec) at the meridian (LHA = 0 deg). At the meridian (Fig 89):

$$\Delta\,(\mathrm{Dec}) = 0.093739 + 0.002851\,(\mathrm{Dec}) \quad (4)$$

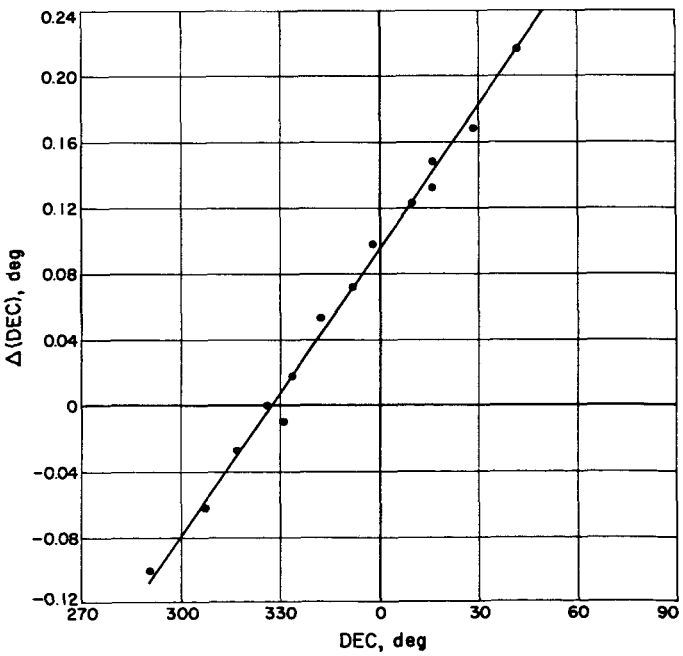

Figure 89. Comparison of equation for Δ (Dec) at the meridian with data

The standard deviation of this fit is 0.008716, which agrees very well with the data from a previous estimate of the Woomera antenna's tracking capability. (The error, Δ (Dec is fully explainable in terms of a radius error in the declination bull gear.) The equation for Δ (Dec) then becomes:

$$\Delta\,(\mathrm{Dec}) = 0.093739 + 0.002851\,(\mathrm{Dec}) + [K\,(\mathrm{Dec})]\,\mathrm{LHA}\sin(\mathrm{LHA}) \qquad (5)$$

The curve in Figure 90 was generated using Equation (5) with $K = 4 \times 10^{-4}$ in the region 270 deg $\leq$ LHA $<$ 0 deg and $K = 10^{-3}$ in the region 0 deg $\leq$ LHA $\leq$ 90 deg. (The factor K appears to be a sinusoidal function of Dec but a quantitative expression cannot be determined without more data.) The shape of the theoretical curve in Figure 90 agrees extremely well with the observed data and the zero-intercept is within the σ value for the function $B_0 + B_1$ (Dec).

2. Local Hour Angle Analysis

Plots of Δ (LHA) vs LHA (Fig 91) are representable as first degree polynomials in LHA; therefore, the Δ (LHA) data for each of the 20 stars were fitted, using the fitting and statistical analysis portion of the star track program, to polynomials of the form:

$$\Delta\,(\mathrm{LHA}) = A_0 + A_1\,(\mathrm{LHA})$$

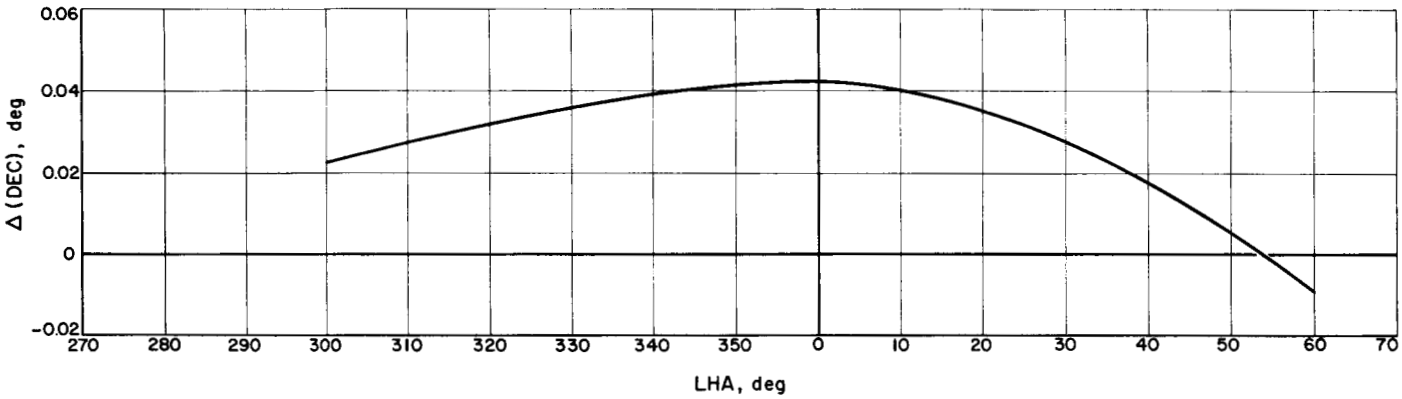

Figure 90. Computed value of Δ (Dec) vs LHA

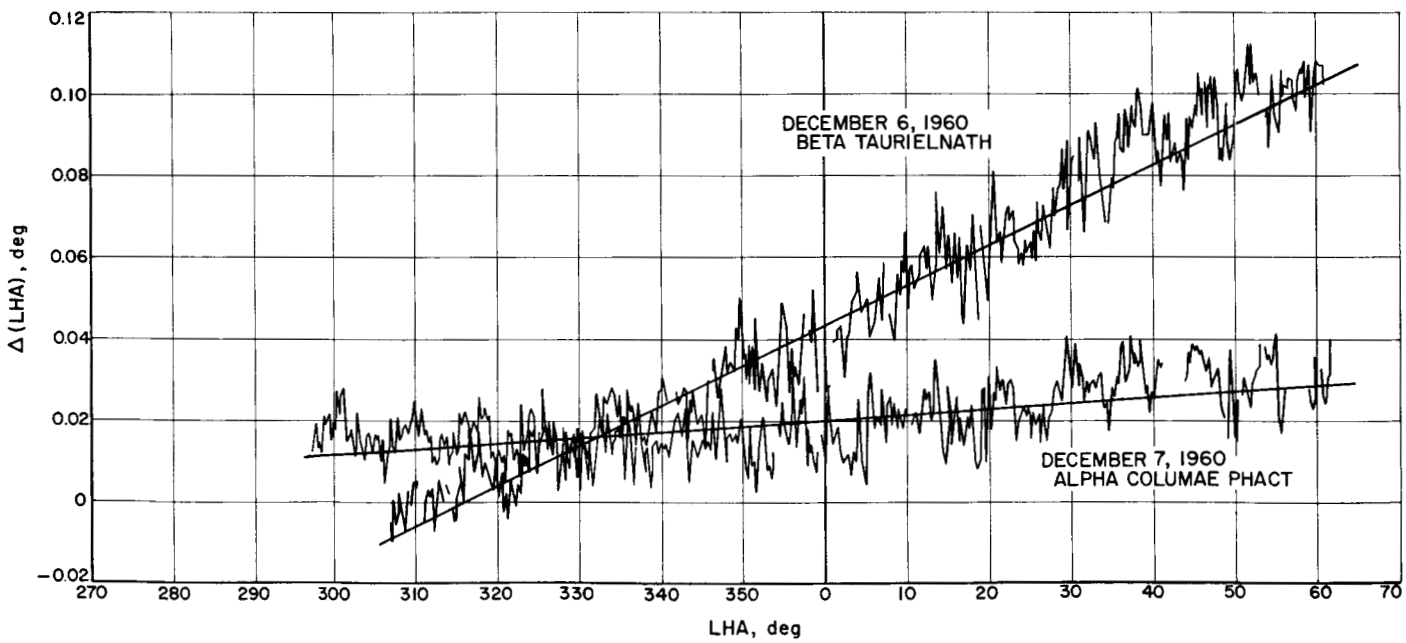

Figure 91. Δ (LHA) vs LHA

For each star it was possible to use the full observed range of LHA. The standard deviations (E $\propto$) from these fits ranged from 0.0043 to 0.0245. Linear fits of the A_0 and A_1 as functions of Dec (Figs 92 and 93) yielded the following results:

$$A_0 = 0.02196 + 0.000383\,(\text{Dec}) \qquad (6)$$

where the standard deviation was 0.0152, and

$$A_1 = 0.000556 + 0.000014\,(\text{Dec}) \qquad (7)$$

where the standard deviation was 0.918×10^{-4}

The coefficients of a linear fit to Δ (Dec) vs LHA showed large deviations from linear fits of A_0 and A_1 for only three stars in the Dec range 290 to 307 degrees and, therefore, these coefficients were omitted from the fits for A_0 and A_1. The above fits and the quantitative mathematical model for antenna systematic hour angle error generated from them

$$\Delta\,(\text{LHA}) = 0.021963 + 0.000383\,(\text{Dec}) + 0.000556\,(\text{LHA}) + 0.000014\,(\text{LHA})\,(\text{Dec}) \qquad (8)$$

are useful, therefore, for the complete declination range investigated except for the region from 290 to 307 degrees.

3. Angular Encoders

In the middle of May a completely new encoding system will be installed at the Woomera station. At the present time the angular encoders are located in the station control room in the servo readout package. This package receives an input from synchro pickoffs mounted on the antenna pinion gears. The new encoders will, as at the Goldstone station, be located on the hour angle and declination shafts. The placing of these encoders on the antenna shafts should reduce the angle tracking jitter introduced in the Woomera evaluation data because of the encoder location.

One effect of relocating the angular encoders can be estimated by examining the standard deviation of the fit of the mathematical model for Δ (LHA). Star tracks performed at the Goldstone station since the relocation of the encoders there gave values of $E \propto$ which lie in the range of 0.0053 to 0.0076. The difference between these values and the larger values of $E \propto$ (0.0043 to 0.0245) for

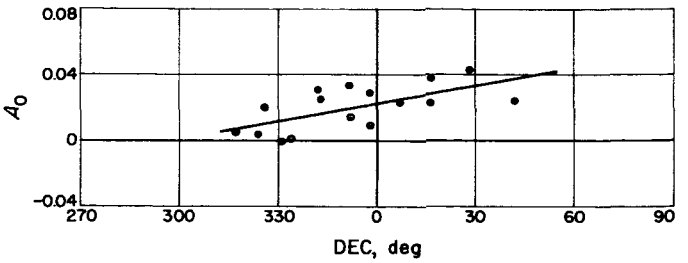

Figure 92. Comparison of fit for A_0 with data

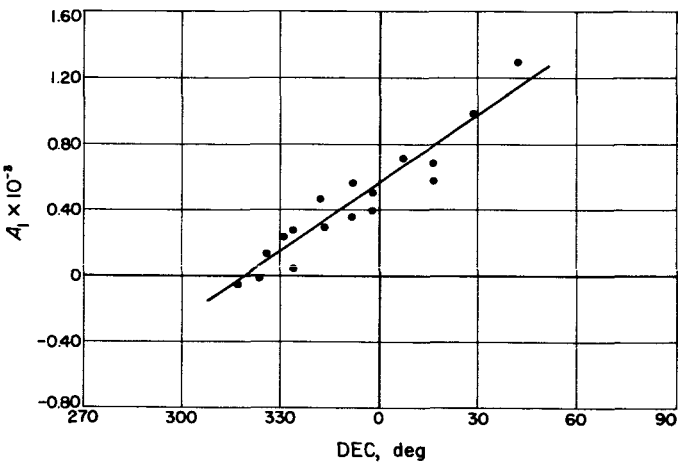

Figure 93. Comparison of fit for A_1 with data

the two stars tracked at Woomera are probably a fair indication of the decrease in tracking jitter that is attained by placing the pickoffs on the hour angle and declination shafts, rather than at the pinion-gears downstream of the hour angle and declination bull-gears.

Because of this planned relocation of the angular encoders, the only further analysis of these data to be done will be to attempt to verify the Δ (LHA) model using tracking data from *Explorer X* (P-14) and to determine the form of Δ (Dec) as a function of LHA. This latter analysis will be attempted since the systematic error (structural deflection of the declination shaft) is independent of the location of the angular encoders. Data for this analysis will be obtained by measuring the elevation angle of the declination shaft at hour angles other than those used in the standard orthogonality tests. Complete system evaluation tests will be performed after the installation of the new angular encoders.

IV. Johannesburg Tracking Station

Construction and installation of the DSIF station near Johannesburg, Union of South Africa is underway. The antenna structure was completed and accepted by JPL on March 25, 1961. Construction proceeded ahead of schedule with only a few days lost due to inclement weather. The control building (Fig 94), collimation tower building, and generator building are under construction at this time. At the present time the electronic subsystems and hydraulic drive system are being installed. This installation includes the cabling between the antenna and the control room and the equipment in the control building console. Completion of the electronics subsystem installation and checkout is scheduled for the middle of June. Operator training and systems tests will be conducted until mid-July when the DSIF net tests for *Ranger* RA-1 take place. Figure 95 shows the latter stages of construction and the finished antenna.

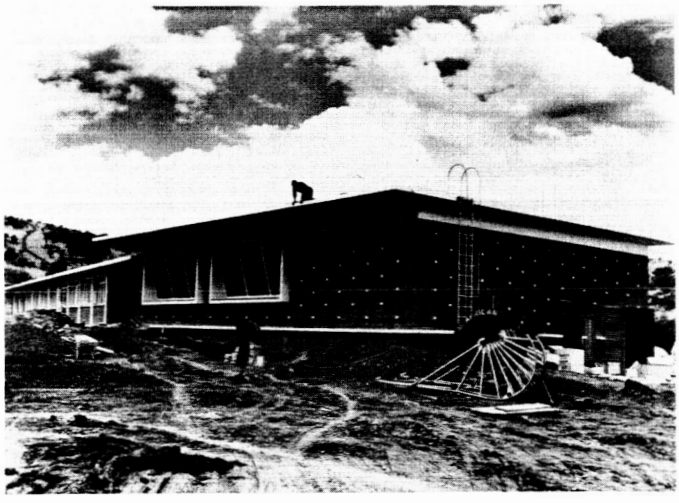

Figure 94. Control building

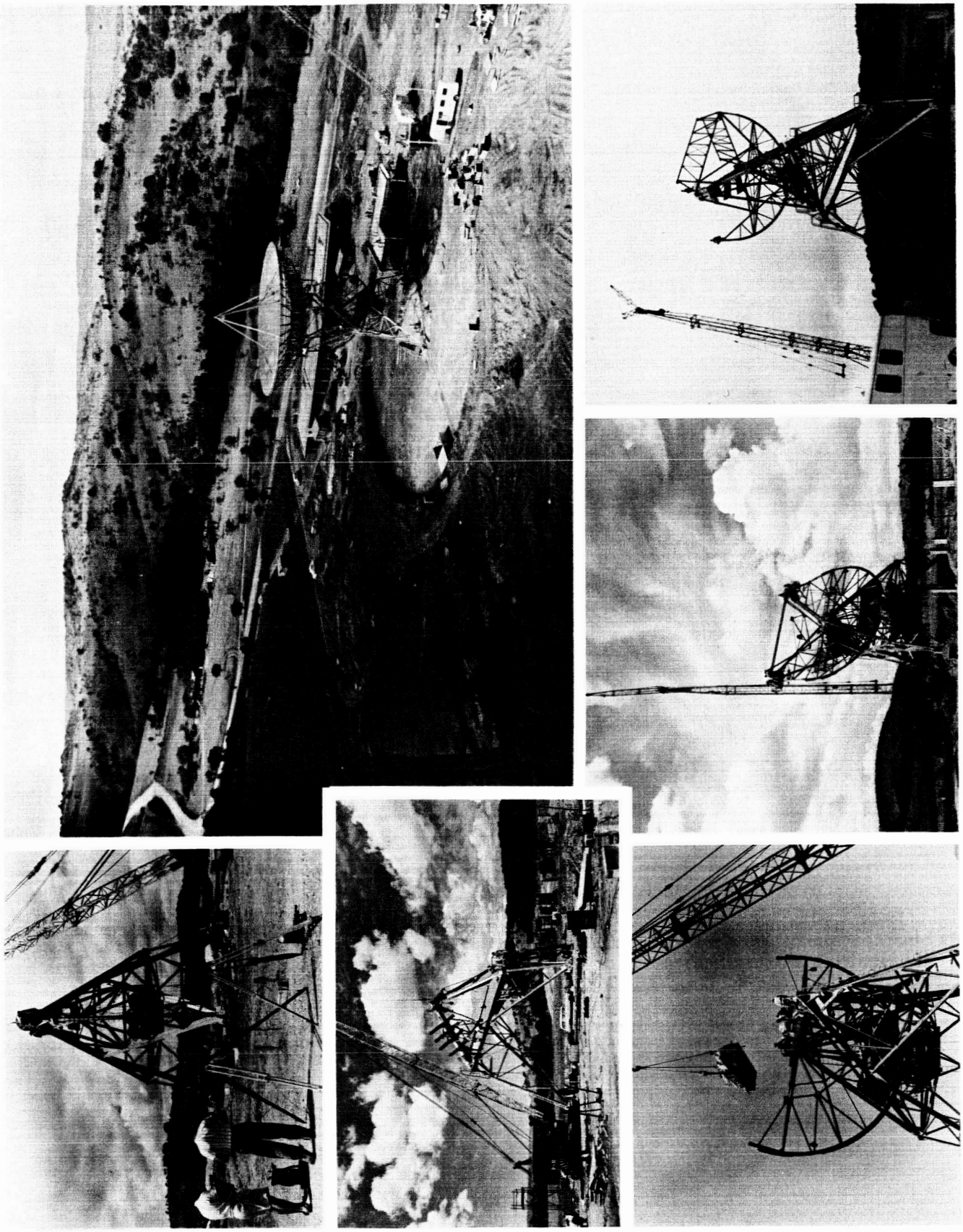

Figure 95. Johannesburg tracking station

V. Mobile Tracking Station

A. Tracking Evaluation

Assessment of the angle tracking errors of the mobile tracking station was performed at Goldstone during the months of January, February, and March. The tests performed consisted of helicopter-theodolite tests, helicopter-TV tests, Venus tracks, stellar meridian crossing observations, and a determination of the effects of polarization on boresight shift. The results of these tests are somewhat academic since the station is now enroute to South Africa but the experience gained by the operating personnel and the data analysis group was invaluable and will result in a reduction in the time required for the station evaluation when it is located in Africa.

Helicopter-theodolite tests. Because the 10-foot parabolic antenna normally operates under a radome, which is transparent to RF but not light, the helicopter-theodolite test was designed. In this test the helicopter carrying an RF beacon is flown on a flight path which brings it repeatedly across one reticle of a T-2 theodolite which is outside the radome. The theodolite is locked at a known angular position in the coordinate being evaluated but is free to track the helicopter in the other coordinate. The antenna tracks the helicopter beacon; tracking data is manually sampled by the theodolite operator whenever the helicopter crosses the reticle which corresponds to the coordinate being evaluated. Since the position of the theodolite is accurately known, the RF boresight error (i.e., the difference between the theodolite angle and the antenna readout angle) can be evaluated. The technique is tedious, difficult, and extremely sensitive both to small errors on the part of the theodolite operator and to weather conditions, since the helicopter must fly a very precise path to stay within the field of view (1° 40′) of the theodolite. Only one coordinate can be evaluated at a time and the results represent, at best, a quasi-static RF boresight error. Five tests were run and the results are summarized in Table 15.

Helicopter-TV tracks. Since the results of the helicopter-theodolite tests were at best inconclusive, it was decided to remove the radome on a calm night and perform a conventional dynamic track of the helicopter. Tracking was accomplished in two-way lock and the boresight shift was recorded by photographing the TV screen presentation of the antenna-mounted TV camera. Two tests were conducted and between the first and second tests the feed was adjusted to remove a −0.1-degree bias azimuth. Ten-point averages were computed for the test data; based on these averages the results of the tests are summarized in Table 16.

Venus tracking. While the radome was removed the TV system was used to track the planet Venus. The results of this test were bad and to a certain extent inexplicable. The error in azimuth was quite likely attributable to the nonlinearity of the TV presentation while the error in elevation, since Venus was quite low in the western sky, would be directly caused by an error in east-west leveling. However, the error implied was greater than 0.1 degree, which is difficult to believe.

Star tracks. Because of this apparent error in leveling, a series of star tracks was attempted. The meridian crossings of nine stars were observed using the reference tele-

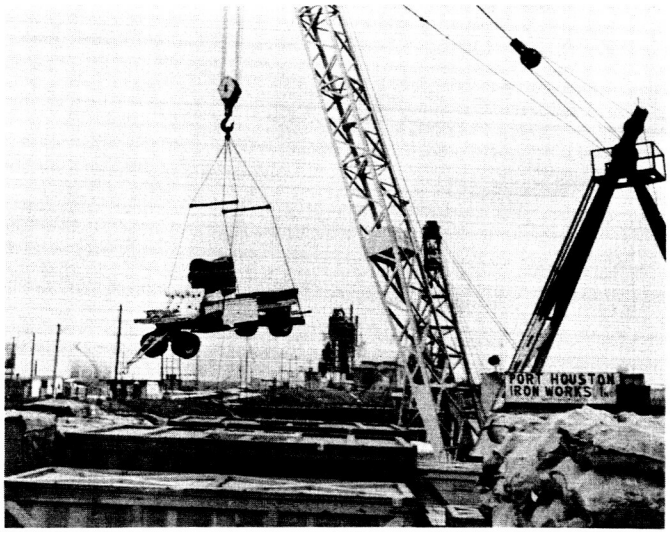

Figure 96. Loading the mobile station for sea shipment

with a scheduled arrival date of May 19. After arrival the vans will travel by highway to the site of the DSIF station near Johannesburg; the other equipment will travel as far as possible by railroad.

C. Installation

Since the mobile station site will already have been prepared, assembly of the station can begin as soon as the station arrives. The preparation of the site consisted of the pouring of the concrete footing and floor for the radome and the concrete base for the collimation tower, the installing of the security fences, and collimation tower guy wire anchors, and the conducting of a survey to establish a base line. Station assembly will begin with the unpacking and locating of the vans (each operational van has most of its equipment tied down within it and additional equipment is tied down in the aisles), generators, air conditioners, and the blower pack for the radome. The pedestal will then be located on the radome floor, the antenna and reflector installed on the pedestal, the collimation tower erected, and power and signal cables laid between the generators, the vans, and the antenna pedestal. Optical targets will be installed and a second order survey performed to locate the antenna pedestal relative to the previously determined base line. The elevation mask of the antenna will then be determined and the radome erected.

Subsystem and system tests will begin after the station has been assembled. Subsystem tests will consist of evaluations of the servosystem, the antenna, the radio system, and the telemetry and data handling systems. After the successful completion of these tests, on June 15, the station will begin system tests which will check the operation of the station as a unit. Initial system tests will consist of countdown operating with RF acquisition of the pole beacon on the collimation tower. Sufficient countdowns will be performed to insure that the station personnel is operating smoothly as a well trained team. Following the countdown operations the station will conduct helicopter tracking exercises (five tracks are presently scheduled) to evaluate the tracking accuracy of the station. In addition to these tracking exercises the station will also engage in a program of star tracking to evaluate pedestal leveling, pedestal and antenna readout, azimuth orientation, and the correctness of the pedestal location in latitude and longitude.

VI. Advanced Antenna System

A. Project Synopsis

A new, large aperture, low-noise, advanced antenna system (AAS) is planned for installation in the NASA–JPL Deep Space Instrumentation Facility (DSIF). The first system, which will be constructed at Goldstone tracking station (GTS), is programmed to be operational by April 1, 1964. The objective of the new antenna system is to provide a substantial increase in the communication capability of the DSIF beginning in 1964 to meet the communications requirements of the NASA lunar and planetary programs.

Chronologically, the present large antenna program has evolved as follows: In 1958, JPL established the Goldstone tracking station with a radio-astronomy type antenna, on a polar mount, and supplemented with high-speed automatic tracking drives and coherent receiving capability. A second 85-foot diameter antenna, on an Az-El mount, was added in 1959 for use as a transmitter in the *Echo* project; the second antenna also permitted station operation as a high capability continuous wave planetary radar, and is now being used in DSIF operational missions to relieve the work level of the first antenna.

Meanwhile, commercial firms were extending their activities within the large antenna field. Some excellent instruments progressed toward completion, and much was learned as to the importance of adequate coordination of design, user requirements, fabrication, erection, and environment. In 1960, NASA Headquarters prepared a preliminary statement of antenna requirements for orientation of advanced program planning.

In September of 1960, a statement of system requirements for DSIF AAS was issued as JPL Engineering Planning Document (EPD) 5. This statement served as the contractual work description for activating a competitive Phase I design study effort.

A review of vendor contacts, directories, technical periodicals and commercial reference sources, established a list of some 300 vendors who professed interest in the antenna area. By NASA Source Evaluation Board Procedures, this list was reduced to a group of firms who were invited to attend a preproposal briefing. A basic management decision was established that consideration could be given only to those firms that had the capability of handling the design and completion of the AAS upon a prime contractual basis.

A formal preproposal briefing was held at JPL on September 29 and 30, 1960, and was followed by a detailed inspection of the existing GTS facilities. Some 40 firms participated. JPL tendered a request for proposal to those firms who had attended the briefing, and subsequently requested consideration. By November 7, 1960, postmark deadline date, 17 firms submitted formal proposals describing a Phase I design study effort for the AAS.

The successful Phase I design study contractors were: Blaw-Knox, Hughes Aircraft, North American Aviation, and Westinghouse Electric.

A precontractual briefing was held at JPL on January 4 and 5, 1961, and was followed by an additional inspection of the GTS facilities (with detailed discussion of some of the system problems associated with present equipment).

The Phase I study parameter ranges would be:

(1) Az-El mounts, Cassegrain dish, trackable to horizon mask.

(2) Focal length to diameter ratio, 0.25 $\pm$0.05.

(3) Diameter, 240 $\pm$24 feet.

(4) Gain improvement over present 85-foot antenna, 9 $\pm$1 db.

(5) Figure of merit improvement (quotient of gain by system noise temperature), 11 $\pm$1 db.

It was concluded that complicated, servo corrected structures apparently are not necessary for the diameters appropriate to this DSIF application. It appeared practical that, below some critical diameter, perhaps 240 feet, depending upon the mounting system and the capabilities of manufacturer, no servo correction of face panels may be required. One of the major points to be established in each of the Phase I design study efforts, is that of the critical diameter for each of the design approaches.

By January 9, 1961 the four Phase I design study contracts were in being and work was in progress. Fourth-week informal engineering conferences with the four individual Phase I study contractors were held between February 7 and 21, 1961. The initial technical direction of each contractor was reviewed in all major areas, and the contractor facilities were inspected. By February 22, 1961, the 2115-mc frequency assignment was approved by FCC Board of Commissioners action for use at GTS. The 2295-mc band had previously been assigned by NASA for deep space use only. Assignment of these frequencies firmly established most of the critical parameters of the AAS. Specifically, these include: size, diameter, beam width, surface tolerance, and pointing accuracy.

On March 2, 1961, representatives of all four Phase I AAS contractors attended the review of RCA Montreal microwave optics work being done under contract to JPL. This work is in support of the AAS program and the results derived have been made available for use, if desired, by the Phase I study contractors.

Eighth-week semiformal engineering conferences were conducted at JPL 14 through 28 March 1961. All four Phase I contractors made separate, detailed, technical presentations on their proposed designs. At this point the basic structural and mechanical elements were reasonably well established and the competitors' emphasis was shifting through the servo and control areas toward the system integration area. Based on these discussions, it still appears that an antenna to the basic requirements of EPD 5 is feasible.

During the period April 14 to 20, 1961, informal engineering conferences were conducted at the contractors' facilities. Remaining technical problems and the work conducted since the eighth-week meeting was reviewed.

Meanwhile supporting studies were conducted by JPL in selected technical areas. This work includes investigation of foundation requirements which bears on the AAS site selection problem, and investigation of pertinent microwave optics design considerations.

B. Supporting Studies

1. Foundation Studies

In examining the foundation requirements for the AAS it became evident that the accuracy required by the antenna placed very stringent demands upon the foundation and soils stability. These rigid requirements stem primarily from the need for an isolated optical tower on which to mount a master equatorial unit which will accurately read out the position of the parabolic surface without reflecting the large structural compliance of the antenna support structure. In order to incorporate this type of optical unit, the antenna must be designed so that the elevation axis and the azimuth axis must intersect. The isolated tower for the optical instrument must be free standing at a minimum height of one-half the reflector diameter, approximately 120 feet. A further requirement is that the optical tower must not rotate as much as 5 seconds of angle in any plane, and must have a resonant frequency a factor of three greater than the response frequency of the servo drive mechanism.

In order to determine the foundation configuration and soils condition requirements necessary to meet the special and stringent conditions noted above, a contract for a Foundation Concept Study was let to the Donald R. Warren Co.

The following requirements were to be met in this preliminary investigation:

(1) Evaluation of appropriate combinations of soil and rock formations with respect to foundation types applicable to the requirements of large, highly accurate antennas.

(2) Specific recommendations on foundation practices required to insure minimal angular deflections (less than 5 seconds of arc maximum) reflected into an isolated centrally located, optical tower. Consid-

eration must be given to those foundation loads which are induced by the optical tower itself; in addition, superimposed foundation pressures from the various load conditions of the antenna structure and loads resulting from seismic and microseismic reactions.

(3) Consideration should be given to the possibility of damping the optical tower to eliminate quickly angular oscillations and to prevent any amplification of such oscillations due to seismic or microseismic activity.

(4) Economic feasibility of various probable foundation types, with a comparison of expected angular deflections under both instantaneous and long term load conditions.

(5) Logistical recommendations with respect to (a) coring operations and requirements, (b) concrete supply and placement requirements, and (c) pile supply and placement requirements.

(6) Specific recommendations are necessary with respect to requirements for initial site selection and for final coring and seismological studies for the determination of finite soil and rock conditions.

The results of this Foundation Concept Study dictate that the optical tower be founded on bedrock in order to meet the rigid angular deflection requirements. The foundation requirements for the antenna structure are less stringent than those of the optical tower, but still indicate a definite need for a stable soil with a relatively high bearing value.

It is now planned to proceed with a comprehensive search of the Goldstone area for an adequate bedrock condition for founding the AAS. The search will be conducted as follows:

(1) Surface review of proposed sites by qualified soil mechanics engineer and geologist for probable bedrock locations.

(2) Geophysical tests on the most promising sites to determine the bedrock profile and to locate undissolved pendants in the form of knolls which could be cut down to expose bedrock.

(3) Coring and laboratory analysis of core samples.

2. *Microwave Optics Design*

The primary purpose of the microwave optics design for the AAS is to maximize the ratio of antenna gain to system noise temperature, for a given diameter antenna. As an additional constraint it is necessary to maintain a very low sidelobe level at angles near the antenna axis, in order to permit tracking close to the sun without undue increase in the antenna excess noise temperature. Quantitatively, the latter requirement is stated so that all sidelobes more than 2 degrees from the antenna axis must be at least 52 db below the on-axis gain; or in other words they must be no higher than about 10 db above the isotropic level.

Partly for operational convenience and partly for electrical reasons, the antenna was chosen to be a Cassegrainian system. For antennas such as the AAS which are very large in terms of wavelengths, Cassegrain optics can, when properly optimized, provide unusually high aperture efficiency and at the same time an extremely low effective noise temperature.

The microwave optics design has been studied both theoretically and experimentally by the four study contractors working on the AAS. In addition, an experimental effort is being sponsored by JPL at the RCA Victor Company, Ltd., in Montreal, Canada. The latter contract is specifically aimed at empirically determining the optimum geometry and any other parameters which may significantly affect the structural design.

A modest analytical study program is being carried out at JPL to evaluate the RF design. Particular emphasis is being placed on improved feed design, the effects which vary with the f/d ratio and the efficiency of the antenna when operated in the monopulse tracking mode.

PART FIVE
JUNO II PROGRAM

The *Juno II* is a four-stage rocket vehicle consisting of an elongated Army *Jupiter* as the first stage, a cluster of 11 solid propellant scale *Sergeant* motors as the second stage, a cluster of three solid propellant scale *Sergeant* motors as the third stage, and a single solid propellant scale *Sergeant* motor as the fourth stage. During 1958 and 1959, this system launched the JPL lunar probes, *Pioneers III* and *IV*, and the IGY satellite *Explorer VII*. *Juno II* has the capability of orbiting payloads in the 100-pound category.

From March 1960 through April 1961, four *Juno II* vehicles have been launched. Two launchings resulted in the orbiting of significant experiments, the *Explorer VIII* ion probe and the *Explorer XI* gamma-ray astronomy experiment. Vehicle malfunctions resulted in the loss of the other two experiments: the Van Allen radiation experiment and the ionosphere beacon. However, the ionosphere beacon mission has been reassigned to the spare vehicle of the *Juno II* series.

Also, in this reporting period, the *Juno II* program was reviewed by a NASA Headquarters Review Team appointed by General Ostrander and headed by Mr. W. H. Kaushagen of Cornell Aeronautical Laboratory. JPL internally conducted a complete engineering review of the cluster system and concluded that only minor procedural changes need be adopted to enhance reliability.

The current status of the program is ten successful missions out of eighteen launchings. Of the eight failures, three are attributable to cluster malfunctions. One vehicle is yet to be launched.

I. Engineering Investigation

A detailed engineering analysis of the *Juno II* cluster was made in September and October 1960, in an effort to provide the largest probability of success for the remaining vehicles. This analysis consisted of four phases. (1) review of the hardware condition, ground assembly and checkout procedures, inspection and balancing procedures, and general quality control; (2) design modifications and structural or hardware changes; (3) engineering telemetry; and (4) dispersion analysis, correlation, and prediction.

At the initiation of this review, fifteen clusters had been launched on two types of boosters with eight of the missions being successful. Thus, a good portion of the review was based on flight experience. Each subsystem and area of the cluster was examined in detail in an attempt to locate any incipient causes of future failures. Special attention was given to those areas which might have contributed to past failures. While no individual item was found to be defective, several recommendations were made and implemented, reflecting a general upgrading of the quality of the installation. These recommendations were in the areas of alignment, balancing, cable routing and tiedown, handling, and inspection.

A redesign of the structure was studied in the form of layout and preliminary detail drawings. These designs provided a more rigid structure, larger separation clearance angles, increased gas venting on separation, and better accessibility. No new design was appreciably lighter than the existing configuration. These redesigns were not incorporated because of short schedule and

small number of flights remaining, as well as the possibility of introducing new and unexpected sources of failure.

The possibility of installing a telemetry system capable of providing engineering information on the separation and flight dynamics was considered. It was found that the vehicle limited weight capability precluded the installation in the payload or cluster of any really worthwhile telemetry. The use of booster telemetry to monitor Stage 2 ignition was rejected on the grounds that propulsion ignition malfunction could be determined from tracking data and that coupling the ignition system and the telemetry system at this late date would increase any possible chance of ignition unreliability.

A study has been made of the general cluster dispersion problem (Table 19) in an effort to correlate past performance, isolate the major causes of this dispersion, and predict the behavior of future flights. Dispersion angle of the cluster (the angle between the actual velocity vector at time t and the velocity vector obtained from a perfect cluster fired with the same Stage 2 and launch-booster constraints) is a function of booster pitch and yaw rates, cluster spin rate, cluster balance, thrust malalignments, thrust, mass flow, ignition and tail-off, motor-to-motor variations, ratios of stage pitch to roll moment of inertia, stage-to-stage principal-axis malalignments, cluster stiffness, and payload weight. Some of these parameters have been different for different payloads. In addition, the dispersion angle of the cluster is a function of the ratio of the precession period to the burning time, the ratio of the precession period to the duration from stage-to-stage ignition, and the phase of the nutation angle at the instant of motor burnout. It was found to be impossible to accurately compute the dispersion of a particular round. This was due to the inability to estimate gas dynamic effects in the cavities during separation, stored elastic energy, Stage 4 nozzle (igniter and timer) blockage, as well as geometric and mass parameters of the cluster.

Flight results could not be correlated specifically due to the almost complete randomness of most of the previously mentioned dispersion-causing parameters. This large number of random effects, most of which are in series with each other, leads to a very wide statistical distribution of dispersion angles. The difference in probability between the most probable dispersion and a dispersion that differs by a factor of 0.5 to 2 is extremely small. A range of possible or probable dispersions (0 to 6 degrees) was computed, and all nonaborted flights fell within this range. The small number of flights compared to the number of random variables precludes any correlation of specific rounds. The over-all conclusion is that the flight dispersions observed to date are representative of the magnitudes of similar future rounds and that these dispersions are normal for this vehicle.

Table 19. Cluster dispersion summary

Number of flights	General results	Detailed comments	Round No.	Actual rpm	Actual dispersion, deg	Computed dispersion, deg
3	Successful	Final dispersion 2 deg; dispersion per stage, low; roll rate of Stage 4 dropped 25%	29 44 47	750 750 —	1.2 0.76 +	3.3 3.3 —
3	Successful, but with high dispersion	Final dispersion 5-7 deg; dispersion per stage, high; Stage 4 roll rate dropped 25% on one flight; no record on others	24 AM11 AM14	750 405 560	4.8 4.7 4.6	3.3 7.9 4.3
2	Failures	Electrical or ignition malfunction	—	—	—	—
1	AM-19, heavy payload	Final deviation less than 2 deg; dispersion per stage, small; stiffened structure	AM19A	428	0.76	0.38

II. Launch Operations

During the period March 1960 through April 1961, four *Juno II* satellite-carrying vehicles were launched. Two of these vehicles, the AM19C Van Allen radiation experiment and the AM19F ionosphere beacon, failed to orbit. However, AM19D successfully orbited the ion probe satellite, and AM19E orbited the gamma-ray astronomy satellite.

1. AM19C Launching

On March 23, 1960, *Juno II* AM19C was launched in an unsuccessful attempt to place the S-46, 22.5-pound Van Allen payload, (Fig 97) into a highly elliptical orbit.

The payload for AM19C was designed to monitor the radiation intensity distribution of the two Van Allen radiation zones over an extended period of time with the objective of establishing the origins, including buildup and decay of radiation, in the two zones and correlating this with solar activity. In addition, the experiment was designed to study the composition of radiation in the two zones, to determine the nature of penetrating components and the energy spectrum of the less penetrating components, and to measure the total energy flux throughout the region of trapped radiation with special interest placed on the outer reaches.

Booster performance was essentially nominal; however, Stage 2 fired under a mean angle of 19 degrees down and 5 degrees right from nominal with approximately correct performance. This large angle of the second stage is very unusual and exceeded all other observed Stage 2 deviations on previous rounds. From this performance it was concluded that there was a cluster malfunction.

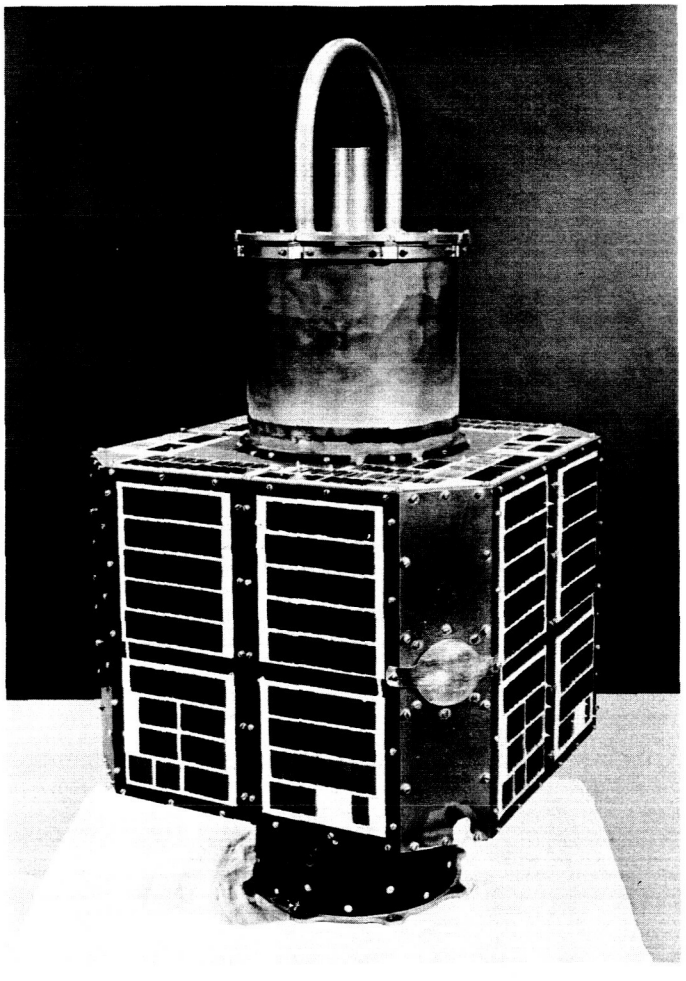

Figure 97. AM19C payload with Van Allen radiation experiment

JPL Cluster 16 was used on this round, and its configuration was essentially that of early *Juno II* rounds (AM11 and AM14 used on the *Pioneer* series, (Fig 98). It did not have the Stage 3 cylindrical support that was flown on Rounds 19A and 16A. There were two reasons for this: first, the payload was very light (22.5 pounds) and, therefore, the cluster did not require the additional structural stiffening; second, the orbit requirements were such that the extra 10 pounds of cylindrical support weight on Stage 3 could not be afforded.

This cluster was delivered to Cape Canaveral on December 3, 1959, and stored until February 16, 1960, when it was sent to the JPL spin building for flight preparation. Initial spin tests for AM19C were accomplished satisfactorily on March 15, 1960.

Although much effort was expended in an attempt to pinpoint the cause of malfunction of the high-speed stages, no conclusive explanation could be obtained. One-motor-out performance of the second stage was examined and found to fit the flight performance reasonably well.

2. AM19D Launching

On November 3, 1960, the *Juno II* AM19D vehicle placed into orbit the artificial satellite S-30, *Explorer VIII*,

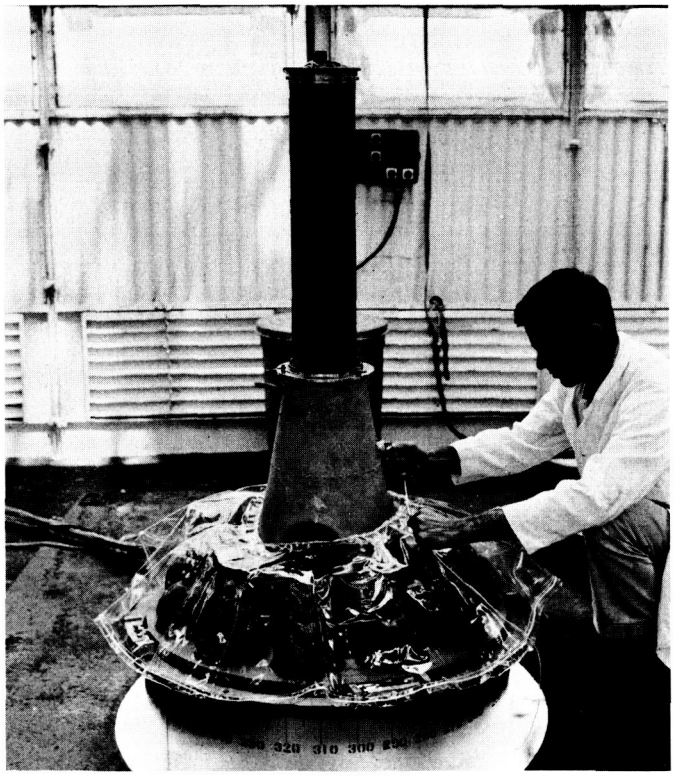

Figure 98. Cluster configuration for AM19C

instrumented to study and report the temporal and spatial distribution of the ionospheric parameters existing between 200 and 1200 km above the earth. The correlative data that was to be taken was comprised of measurements of the charge accumulations on the surface of the satellite and the relation of this data to electrical drag and density of the medium, and measurements of the frequency, momentum, and energy of micrometeorite impacts.

Both the *Jupiter* booster and JPL cluster performed close to preflight predictions, as shown in Table 20. JPL Cluster 17 (Fig 99) used on this round was identical to the cluster used on AM Round 19A (or 16A) with a support cylinder added to the Stage 3 cone. This cylinder was again required because payload weight was in the range of 92.5 pounds and the cluster needed the additional rigidity.

This cluster was delivered to Cape Canaveral on May 2, 1960 and stored in the AMR magazine until September 27, 1960, when it was delivered to the JPL spin building for final assembly. By October 25, 1960, the cluster assembly work and payload mating had been completed, and the cluster was sent to the pad for mating with the *Jupiter*. The initial spin test was then conducted satisfactorily as was the plug drop test in which fuzes (simulating Stage 2 igniters) were fired through the composite *Jupiter* cluster wiring.

The countdown on October 3, 1960, was marred only by the necessity of removing the payload for a minor repair after it had been mated to the cluster. However, the repair was made, the payload remounted on the cluster, and the launching successfully executed within the allowed firing window.

3. AM19F Launching

On February 24, 1961, *Juno II* AM19F (Fig 100) was launched in an unsuccessful attempt to place the 75 pound, S-45 ionosphere beacon satellite (Fig 101) into orbit. The payload for 19F was designed to provide a means to study the propagation of signals through the ionosphere. These signals would enable the acquisition of data relative to ionospheric absorption anomalies, in-

Table 20. Orbit characteristics of *Explorer VIII*

Characteristic	Predicted	Actual
Perigee, km	395	370
Apogee, km	2375	2341
Eccentricity, km	0.1276	0.1275
Inclination, deg	50.33	49.9
Period, min	113.3	112.7

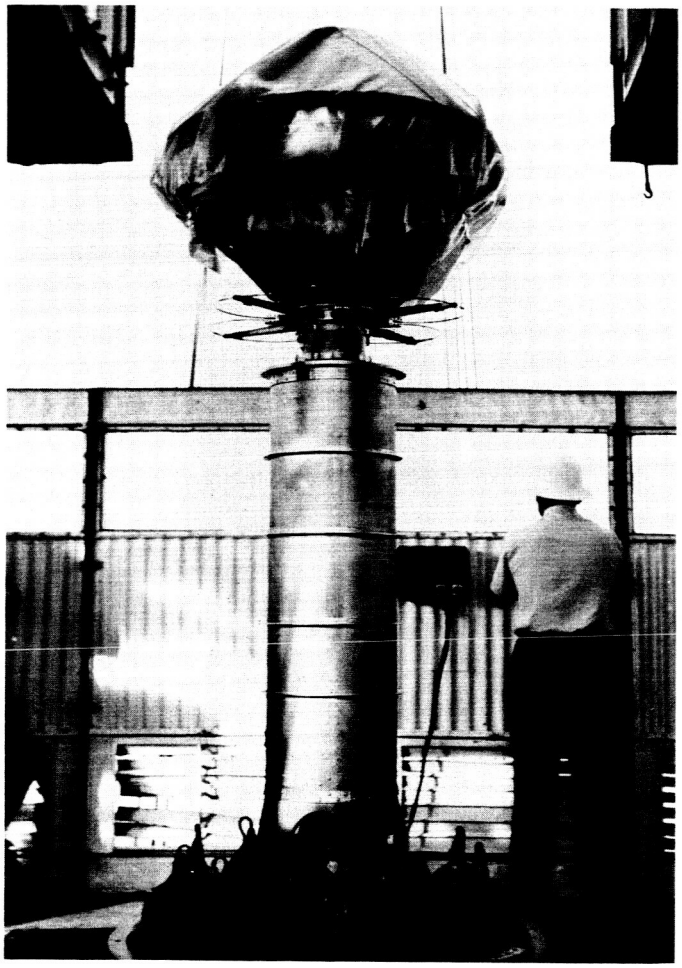

Figure 99. Cluster configuration for AM19D

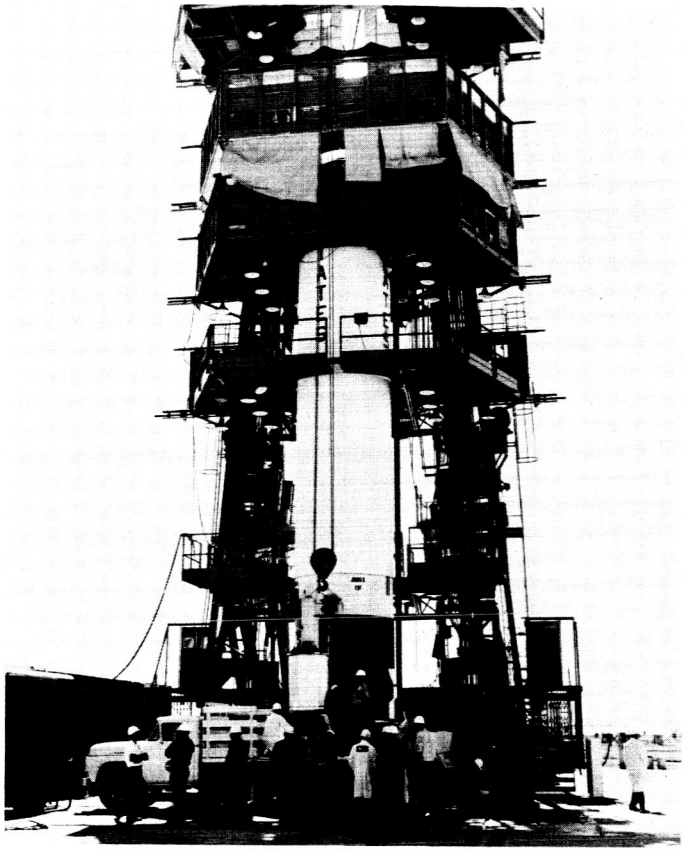

Figure 100. *Juno II* AM19F

tegrated electron density, faraday rotation measurements, and a possibility of transmission time delays.

As detailed in Table 21, booster performance was essentially normal until first separation (booster tankage from instrument compartment). While evidence is inconclusive, a possible mode of failure is that the cable from the angle-of-attack meter (shown in Fig 102) came free from the side of the shroud (held in place only by a potting compound) and interfered with the rotation of the payload. This interference led to the displacement of the payload, the unseating of Stage 4, the destruction of the Stage 3 and 4 timer, and eventually to the loss of spatial attitude control of the instrument compartment. This theory is supported by the dynamic condition of the cluster returning to normal shortly after the ejection of the shroud (possibly permitting the escape of the unseated Stage 4 and payload).

Stage 2 was observed to fire (with approximately correct performance) by the Lincoln Laboratory radar facil-

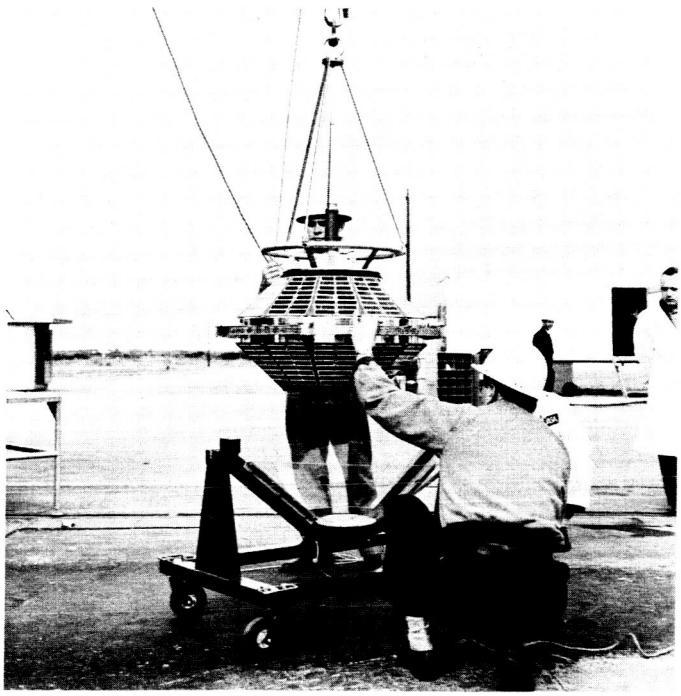

Figure 101. AM19F payload with ionosphere beacon

Table 21. Initial data on Flight AM19F

Event	Predicted time, sec	Range time, sec	Universal time
Range-zero time[a]	0	0	1913:13
Liftoff time (first vertical movement of vehicle)	0	0	1913:13
Booster: cutoff	179.3	178.5	1916:11.5
Booster: separation	186.3	186.5	1916:19.5
Signal from angle-of-attack measurement lost	—	188.1	—
Pitch and yaw gyros start to oscillate at 3 to 4 cps	—	188.1	—
Cluster drive motorcurrents go to full scale	—	188.7	—
Platform rolls greater than 15 deg (essentially lose reference)	—	190.3	—
Payload transmitter signal lost	—	204	—
Shroud separation (no indication of shroud kick motor firing)	214	214	1916:47
Cluster dynamic condition returns to normal	—	221	—
Stage 2 ignition	432	473	1921:6
Stage 3 ignition			Not observed
Stage 4 ignition			Not observed
Launch azimuth			44° East of true North

[a]The instant chosen as range-zero time is the first whole-number second occurring immediately prior to liftoff.

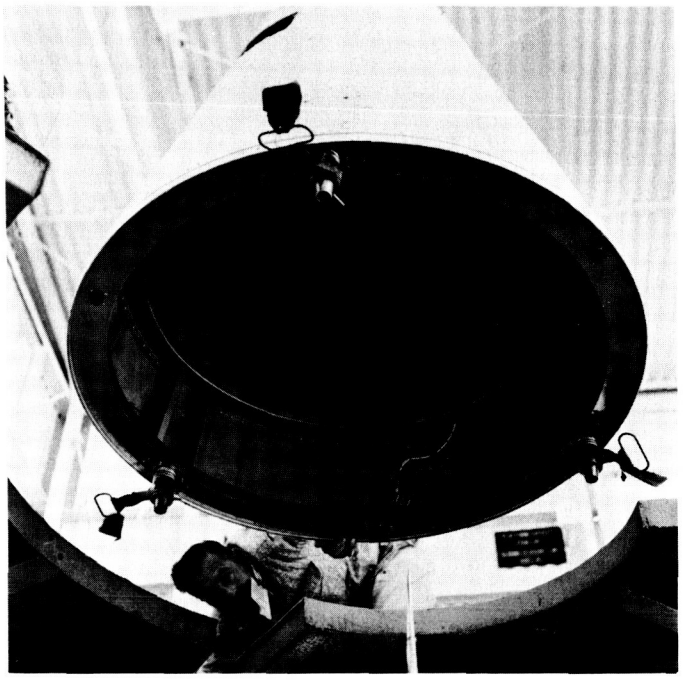

Figure 102. AM19F shroud

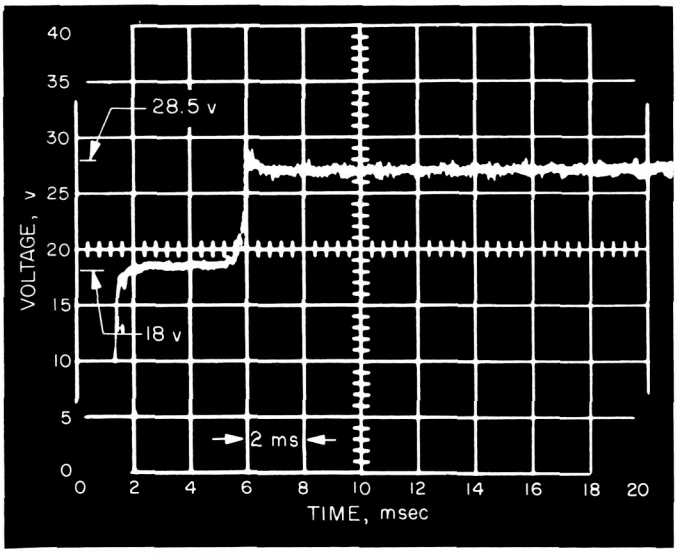

Figure 103. Second stage ignition characteristics

ity; however, neither Stage 3 nor Stage 4 was observed to fire, supporting the theory that the timer was destroyed.

Another possible mode of failure is that the Stage 3 to Stage 4 shear pins failed prematurely due to negative *g* loads. After considerable investigation this possibility was judged highly improbable and no changes have been made in the method of shear-pinning the high-speed stages. The criteria governing shear pin strength and design were again reviewed and judged adequate for the existing cluster dynamic environment.

JPL Cluster 19 used on this round was identical to Cluster 17 used on AM19D. Prior to the launching of this vehicle, the JPL engineering review team expressed interest in obtaining test information on the second stage ignition level and squib time delay as a function of the combined cluster–*Jupiter* circuitry. To obtain this information, simulated igniters (identical to flight igniters with the exclusion of pyrotechnic material) were connected to the Stage 2 harness. An oscilloscope was also connected into this harness and equipped with a polaroid camera to record the ignition sequence. Figure 103 shows the actuation time of the eleven igniter simulators, and it can be seen that there was approximately a 4-millisecond time period from power first being supplied until the first squib was activated. The remaining 21 squibs all fired within a 0.5-millisecond time period. The voltage rose from approximately 18 volts with full squib load to 28.5 volts for no load. The important time period (as far as Stage 2 ignition is concerned) is from that time the first squib ignites until the last squib ignites. In this particular case the 0.5-millisecond time period is acceptable considering the fact that Stage 2 maintains electrical contact for 12 milliseconds under full thrust conditions.

4. AM19E Launching

On April 27, 1961, the *Juno II* AM19E vehicle placed into orbit the artificial 85-pound Satellite S-15, *Explorer XI*, the gamma-ray astronomy satellite. This satellite (Fig 104) has the primary objective of detecting and mapping the high-energy gamma rays resulting from neutral pi-meson (pion) decay and relating this data with the density of cosmic-ray flux and interstellar matter. The secondary objective is to measure the ratio of the high-energy gamma rays reflected by the earth's atmosphere to the quantity of gamma rays falling upon the earth.

Both the *Jupiter* booster and the JPL cluster performed close to preflight predictions, as shown in Table 22. JPL Cluster 18 used on this round was identical to the cluster used on 19D. The countdown proceeded smoothly without interruption with the exception of a 5-minute hold at X − 15 minutes for an AMR computer check.

Table 22. Orbit characteristics of *Explorer XI*

Characteristic	Predicted	Actual
Perigee, km	475	497
Apogee, km	1832	1793
Inclination, deg	28.307	28.49
Period	108.06	108.1

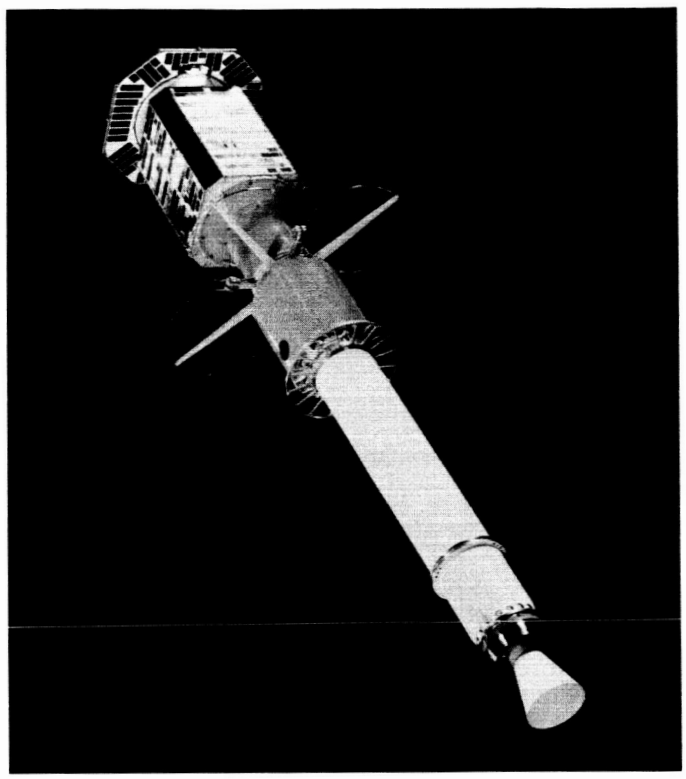

Figure 104. AM19E gamma-ray astronomy satellite

References

1. *Scientific America*, Vol 202, No. 5, p 69, May 1960.
2. Viterbi, A. J., *On Coded-Coherent Communications*, Technical Report No. 32-25, Jet Propulsion Laboratory, Pasadena, August 15, 1960.
3. Lawton, J. G.,"Theoretical Error Rates of Differentially Coherent Binary and Kineplex Data Transmission Systems," *Proceedings of the IRE*, Vol 47, pp 333–334, February 1959.
4. Cahn, C. R., "Comparison of Coherent and Phase Comparison Detection of a Four Phase Digital Signal," *Proceedings of the IRE*, Vol 47, p 1662, September 1959.
5. Glenn, A. B., "Comparison of PSK-AM Versus FSK-AM and PSK Versus FSK Binary Coded Transmissions," *IRE Transactions on Communications Systems*, CS-8, No. 2, p 87, June 1960.
6. Daelz, M. L., Heald, E. T., and Martin, D. L., "Binary Data Transmission Techniques for Linear Systems," *Proceedings of the IRE*, Vol 45, No. 5, pp 656–661, May 1957.
7. Barry, G. and Garabedian, A., *Performance of Predicted Wave Systems in the Presence of Additive, White Gaussian Noise*, Engineering Report No. CER-W592, Collins Radio Company, Newport Beach, California, January 20, 1958.
8. Landee, R. W., *A Method of Generating an Unambiguous Local Phase Reference for Data Detection Applications*, Technical Memorandum, Collins Radio Company, Newport Beach, California, December 19, 1960.
9. Coggshall, J. C. and Nybo, R., *Technical Report on the TE-290 Data Terminal Set*, Collins Radio Company, Newport Beach, California, 1960.